Development of a Performance-based High Pressure Feed-water Heater Model for Flownex SE

University of Cape Town

Prepared by:

MATETE THAKASO

THKMAT002

Department of Mechanical Engineering

University of Cape Town

Supervisor:

Dr WIM FULS

NOVEMBER 2014

Submitted to the Department of Mechanical Engineering at the University of Cape Town in partial fulfilment of the academic requirements for a Master's of Science degree in Mechanical Engineering

Key Words: Feed-water heater, Heat transfer coefficients, modelling, Flownex SE, Pressure drop.

The copyright of this thesis vests in the author. No quotation from it or information derived from it is to be published without full acknowledgement of the source. The thesis is to be used for private study or non-commercial research purposes only.

Published by the University of Cape Town (UCT) in terms of the non-exclusive license granted to UCT by the author.

University of Cape Town

Abstract

Feed-water heaters (FWHs) are an integral part of the power plant with respect to the overall heat recovery, and thus its efficiency. While the main purpose of the FWHs is to heat up the feed-water before being sent to the boiler, there are more added advantages owing to the installation of this equipment to the power plant such as less heat being removed to the atmosphere at the condenser. This report aims at understanding the different types of FWHs in operation and understanding how heat is transferred from the bled steam into the feed-water, and using the understanding to model a transient FWH. The FWH model is a building block towards building a complete transient power plant model. Process operations are all subject to constraints of some sort. The limitations can be in the form of physical geometry, process parameters or lack of correlations that relate known data. The constraints vary in their complexity, and depending on the type of constraints a different mathematical modelling technique can be applied to implement the FWH model. The grey-box modelling technique was chosen to be the appropriate one for analysis as it captures the dynamics that depend on the first principles and correlations whilst still using the global inlet and outlet properties of the FWH [1].

The FWHs have three zones; de-superheating, condensing and sub-cooling zones. The heat transfer characteristics of the three zones are different, and thus their heat duties with the condensing taking a significant amount of the heat duty. The heat duties of the different zones are determined and condensing zone takes above 80% of the heat transfer for the case study taken in this report. Most research on FWH modelling combines the heat transfer coefficient (HTC) of all three zones. But in this report only the condensing zone overall HTC is determined from assuming saturation temperature is taken at the inlet pressures of the two streams for the FWH. The overall HTC takes into consideration the conductivity of the heat exchanger (HX). The algorithm used, converts the FWH high level inputs into heat transfer characteristics for that FWH. The Heat on the two remaining zones is added as heat input on the model and varies with varying load conditions.

The results from build simulation models show good agreement with acceptance data from the Kriel power station which was used as a case study to validate the model. The temperature and energy analysis in steady state showed that the modelling tool, Flownex, predicted the energy and temperature distributions accurately. This is also seen in the transient model built during load changing.

Declaration

I, Matete Thakaso, hereby declare the work contained in this dissertation to be my own. All information which has been gained from various journal articles, text books or other sources has been referenced accordingly. I have not allowed, and will not allow, anyone to copy my work with the intention of passing it off as their own work or part thereof.

Signed by candidate

_____

Matete Thakaso

Acknowledgements

I would like to thank the following people for their contribution to this thesis.

Dr W. Fuls, my supervisor, for the boundless knowledge he shared and the patience, without whom this work would not have been achieved. I have learnt from him more than what is written in this thesis. Words cannot describe how thankful I am.

Prof L. Jestin & Prof P Rousseau for their advice, technical support and motivation in getting the work done and for the side exercises they gave to broaden my knowledge scope during this work.

I would also like to thank my colleagues in the Energy Efficiency Centre for their different contributions in my work, the office discussions. I would specifically like to thank Mr. Rahendra Neerputh for making available to me all plant data used in this work.

To my financial sponsors EPPEI through the Department of Mechanical Engineering, I am extremely grateful. If it wasn't for the opportunity they granted me, my studies would not have been possible.

To my friends, both at school and from back home, for the moral support and believing in my ability. I also thank Miss Nthateng Mphofu for proofreading my work.

My family, who listened and encouraged and whose love and support are one of a few unconditional things in my life.

Lastly and most importantly, I thank God for the opportunities and blessings.

Table of Contents

List of Figures vi
List of Tables x
List of Nomenclature xi
1. Introduction 1
1.1 Background to the Study 1
1.2 Objectives of the Study 1
1.3 Scope and limitations of the study 2
1.4 Plan of Development 3
2. Literature Review 4
2.1 Flownex Introductory 4
2.2 Overview of closed FWHs 8
2.3 Modes of Heat Transfer 15
2.4 Transient Heat Transfer 25
2.5 Pressure Drop Correlation Review 39
2.6 Level and Level Control in FWHs 42
2.7 Modelling Techniques 44
2.8 Previous Mathematical Models of FWHs 49
3. Model Development 53
3.1 Overview of Model Development 53
3.2 Operating conditions 53
3.3 Determining the Heat Transfer Characteristics 55
3.4 Thermal Mass Determination 61
3.5 Pressure Drop Determination 64
3.6 Detail Model Description 64
3.7 Pre-processing Results and Model Implementation 75
4. Model Validation, Observations and Discussions 79
4.1 Steady State Tests 79
4.2 Transient Tests 82
5. Conclusions and Recommendations 89

5.1 Steady State Model 90
5.2 Transient State Model 91
5.3 Closing Remarks 91
6. List of References 92
Appendix A. Methodology Summary 98
Appendix B. Typical HTCs Calculation 102

List of Figures

Figure 2-1: Flownex pipe component with input options [4]. 4
Figure 2-2: Flow resistance component with inputs options [4]. 5
Figure 2-3: Two-phase tank component with inputs options [4]. 6
Figure 2-4: Boundary condition with inputs options [4]. 7
Figure 2-5: Heat transfer component and a schematic with convection and conduction [4]. 7
Figure 2-6: Restrictor with discharge coefficient element and its input options [4]. 8
Figure 2-7: Feed-water traces on a T-s diagram for Rankine cycle. 9
Figure 2-8: Rankine cycle components with heater in place. 10
Figure 2-9: Tube-sheet and header type FWHs being assembled [7]. 11
Figure 2-10: Temperature profile of the two fluids in a parallel-flow HX and a counter flow HX. ... 12
Figure 2-11: Three zone U-tube FWH [9]. 13
Figure 2-12: Header-type FWH [15]. 13
Figure 2-13: One-dimensional conduction through a plane wall. 15
Figure 2-14: Boundary conditions of a typical tube cross-section working as a HX 16
Figure 2-15: Condensing modes for condensation over a tube bundle [15]. 19
Figure 2-16: Flow disturbance due to baffles and the different streams created due to baffles [28]. 20
Figure 2-17: Small section of a counter-flow HX. 21
Figure 2-18: One-dimensional cross-section of a HX. 22
Figure 2-19: Counter flow HX effectiveness variation with NTU for different heat capacity ratios. 24
Figure 2-20: Parallel flow HX effectiveness variation with NTU for different heat capacity ratios... 25
Figure 2-21: HX Exit and wall transient temperature for different NTU [36]. 27
Figure 2-22: Geometry and parameters involved in the lumped system analysis. 29
Figure 2-23: Temperature profile or response of lumped system for different b values. 30
Figure 2-24: Dimensions of a tube working as a HX. 31
Figure 2-25: Instantaneous Temperature Field within HE with n=3 versus n=6. 32
Figure 2-26: Temperature profile as a function of radius with increasing time (Analytical). 33

Figure 2-27: Temperature profile as a function of time with increasing radii (Analytical). 34

Figure 2-28: Comparison between Flownex and analytical results for an infinitely long tube subjected to convection at the boundaries to induce transients where 4 nodes and time step of 0.1s were used in Flownex [40]. 35

Figure 2-29: Heat transfer from the condensate to the feed-water in a typical sub-cooling zone during a simulated transient. 36

Figure 2-30: Typical discretised HX material with discrete temperatures. 37

Figure 2-31: Heat energy absorbed (red) by HX and the difference of energy into and out of a HX. 38

Figure 2-32: Maximum difference in energy absorbed and Q_{in}–Q_{out}, % difference for different increments. 39

Figure 2-33: Pipe exit and entrance losses to and from a large reservoir 40

Figure 2-34: Cross-sectional view of a FWH showing baffles, baffle window and the flow directions on each segment. 41

Figure 2-35: Drain valve position on a FWH. 43

Figure 2-36: Illustration of how the TTD and the DCA are determined from a typical heater. 43

Figure 2-37: FWH level vs TTD/DCA [48]. 44

Figure 2-38: White box modelling flow diagram. 45

Figure 2-39: Black box modelling flow diagram. 45

Figure 2-40: Grey box modelling flow chart. 46

Figure 2-41: Series Hybrid grey-box Modelling. 48

Figure 2-42: Parallel Hybrid grey-box modelling. 48

Figure 2-43: Effect of level on overall heat transfer by drain cooler approach [59]. 50

Figure 2-44: Comparison of calculated and actual feed-water outlet temperature [51] 51

Figure 3-1: Kriel power station [3] 54

Figure 3-2: Data from heat balance of Kriel power station 55

Figure 3-3: Temperature profile of a typical three zones FWH. 56

Figure 3-4: De-superheating energy vs feed-water mass flow rate of HPH 7. 58

Figure 3-5: Condensing zone temperature profile. 59

Figure 3-6: Summary of the tube layout in HXs and the accompanying characters in tube count analysis. 62

Figure 3-7: Schematic drawing of a FWH indicating dimensions and the clearance of tubes to the end cap. 63

Figure 3-8: Complete transient model of a FWH showing with three different zones. 65

Figure 3-9: De-superheating zone showing both inputs of shell and tube sides. 66

Figure 3-10: Sub-cooling zone with the data link as heat transfer element. 68

Figure 3-11: FWH shell and inputs required in the model. 69

Figure 3-12: Condensing zone shell side inputs. 70

Figure 3-13: Heat transfer element connecting shell and tube sides. 70

Figure 3-14: Convection HTC inputs on a condensing zone. 71

Figure 3-15: Typical HPH 7 high level inputs and results. 72

Figure 3-16: Inputs to the shell side inlet properties. 72

Figure 3-17: Steady state Flownex model of a FWH 73

Figure 3-18: Inputs of the heat transfer without conducting layers. 75

Figure 3-19: Condensing zone section showing inlet and outlet quality, and heat energy without conduction 76

Figure 3-20: Inputs to the conductive layers option. 76

Figure 3-21: Condenser section showing inlet and outlet quality, and heat energy with conduction. 77

Figure 3-22: Feed-water side HTC varying with load. 77

Figure 4-1: Designer set-up to determine the required Bled steam mass flow for thorough condensation. 79

Figure 4-2: Percentage error in the model results for different load conditions. 81

Figure 4-3: Exit temperatures of the two FWH streams at 80% load. 83

Figure 4-4: Bled steam and condensate drain flow rate, and level for changing load characteristics (80% to 100%). 84

Figure 4-5: condensate and feed-water temperatures for changing load conditions (80% to 100%). 85

Figure 4-6: Heat transfer across FWH and the level for changing load conditions (80% to 100%). .. 86

Figure 4-7: HPH 6 corrosion at Kriel power station [3]. 87

Figure 4-8: Plant data for HPH7 over 14 hours [3]. 87

Figure 4-9: Comparison between acceptance test results and Flownex model results. 88

List of Tables

Table 3-1: Inlet conditions of the HPH 7. 55

Table 3-2: HPH 7 shell geometric data [63]. 61

Table 3-3: Illustration of tube mass determination showing required parameters. 63

Table 4-1: Flownex steady state model results. 80

Table 4-2: Effect of pressure drop on FWH performance. 80

Table 4-3: Actual FWH 7 working data. 81

List of Nomenclature

General symbols

$\Delta H`_{fg}$	Available latent heat [J/kg]
ΔP_b	Pressure drop across baffles [Pa]
ΔT_{LMTD}	Log Mean Temperature difference [K]
A	Area [m^2]
b	The reciprocal of the time constant [1/s]
Bi	Biot number [-]
c	Constants [-]
C	Heat capacity [W/K]
C_r	Ratio of minimum to maximum heat capacities [-]
D	Diameter [m]
F	Friction factor [-]
G	Mass flow per area [kg/m^2s]
h	Specific Enthalpy [J/kg]
h_c	Heat transfer coefficient [W/m^2K]
h_{fg}	Latent heat [J/kg]
J_0	Bessel function of first order [-]
k	Thermal conductivity [W/mK]
K	Secondary losses friction coefficient [-]
L	Length [m]
L_C	Characteristic length [m]
N	Number of rows of tubes in HX [-]
Nu	Nusselt number [-]
P	Pressure [Pa]
Pr	Prandtl number [-]
P_{sat}	Saturation pressure [Pa]
Q	Heat transfer [W]
R	Radius [m]
Re	Reynolds number [-]
T	Temperature [$^\circ$C]
U	Overall heat transfer coefficient [W/m^2K]
v	Velocity [m/s]
V	Volume [m^3]

X	Quality [-]
Z	Adjustment factor for LMTD [-]

Greek symbols and subscripts

μ	Dynamic viscosity [kg/ms]
ρ	Density [kg/m^3]
v	Specific volume [m^3/kg]
ζ	Vapour sectional area
φ	Two phase multiplier [-]
ε	Effectiveness [-]
τ	Dimensionless time [-]
δ	Radial thickness of a tube [m]
λ_n	Eigenvalues of the Bessel function [-]
a	Condensation HTC factor [-]

c	Cold stream [-]
h	Hot stream [-]
f	Saturated liquid [-]
g	Saturated vapour [-]
w	Properties of the heat exchanger wall [-]
l	Liquid state

Acronyms and Abbreviations

CL	Angle tube layout constant
CTP	Tube count constant
FWH	Feed-water Heater
HPH	High Pressure Heater
HTC	Heat Transfer Coefficient
HX	Heat Exchanger
LMTD	Log Mean Temperature Difference
LPH	Low Pressure Heater
NTU	Number of Transfer Units
PR	Tube pitch to radius ratio
TTD	Terminal Temperature Difference

1. Introduction

1.1 Background to the Study

The Specialization Centre for Energy Efficiency in the Department of Mechanical Engineering is developing a transient thermal-hydraulic power plant model using the Flownex Simulating Environment. The model will be used to simulate the process performance of individual components. It will also be used to analyse Eskom power plants in order to conduct power plant fault finding and to investigate the behaviour of the plant as a whole under different load characteristics and transients.

This project focuses on modelling the Feed-water Heater [FWH] of a typical power plant using heat balance data as input.

1.2 Objectives of the Study

1.2.1 Purpose of Study

A FWH may be modelled in one of the two different ways. They are the performance- and design-based approaches [2]. In the performance-based approach, a relatively small amount of parameters are specified by the user to represent the overall behaviour of the FWH. These would typically be process parameters observed or required under various load conditions. On the other hand, in design-based approach, a detailed analysis of the heat transfer and flow phenomena is performed internal to the heater so that the required amount of information to resolve the FWH within the system components is developed. This approach requires an extensive collection of input data that describe the heater internals in detail. This approach is very time consuming, and often the detail information is not known to the end user (in this case Eskom).

The purpose of this study is therefore to develop a methodology that can be followed to define a FWH in Flownex with minimal inputs required. The eventual model will be able to predict the heater's performance under various load conditions, as well as during moderate transient events. As a case study the Kriel HPH 7 is used in this report. This is because of the difficulties faced by Kriel operators where only unit 5 has credible results while other units' control and instrumentation requires upgrade. And a methodology for predicting some of the heaters' performance based on known inlet conditions would help overcome some of the problems outlined in [3].

1.2.2 Problems to be investigated

The following questions will be investigated and answered by this study:

- How can the different heat exchanger (HX) zones, namely the de-superheating, condensing and sub-cooling be separated from each-other without knowing the internal geometry?
- What level of sophistication is needed to model the various zones in Flownex?
- How can the heat transfer characteristics of the different zones be determined using only plant data at various load conditions?
- What information is needed to appropriately incorporate the thermal mass and volumes of the heater, again without detail internal information?
- How will the thermal inertia and effect of conductivity through the pipe wall affect the overall model, and how should that be incorporated?
- How can one determine the level in the vessel, and apply an appropriate Flownex element which would mimic the control system?

This study will address all the above questions, and attempt to offer solutions of appropriate methods for dealing with these.

1.3 Scope and limitations of the study

Because the details of flow phenomena that occur in the respective streams of the FWH are not modelled, the combined model will not be able to predict some local effects. This may result in inaccuracies when compared to actual plant data, especially during fast transients, or process conditions that extend far beyond the typical operating range.

In determining the heat transfer characteristics, average fluid and material properties will be used. This could further reduce the accuracy for off-design operation conditions.

The model will be built with level control capabilities but no control loops will be added to actually control the level. This is considered outside the scope of the study, and would form part of a separate project where the complete power plant control system will be added to the various components.

The method will be developed and tested on a tube-sheet horizontal high pressure FWH. Some of the methods would apply to vertical heaters, or header-type heaters, but this study will not attempt to produce solutions for all of these.

1.4 Plan of Development

To model a FWH, it is important to understand the basic phenomena behind heat transfer and pressure drop which are what determines the performance of a FWH. Chapter 2 outlines the background theory and mathematics required in a holistic model of a FWH. This chapter begins with an overview of the Flownex Simulation Environment which is the platform in which the model will be built. It then discusses a closed FWH, purpose and different types in service at Eskom. It continues by looking at heat transfer in steady state and transient state scenarios, and the heat transfer coefficients (HTCs) for the different flow regimes and fluid states. The pressure drop through a FWH is often negligible in the overall process, but it was studied for a better understanding of the response of the Flownex model. The concept of level control within a heater shell is discussed, and then some techniques of process modelling in engineering are looked at. Chapter 2 is completed by looking at some previous works by other authors in formulating the model of a FWH and discusses the concepts of white-, black-, and grey-box modelling.

Chapter 3 presents the methodology and logic in developing the FWH model. It first looks at the mass and energy balances of a FWH. Then the method followed in determining the HTC and heat duties for the different zones is outlined. The thermal mass estimation and methods used before are also presented with case study done for high pressure heater (HPH) 7. The preliminary checks to validate the model are also presented in this chapter. The Flownex model is then outlined, with all the components' contributions towards the whole model. The complete steady state and transient models are finally presented.

Chapter 4 gives the results for both the transient and steady state models with the plant data and comparison is made to gain confidence in the Flownex models. The results of the models are discussed with the aid of the literature presented in Chapter 2.

Chapter 5 discusses the usability of the models, shortfalls and recommendations for further work on the topic.

2. Literature Review

2.1 Flownex Introductory

This section is a brief introduction to Flownex and how it works, and most of the explanations are based on information from the software manuals [4] and [5]. "*Flownex is an integrated systems computational fluid dynamics (CFD) code used for design, optimization and simulation of complete thermal-fluid systems*" [4]. "*It solves partial differential equations for mass, momentum and energy conservation to obtain the mass flows, pressures and temperature distributions throughout the network*" [5]. The Flownex library contains simple components like pipes, pumps, heat transfer elements, valves etc. which can be connected and interconnected to form any desired network. The key components used in the model are outlined below.

Pipes:

Figure 2-1 shows the representation of a pipe in Flownex. The geometry of the pipe can be specified by giving the cross-sectional area or diameter with the length. The pressure losses in pipes are of two forms, the primary and secondary losses.

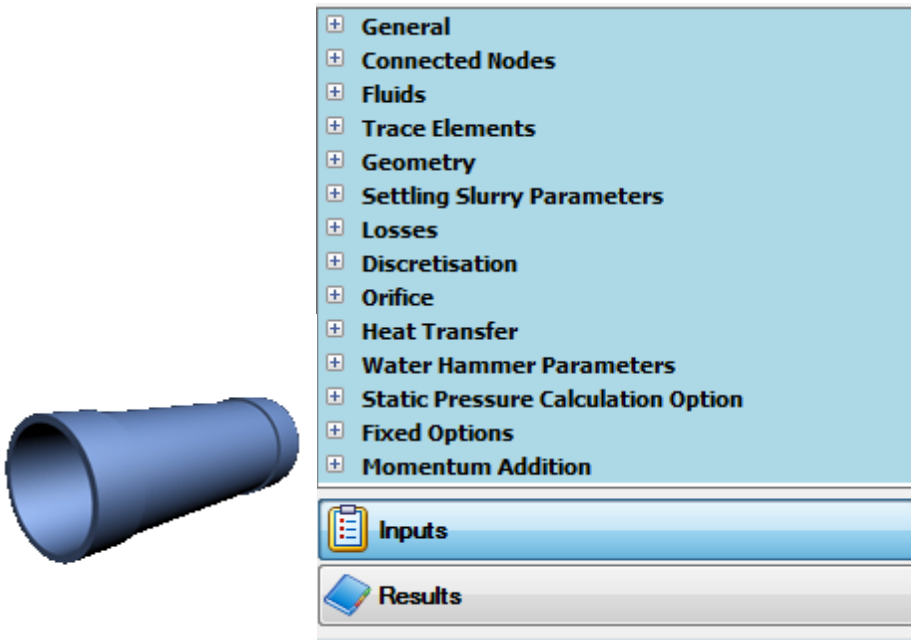

Figure 2-1: Flownex pipe component with input options [4].

Sudden changes in working conditions of a fluid in a pipe may cause a pressure pulse in the pipe, a phenomenon known as water hammer, and this can be captured in Flownex pipes. A pipe has capability of having a valve in the form of an orifice. The orifice can only be specified for pipes with a single increment, once there is more than one increment the orifice option disappears. Under

the discretisation option, the pipe can be subdivided into several sections to better follow the change in fluid properties or heat transfer along the pipe. Also, if there are several pipes of the same characteristics, the "number of parallel" pipes option can be specified.

Flow Resistance:

A flow resistance component is mostly used to model pressure drop across HXs, valves, ducts etc. It is often used as "connector" between other elements where the actual pressure drop is insignificant by defining a large flow admittance value.

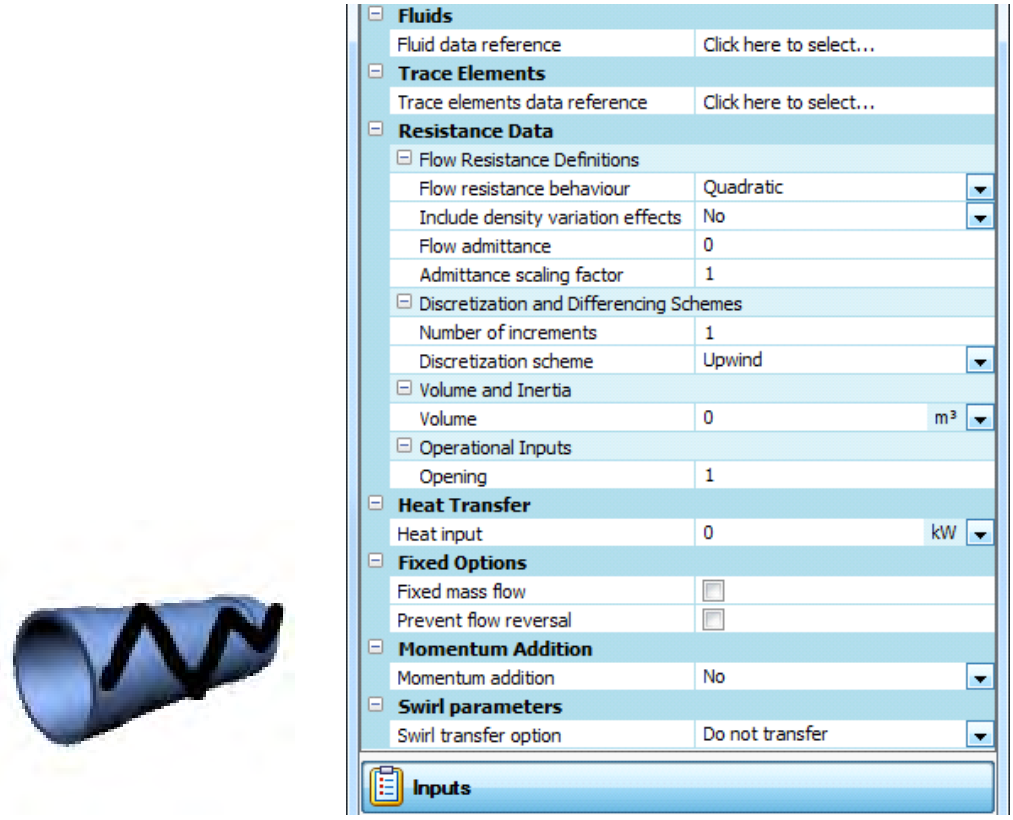

Figure 2-2: Flow resistance component with inputs options [4].

Only a constant heat input can be specified in this component. The capability of preventing flow reversal can be used to model non return valves with the flow resistance element.

Two-phase tank:

Two-phase tanks are used to model cavities/tanks which contain a fluid with different phases. The level of liquid in the tank is calculated from the fluid quality, hence making it possible to track it during transients. Entrances and exits to the two-phase tank can be specified by specifying the volume fraction of the component connected to the tank as shown in Figure 2-3. This allows one to extract either saturated liquid or gas, depending upon the current level relative to the pipe extraction height.

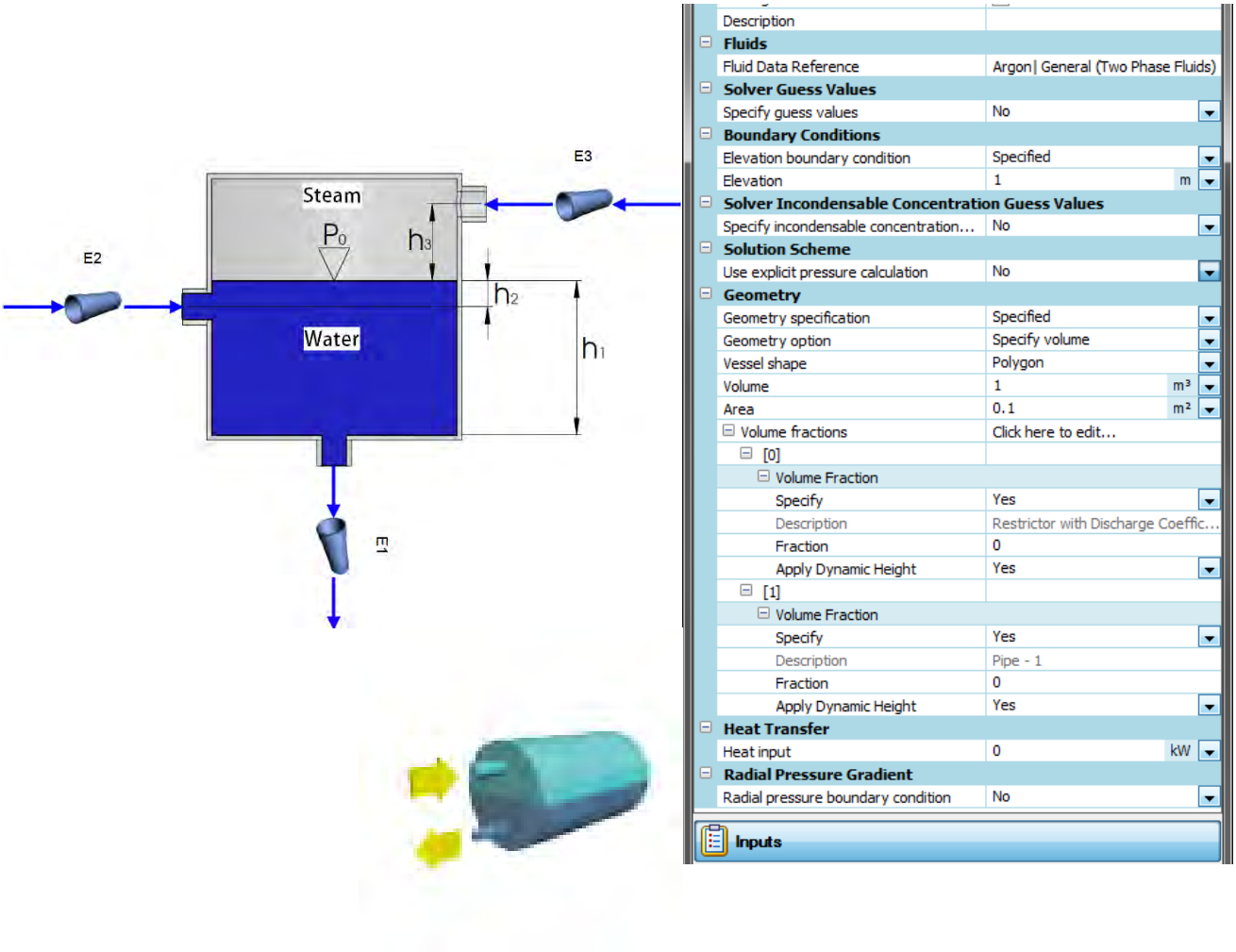

Figure 2-3: Two-phase tank component with inputs options [4].

The geometry and orientation of the two-phase tank can also be specified depending on the problem being solved. Also, because some components are located an elevation higher than other, there is an elevation specification option. The two-phase tank is in fact only a special case of the generic node component. Nodes are used to link other components (defined as elements) in Flownex. Elements have only one inlet and outlet, but a node can have multiple ports.

Boundary condition:

The boundary condition component is used to specify the conditions at a specific node in the network. It is represented as shown in Figure 2-4 in Flownex, and can only be connected to nodes and similar special node types, not elements. Only a few combinations of inputs at a single boundary can be specified. These are outlined in [4].

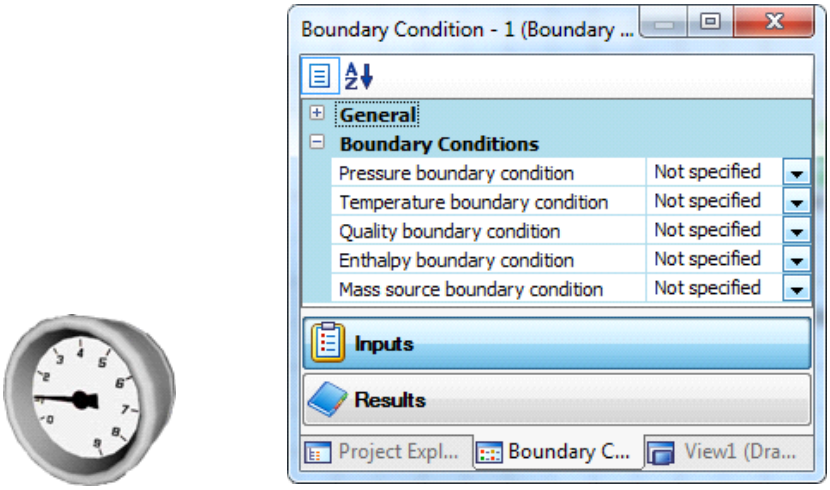

Figure 2-4: Boundary condition with inputs options [4].

Heat transfer element:

The heat transfer element is used to model convection, conduction and radiation to and from elements and nodes.

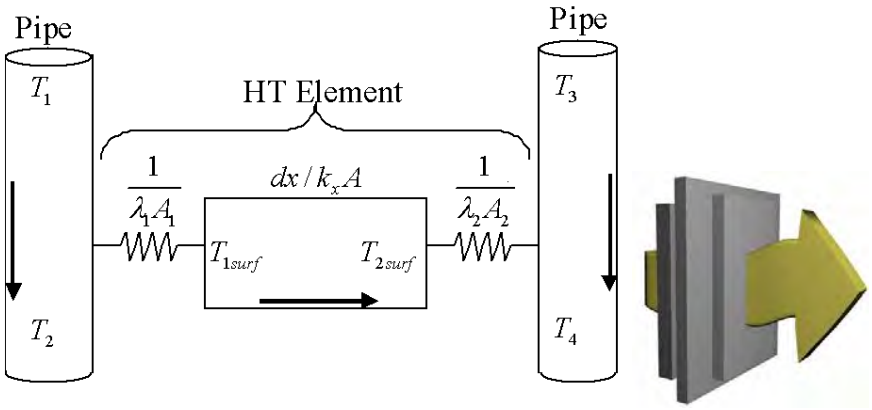

Figure 2-5: Heat transfer component and a schematic with convection and conduction [4].

Figure 2-5 shows a heat transfer element with convective heat transfer on both ends of a solid material, and the conduction through the material. The same idea is used to build the heat transfer between steam and feed-water in a FWH. The inputs and specifications of a heat transfer element will be shown in the model description to show which inputs are of relevance in the model in section 3.6.

Restrictor with discharge coefficient:

The restrictor with discharge coefficient can be used in throttling processes and/or similar processes. It uses the cross sectional area of flow and the discharge coefficient to determine the pressure drop due to a certain flow rate. Figure 2-6 shows the restrictor component and the inputs box. The “Cross sectional option” can be changed between Area and Diameter.

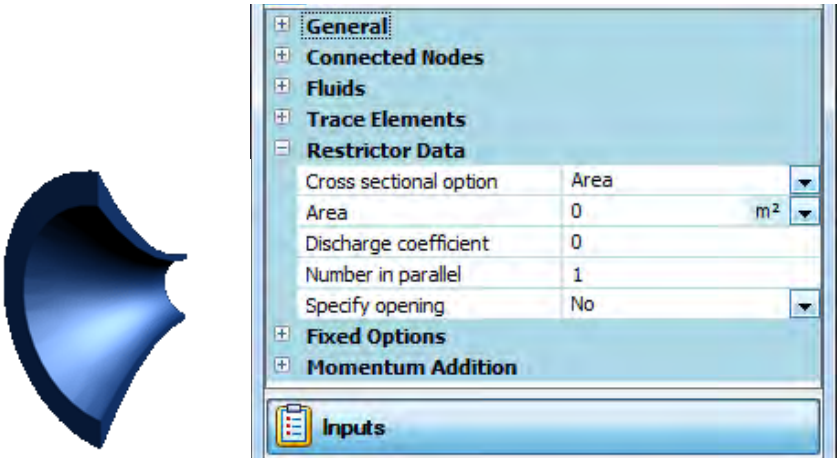

Figure 2-6: Restrictor with discharge coefficient element and its input options [4].

External software:

Flownex allows for the linking of various other software tools into the network. This allows one to perform calculations externally and feeding the answers into the components. In this project Excel and Mathcad components are used to do calculations external to Flownex algorithms. Also, the results from the Flownex runs can be reported into an Excel sheet for later analysis. All the components discussed above have significance towards building a FWH model and it will be explained in detail how each of them contributes in the overall model.

Flownex version 8.3.7.2310 is used to model the FWH in this report.

2.2 Overview of closed FWHs

2.2.1 Purpose of a closed FWH

Most power plants make use of the Rankine vapour cycle for converting the thermal energy (obtained from burning fuel) into electrical energy. The ordinary Rankine cycle can be summarised as a series of four events in a closed loop on a T-s diagram (see Figure 2-7):

1. The working fluid in the Rankine cycle is pumped from a low to a higher pressure, and this is ideally an isentropic process. The pumping of a fluid requires some form of power input to the system;

2. The pressurised fluid is channelled into a boiler for constant pressure heating until it reaches superheated vapour. The heat source in more than 90% of ESKOM power plants is either coal or a nuclear reactor;

3. Superheated vapour then expands through a series of turbines which then drives an electrical generator. This process, like pumping, is ideally an isentropic one. As the steam expands and loses its energy the temperature and pressure decreases;

4. The resulting vapour is then collected in a condenser for cooling to saturated liquid. The resulting liquid is then fed back to the pump and the cycle repeats [6].

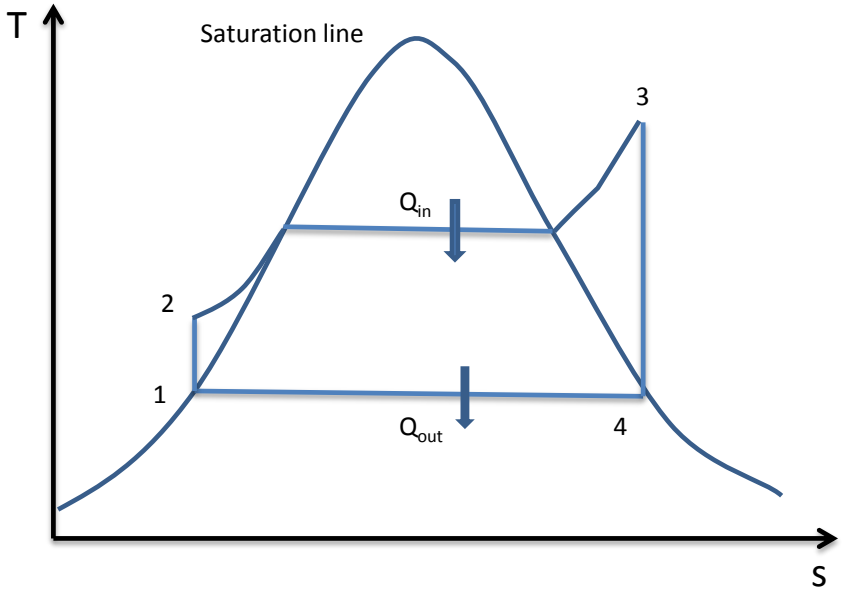

Figure 2-7: Feed-water traces on a T-s diagram for Rankine cycle.

Developments have been made to improve the Rankine cycle efficiency, and one of those was to add a FWH between a condenser and a feed pump for regeneration. One of the benefits of adding a FWH is a reduction in the energy requirement to heat the high pressure feed-water in the boiler to its saturation temperature [7].

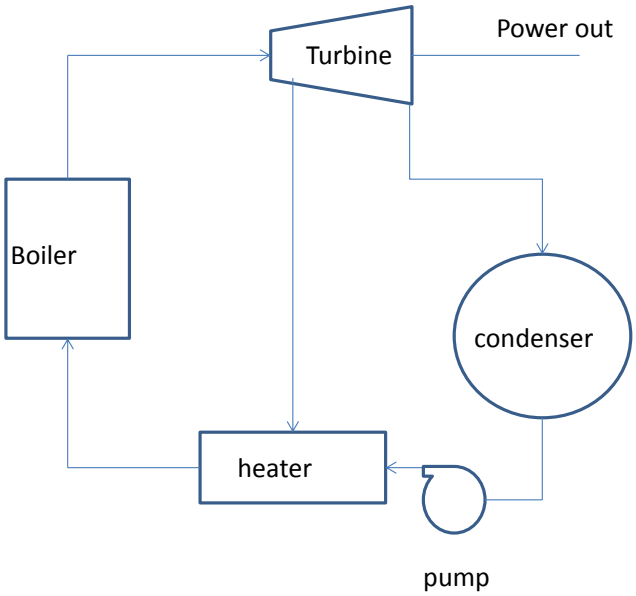

Figure 2-8: Rankine cycle components with heater in place.

Figure 2-8 shows a common implementation of the FWH where the feed-water is heated using steam extracted from the turbine. The consequence is that there will be less steam to be condensed. This may not be seen to increase the efficiency directly, but it cuts on the costs of heating in the boiler and reduces the size of the condenser and low pressure turbine [8].

FWHs also improve the life expectancy of the boiler and turbine. A turbine operating with FWH extraction expands less steam and therefore lower forces acting on the turbine blades. A boiler without FWHs upfront needs to introduce higher amounts of heat into the furnace, thus creating higher thermal stresses [9]. These last two benefits are of particular importance for a plant that has been designed with FWHs, but is operated with some out of service.

2.2.2 Types of FWHs and Construction

This study will only focus on closed FWHs, where the feed-water and bled steam streams do not mix. There is also an open-type FWH, where the bled steam mixes into the incoming feed-water stream, and is taken onwards to the boiler.

Closed FWHs can be classified according to the operating pressure of the feed-water stream into either a high pressure (HPH) or low pressure (LPH) heater. The HPHs are placed between the boiler feed-water pump and the boiler, which implies that they operate at approximately the boiler pressure. The LPHs are placed between the condensate pumps and the boiler feed-water pumps, and operates at a pressure in-between the condenser and boiler pressure [10].

The arrangement of the tubes inside the heater differentiates the type of FWHs, with the main types being the tube sheet and the header type. Tube sheet heaters were conventionally used until the introduction of the header heaters. And in some old plants in the ESKOM fleet the header types are replacing the tube sheet heaters. The header type heaters have gained more use within ESKOM plants due to their ability to withstand high thermal gradients within the header section, due to reduced thickness [7]. Due to their ability to withstand high thermal stresses they are used mainly as HPHs. In tube sheet FWHs, the feed-water flows in a group of U-shaped tubes which is connected to a common tube sheet. Header type FWHs can have multiple passes of the feed-water tubes, and they start and end in separate headers as shown in Figure 2-9.

a) Tube-sheet FWH being assembled

b) Header type FWH being assembled

Figure 2-9: Tube-sheet and header type FWHs being assembled [7].

FWHs can also be classified by orientation in operation as either the horizontal or vertical FWH. The horizontal FWH requires more space for installation compared to the vertical, but has an advantage of smooth condensate level change in drastic operating changes. This is because a big change in condensate volume only causes a small change in level [11]. The vertical FWH can be classified further into two types, the channel up or channel down depending on the position of the sub-cooling section [12].

Inside the FWH there may be baffles to direct the flow of the bled steam through the shell. The FWH can be arranged for the fluids to either flow in parallel, counter-flow, cross-flow or any combination of these three. In an ideal parallel flow closed FWH the temperature of the feed-water and that of steam at the outlet will be the same [13]. And Figure 2-10 shows a typical temperature profile for both the parallel and counter flow HXs.

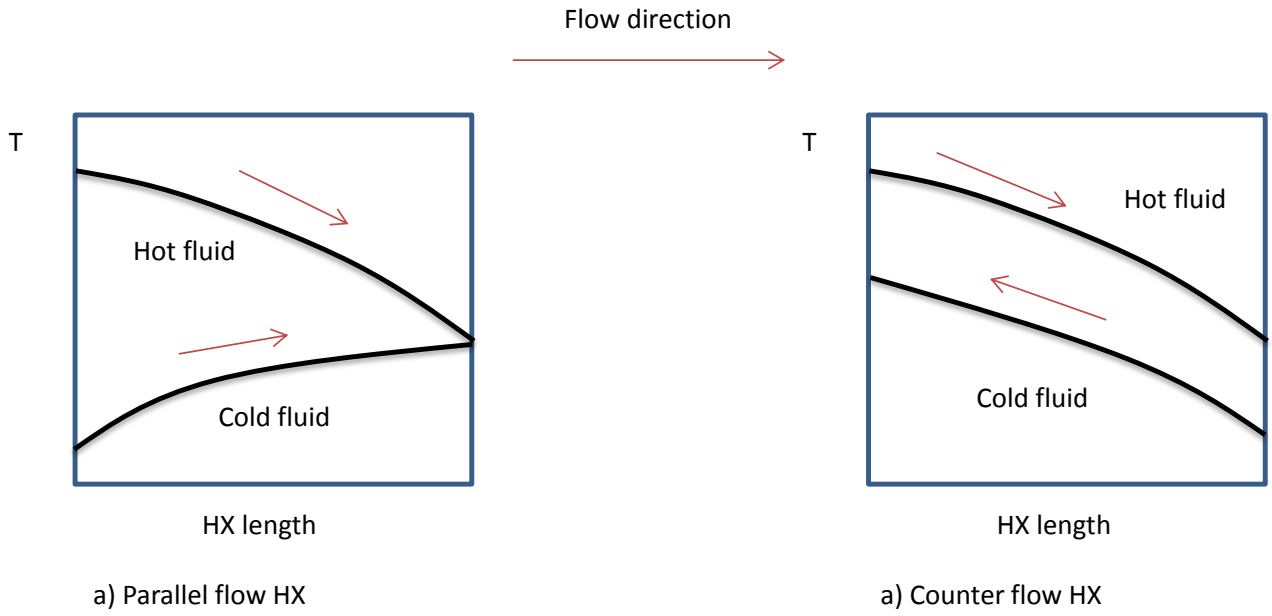

Figure 2-10: Temperature profile of the two fluids in a parallel-flow HX and a counter flow HX.

Counter-flow closed FWHs are the most widely used ones because of their higher effectiveness in heat transfer. This is because the feed-water at exit can reach temperatures higher than that of the bled steam at exit as can be seen in Figure 2-10. The fluid flow can also be arranged in a cross flow manner. This is where the fluids flow at right angles to each other in a HX. In most FWHs, the flow inside is a combination of cross flow and one of parallel or counter flow.

Closed FWHs can also be classified by the number of heat transfer zones within the shell. They are either single zone, double zone or three zones heaters. These zones are the de-superheating zone, condensing zone and the sub-cooling zone, and will be looked into in detail the next section. Hussaini and Zubair [14] talk about the reasons for having different zones in a heater, with the main one being the steam properties which depends on the extraction points of the steam from the turbine. All heaters have the condensing zone and some may have the de-superheating or sub-cooling or in some cases both depending on the steam properties and FWH downstream process equipment. Figure 2-11 shows a tube sheet FWH with all three zones in place.

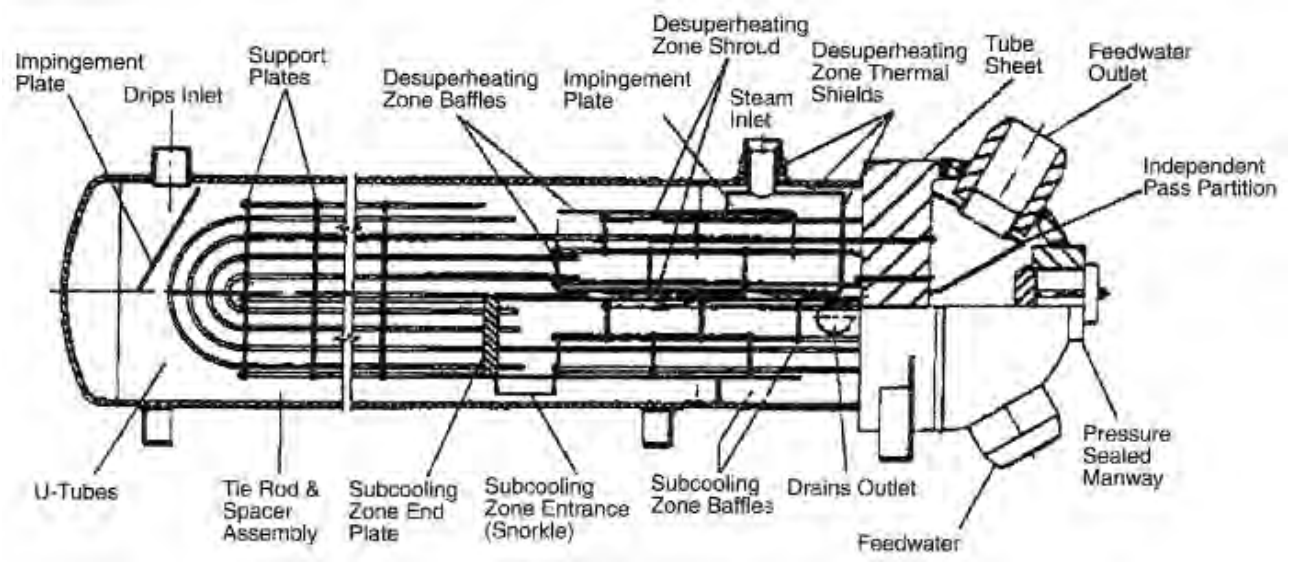

Figure 2-11: Three zone U-tube FWH [9].

Figure 2-12 shows another type of a FWH, the header type heater, with the feed-water inlet and outlet headers marked as 1 and 2 respectively. From Figure 2-12 it can also be seen that there are effectively four tube passes in this kind of FWHs.

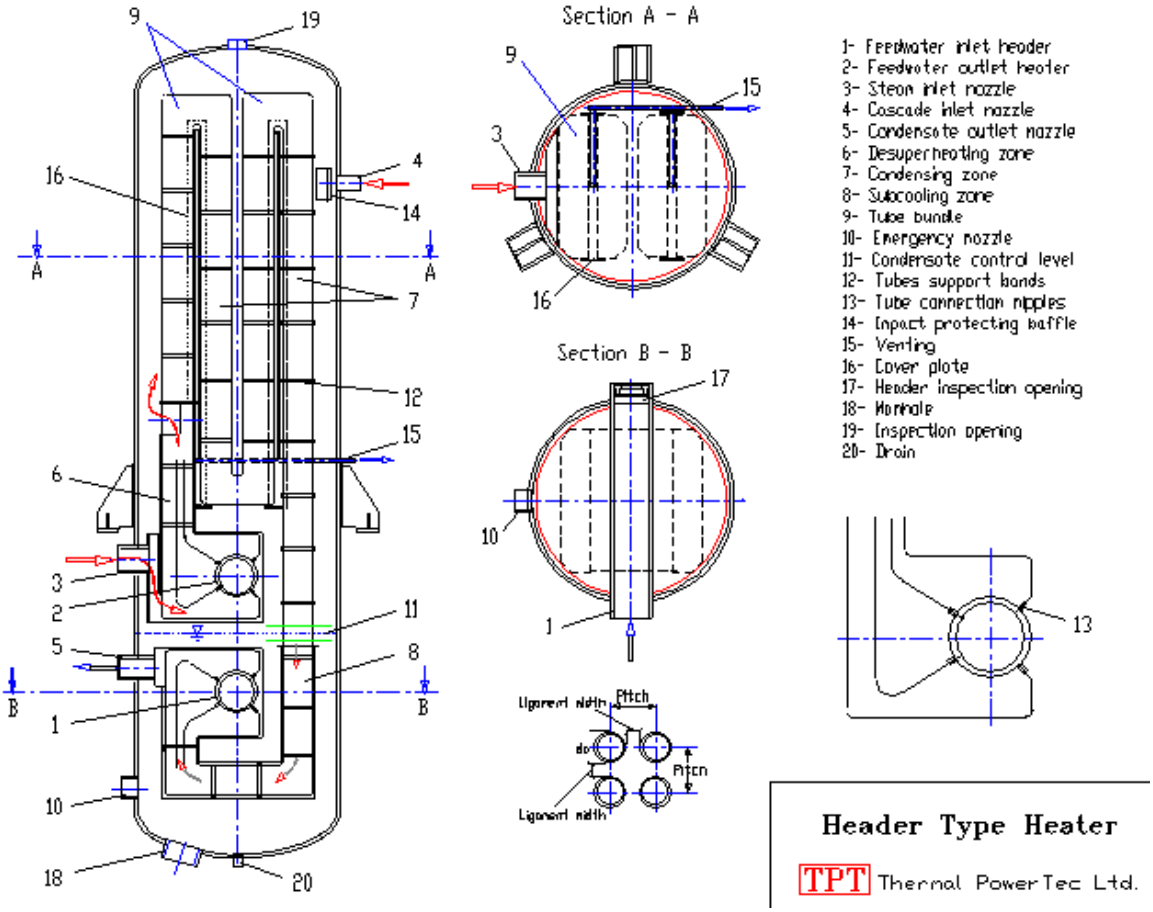

Figure 2-12: Header-type FWH [15].

The purpose and importance of each zone is discussed in the following section.

De-superheating zone

The de-superheating zone serves to bring the steam temperature down to closely saturation conditions. The flow velocity is increased by adding baffles to enhance the HTC while steam is in the gaseous phase. This is to reduce the size of the HX in the de-superheating zone, and hence reducing the overall size of FWH. The tube wall temperature at the outlet of the de-superheating zone should preferably be 5°C above saturation temperature of the bled steam [14]. This is to prevent tube bundle erosion and maintain a dry wall condition at the de-superheating zone.

Condensing zone

After the de-superheating zone, the saturated steam enters the condensing zone where it releases its latent heat as it goes from vapour to liquid. Condensation occurs ideally at a fixed saturation temperature. This temperature is driven by the pressure in the condensing zone. It may be lower than at the FWH steam inlet because of the pressure drop from the baffles in the de-superheating zone. For mathematical modelling purposes this pressure drop is neglected, as the actual pressure drop cannot be determined without knowing the detail geometry of the heater [16]. The condensing zone covers the largest area of heat transfer area in the heater and hence carries the most heat duty [14].

Sub-cooling zone

In the sub-cooling section (also called the drains cooler), the condensate comes into contact with the feed-water tubes from the inlet side of the HX. The condensed liquid will have some level within the shell side, so parts of the tubes are submerged. Very often a specific cavity is created which is flooded with steam condensate, thus ensuring contact with the feed-water tubes. The sub-cooling is mainly in place so that the saturated liquid, after condensing, does not immediately go into pipeline towards the next heater and end up flashing back to steam due to pressure drop [17].

2.3 Modes of Heat Transfer

2.3.1 Conduction Heat Transfer

The rate of heat transfer in a HX depends partly on the material being used as a barrier between the two streams. If the material has a low conductivity, it will require a large temperature difference to conduct the necessary heat [18]. Heat conduction is a mode of heat transfer, mostly in solid, whereby heat is transferred across the particles of material due to a temperature gradient. The simplest conduction situation is when there is a steady state heat transfer without energy source as shown in Figure 2-13 below.

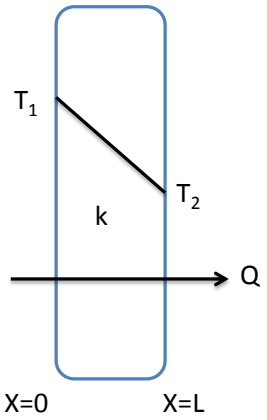

Figure 2-13: One-dimensional conduction through a plane wall.

The ordinary differential equation for heat conduction on a flat plat plate or wall is given below:

$$\frac{d^2T}{dx^2} = 0 \tag{2-1}$$

The boundary conditions for the wall are the temperatures $T=T_1$ at one end, $x=0$, and $T=T_2$ at the other end, $x=L$. The solution for the differential equation with the imposed boundary conditions simplifies to:

$$T = T_1 + (T_2 - T_1)\frac{x}{L} \tag{2-2}$$

And the heat transfer going through the wall according to Fourier's law of conduction [19] is given as:

$$Q = \frac{kA}{L}(T_1 - T_2) \tag{2-3}$$

The idea of conduction can be extended to cylindrical coordinates to get a better understanding of conduction across pipes/tubes, which are of interest when dealing with FWHs. The heat conduction equation in cylindrical coordinates is given as:

$$\frac{1}{r}\frac{d}{dr}r\frac{dT}{dr}=0 \tag{2-4}$$

The general solution, at any radius, to the above equation is given by:

$$Q=-k\left(2\pi rL\right)\left(\frac{dT}{dr}\right) \tag{2-5}$$

Solving and rearranging the above equation for boundary conditions shown in Figure 2-14 gives the heat transfer per unit length as:

$$Q=\frac{-2k\pi r(T_1-T_2)}{\ln\frac{r_2}{r_1}} \tag{2-6}$$

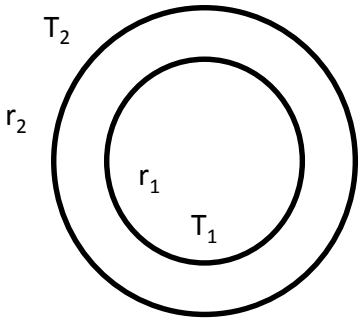

Figure 2-14: Boundary conditions of a typical tube cross-section working as a HX

From equation (2-6) it is evident that the conduction heat transferred depends on the ratio of the outer to the inner radius of the pipe. So, for a given material of known conductivity, the ratio of the radii drives the amount of heat energy the pipe HX can transfer. A larger radius ratio (thick pipe) decreases the ability of the pipe to transfer heat.

2.3.2 Convection Heat Transfer

Convective heat transfer can be thought of as a mode of heat transfer where heat is transferred from/to a solid surface by the motion of fluids adjacent to the solid surface [20]. In most cases, as in the FWH, there are two fluids on either sides of the surface exchanging heat with a solid interface. The heat exchange depends on the boundary conditions at the surface exposed to the flowing fluids, as well as the fluid flow structure. It combines the effects of inter-fluid conduction and fluid motion, and generally the faster the fluid motion the greater the convective heat transfer [20].

Three important dimensionless quantities are used in convective heat transfer modelling. The first is the Reynolds number (*Re*) which relates the inertial forces of the fluid to the forces due to the viscosity of the same fluid. The Prandtl (*Pr*) number is the ratio of the momentum diffusivity to thermal diffusivity, and mainly depends on the fluid characteristics. It compares how quickly heat diffuses compared to its velocity or momentum [20].

The Nusselt number (*Nu*) for internal flow is the ratio of the convective conductance to the amount of pure molecular thermal conductance [11]. It can also be expressed as a function of Prandtl and Reynolds number.

The relationship between *Nu*, *Re* and *Pr* depends on the flow conditions during heat transfer.

$$Nu = f(\mathrm{Pr},\mathrm{Re}) = \frac{h_c L}{k} \tag{2-7}$$

Where h_c is the HTC, which is the proportionality between the actual heat flux and the driving factor which is the temperature difference. In the following sub-sections, it will be shown as to how the above mentioned dimensionless quantities relate for different scenarios in heat exchanging.

Turbulent flow inside a pipe:

For a pure liquid fluid in a pipe in the turbulent flow regime, where $\mathrm{Re} \geq 4000$, the heat transfer is given by a Dittus-Boelter correlation [21] [10], given as:

$$Nu = 0.023\mathrm{Re}^{0.8}\,\mathrm{Pr}^{n} \tag{2-8}$$

Where the exponent is given as:

n = 0.4 for heating,

n = 0.3 for cooling.

The correlation by Colburn and Kern is also widely used [22]. Colburn and Sieder Taite use the same formulation as in the Dittus-Boelter. However, they remove the dependability of cooling or heating by taking into account the effect of viscosity difference of the bulk fluid and that at the boundary layer, near the wall [21]. The Kern formulation tries to incorporate the fact that the HTC should be linear in the intermediate region in his formulation [10].

Laminar flow inside a finite tube length:

When the fluid is flowing in the tubes and the flow is a fully developed laminar, i.e. $\mathrm{Re} \leq 2300$, Seider and Tate [22] give a correlation for a finite length, *L*, of tube as:

$$Nu = \frac{hd}{k} = 1.86\left(\mathrm{Re}\,\mathrm{Pr}\left(\frac{d}{L}\right)\right)^{\frac{1}{3}}\left(\frac{\mu_w}{\mu_b}\right)^{0.14} \tag{2-9}$$

The limitation to this approach is for tubes with a diameter to length ration which is relatively large, which results in the HTC that approaches zero. The Hausen correlation gives a more conservative approximation to the average HTC for laminar flow where the wall temperature is considerably constant [21], and is given as:

$$Nu = \frac{hd}{k} = 3.66 + \frac{0.668\,\mathrm{Re}\,\mathrm{Pr}\left(\frac{d}{L}\right)}{1 + 0.4\left[\mathrm{Re}\,\mathrm{Pr}\left(\frac{d}{L}\right)\right]^{\frac{2}{3}}} \tag{2-10}$$

Transition regime flow inside a finite tube length

In the transition regime between laminar and turbulent flow, the Hausen correlation [21] is the most widely accepted correlation to estimate the HTC and is given as follows:

$$Nu = \frac{hd}{k} = 0.116\left(\mathrm{Re}^{\frac{2}{3}} - 125\right)\mathrm{Pr}^{\frac{1}{3}}\left(\frac{\mu_w}{\mu_b}\right)^{0{,}14}\left(1 + \left(\frac{d}{L}\right)^{\frac{2}{3}}\right) \tag{2-11}$$

Another alternative to estimate the HTC in the transition regime is to use linear interpolation between the laminar and turbulent formulations at the actual Reynolds number.

Condensation on the outside of a horizontal tube:

For vapour condensing outside a pipe of diameter D_o, the HTC is given by Kern [23] as:

$$h_0 = a\left[\frac{k^3\,\mathrm{g}(v_g - v_f)\Delta H`_{fg}}{\mu_f D_o (T_f - T_w) v_f{}^2 v_g}\right]^{\frac{1}{4}} \tag{2-12}$$

Where a is a fitness correlations, and

a = 0.725 for horizontal pipes

a = 0.943 for vertical pipes

The subscript *f* indicates the fluid/liquid while *g* indicates gaseous/vapour form for properties. To account for the non-linear temperature profile across the length of a pipe, the available latent heat, $\Delta H'_{fg}$ is used and given as:

$$\Delta H`_{fg} = h_{fg} + 0.68C_p(T_f - T_w) \tag{2-13}$$

And the average film temperature, T_f, is given as a function of the wall temperature and the bulk fluid temperature as seen below:

$$T_f = 0.375(T_b - T_w) + T_w \tag{2-14}$$

In order to fully understand condensation on the outside of pipes in FWHs, the concept of condensation over a single pipe is extended to condensation on tube bundles. There are considerations that have to be looked at when modelling condensation on a bundle of tubes. Firstly, the way in which the condensate flows from the top tube to the bottom ones has to be taken into account. In some cases this happens to the extent that some of the bottom tubes are sub-cooling and not condensing in FWHs. Figure 2-15 shows the different modes of condensing to illustrate the point. Secondly, if the influences of vapour shear are taken into consideration then McNaught correlation [24] is the best available to predict the HTC for turbulent flow over tube bundle.

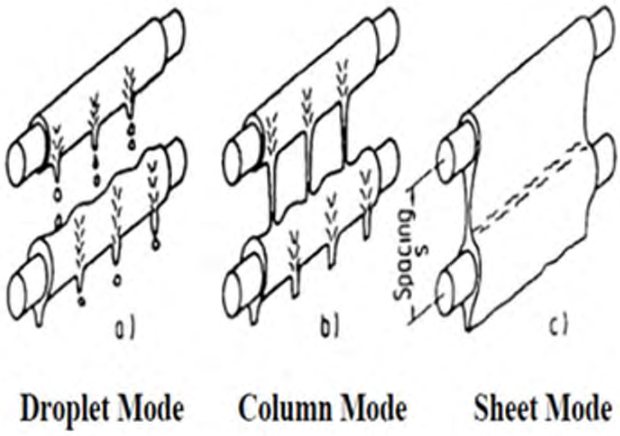

Figure 2-15: Condensing modes for condensation over a tube bundle [15].

The effects of this are analysed in [25], but if this effects are ignored then the mean heat transfer for *N* tubes is given as:

$$h_c = 0.728\left(\frac{g(Nd_o\mathrm{k})^3(\rho_f - \rho_g)\Delta H`_{fg}}{(T_f - T_w)\mathrm{v}_f}\right)^{\frac{1}{4}} \tag{2-15}$$

The heat transfer on a single N-th row tube is approximated by different authors, but was shown in [25] that most of the formulations were over conservative and resulted in condensers that were consistently over-surfaced. To improve this, a new correlation was given in [26] for the N-th tube row in a bundle h_{CN}:

$$\frac{h_{CN}}{h_o} = N^{-\frac{1}{6}} \tag{2-16}$$

Where, h_o is the HTC for the top tube as shown above in equation(2-12).

Flow across a tube bank – single phase on the shell side:

The HTC on the shell side of the de-superheating zone is often increased by employment of baffles as already mentioned, and the effects of baffles are illustrated in Figure 2-16. This is mainly because the baffles disturb flow and create turbulence in the process. Also, the baffles can be seen to direct flow to be partly cross flow which result in a higher heat transfer than flow parallel to the pipe. McAdams [27] gives a correlation where the baffles are not considered and flow is turbulent. The effective diameter for flow on the shell is used in the analysis, and the HTC is given as follows:

$$h_o = 0.36\frac{k}{D_e}\mathrm{Re}^{0.55}\mathrm{Pr}^{\frac{1}{3}}\left(\frac{\mu_b}{\mu_w}\right)^{0.14} \tag{2-17}$$

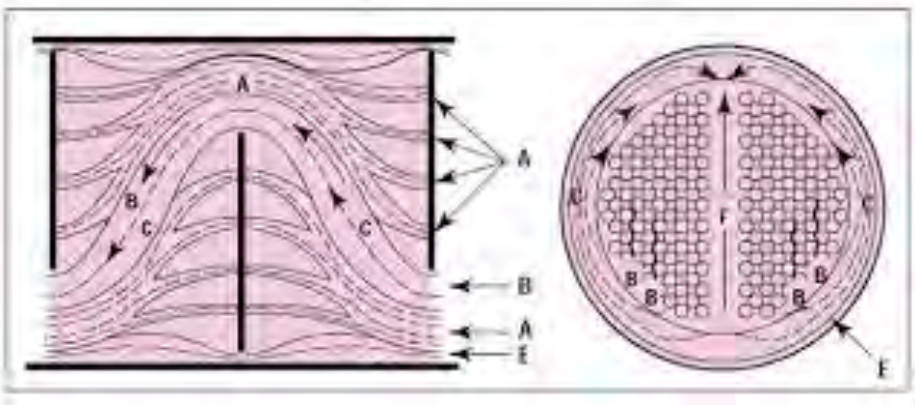

Figure 2-16: Flow disturbance due to baffles and the different streams created due to baffles [28].

The Kern correlation for HTC on shell side is the most simplistic approach as it does not take into consideration the different flows indicated on Figure 2-16. It only takes the main flow, shown as B, and uses it as though it was a simple cross flow over tubes to determine the HTC [27]. Bell-Delaware correlation, on the other hand, takes into consideration the effects of the different flows and geometry and other different factors as outlined by Thome [28]. The most widely used correlation is the Taborek correlation [27] [28], and Flownex also applies it for flows over tube bundles. It is applicable for turbulent flows and the Reynolds number is based the outer diameter of the tubes. The correlation uses the cross flow average velocity and is given as follows:

$$h_o = 0.2\frac{k}{d_o}\mathrm{Re}^{0.6}\mathrm{Pr}^{0.4} \tag{2-18}$$

Summary

This sub-section gave a summary of the different ways or correlations for determining HTCs for different flow regimes on both the tube and shell side of a HX. It is worth noting that none of the correlations quoted above claim to be 100% correct, and research is still ongoing to produce more accurate correlations.

2.3.3 HX Analysis

For a finite section of pipe (see Figure 2-17 below) working as a HX between a hot and cold stream of fluids, the heat flow rate from the hot fluid can be quantified in three different ways as described in the next sub-sections.

In all the explanations and equations, reference to all quantities is made to Figure 2-17.

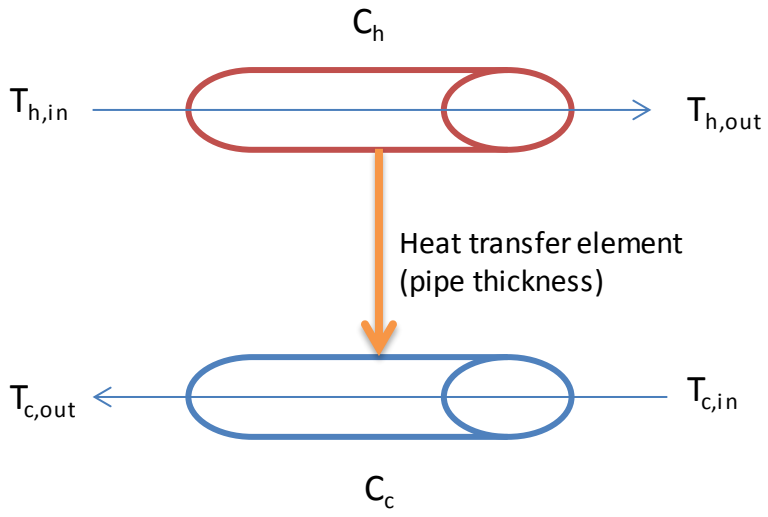

Figure 2-17: Small section of a counter-flow HX.

Fundamental Approach

The heat rate can then be quantified as:

$$Q = UA(T_{h,av} - T_{c,av}) \tag{2-19}$$

Where, U is the overall HTC of a HX and A is the heat transfer area. The combination of U and A is defined as the inverse of the total resistance between the two fluid streams [29]. This method only allows for small changes in temperature from inlet to the outlet of the streams such that the average temperature is a good approximation of the temperature difference between the two streams. Hussaini and Zubair [14] use this approach in the area allocation method for FWH design. Here the pipe was discretised into small sections such that the inlet temperatures of each section

can be used to calculate the local heat transfer. The conservation of energy for each stream is used to determine the inlet conditions for the next pipe segment.

The overall HTC is the total resistance of the two fluids and the exchanger element against heat flow from the hot to the cold stream and is given as:

$$UA_{ave} = \left[\frac{1}{h_i A_i} + \frac{r_i \ln\left(\frac{r_o}{r_i}\right)}{kA_{ave}} + \frac{1}{h_o A_o} \right]^{-1} \tag{2-20}$$

Where, the inner and outer convective HTCs are shown with the subscript *i* and *o* respectively, as well as the inner and outer radius of exchanging tube with conductivity, *k*. The overall HTC comes from the fact that the energy lost from the hot stream is the heat energy transferred across the HX into the cold stream.

The energy conservation equations are presented with the aid of Figure 2-18.

$$Q = UA_{ave}(T_h - T_c) = h_c A_i (T_{wc} - T_c) = \frac{kA_{ave}}{L}(T_{wh} - T_{wc}) = h_h A_o (T_h - T_{wh}) \tag{2-21}$$

The three above equalities are combined to give:

$$T_h - T_c = Q\left[\frac{1}{h_c A_i} + \frac{1}{\left(\frac{kA_{ave}}{L}\right)} + \frac{1}{h_h A_o} \right] \tag{2-22}$$

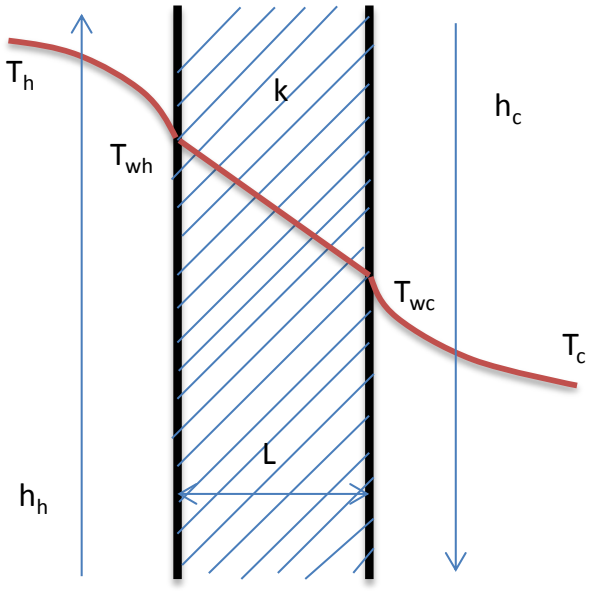

Figure 2-18: One-dimensional cross-section of a HX.

Log Mean Temperature Difference method (LMTD)

The Log Mean Temperature Difference (LMTD) method is developed from the integral solution of equation (2-19) where the tube length is infinitesimal. The LMTD assumes that the fluid properties such as the heat capacity remain constant and is either pure counter-flow or parallel-flow. The LMTD gives an exact solution of a finite size HX.

The heat transfer can be written as:

$$Q = UA(\Delta T_{LMTD}) \tag{2-23}$$

With

$$\Delta T_{LMTD} = \frac{\Delta T_1 - \Delta T_2}{\ln\left(\frac{\Delta T_1}{\Delta T_2}\right)} \tag{2-24}$$

ΔT_1 and ΔT_2 are the temperature differences of the streams on side 1 and side 2. The LMTD method requires that all the inlet and outlet temperatures of a HX be known in order to quantify the heat rate across it.

It must be noted that an adjustment factor *Z* is required to the LMTD for other configurations like cross-flow, or multiple passes.

Effectiveness-Number of Transfer Units (NTU) formulation

The effectiveness-NTU method is usually used to calculate the heat rates across the HX in situations where only the inlet conditions are known.

NTU is defined as the number of transfer units, and can be thought of as the capability of a HX to transfer heat. It is the ratio of the overall thermal conductance to the smaller of the heat capacities (C_{min}), one with least capability of absorbing or releasing the available heat energy [30] [31]. The heat capacity is the product of the fluid mass flow, and its specific heat.

$$NTU = \frac{UA}{C_{\min}} \tag{2-25}$$

The heat transfer in a HX reaches the maximum value when either one of two scenarios happen. Firstly, whenever the cold fluid is heated up to get to the inlet temperature of the hot fluid and the cold fluid cannot gain anymore temperature. Secondly, when the hot fluid is cooled to go to the same temperature as that of the cold fluid at its inlet and cannot be cooled any further [32]. These

two limiting factors can never be reached at the same time unless the two fluids have the same heat capacities. So the smaller of the two heat capacities limits the amount of heat transfer it absorbs from the hot side or can give to the cold side. So for any HX, the maximum heat transfer that can be exchanged is given to be:

$$Q_{\max} = C_{\min}\left(T_{h,in} - T_{c,in}\right) \tag{2-26}$$

The effectiveness of the HX is the ratio of the actual amount of heat exchange to the maximum that can be achieved shown in equation(2-26), and thus is a measure of how close the HX is to the ideal case. The derivations of the different effectiveness for various flows are shown in [32] and the results are only quoted in this report. Only the effectiveness of the parallel and counter flow HXs are presented with their accompanying graphical illustration of how the effectiveness changes with NTU for different fluids capacity ratios.

The effectiveness for counter flow is given as:

$$\varepsilon = \frac{1 - e^{-NTU(1-C_r)}}{1 - C_r e^{-NTU(1-C_r)}} \tag{2-27}$$

Where, C_r is the ratio of the minimum to the maximum heat capacities of the two streams. Figure 2-19 shows how the effectiveness changes with the NTU for the different fluids capacity ratios for a counter flow HX. As NTU increases, the HX is more effective if the combined heat capacity mass flow rate of one stream is very low compared to the other.

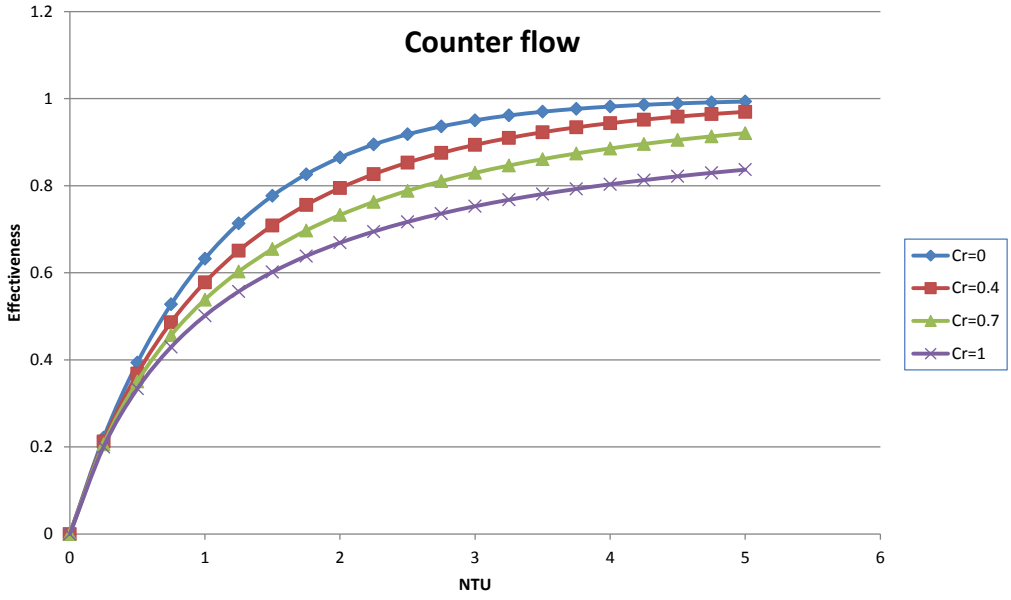

Figure 2-19: Counter flow HX effectiveness variation with NTU for different heat capacity ratios.

The effectiveness for parallel flow is given as:

$$\varepsilon = \frac{1 - e^{-NTU(1+C_r)}}{1 + C_r} \tag{2-28}$$

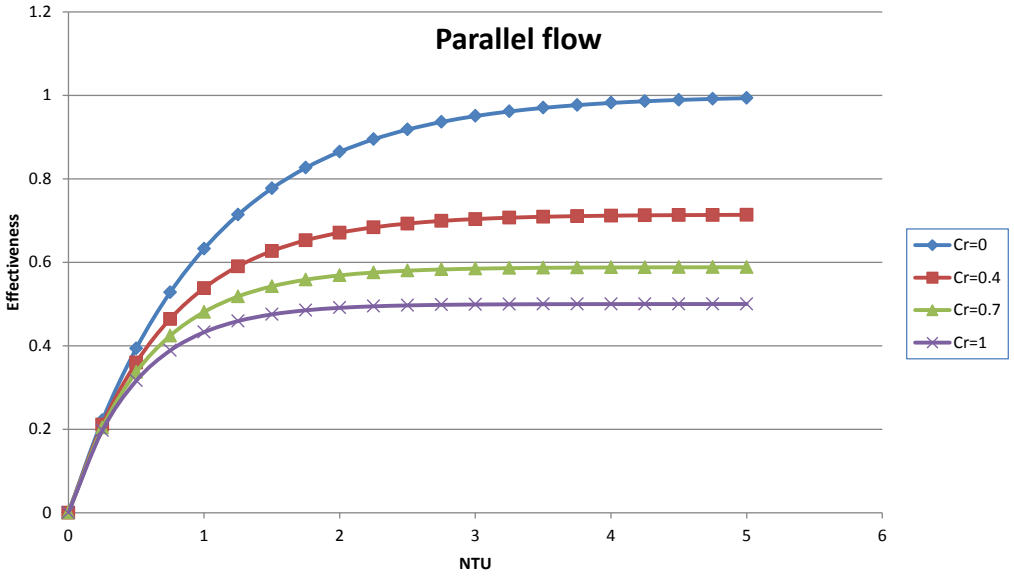

Figure 2-20: Parallel flow HX effectiveness variation with NTU for different heat capacity ratios.

The effectiveness of a parallel HX is strongly driven by the ratio of the fluids capacities, and as seen from Figure 2-20 for a HX with fluids that have same heat capacities the effectiveness is limited to 0.5. Also, comparing the effectiveness of the parallel and counter flow HXs for same fluids it is evident that for the same NTU the effectiveness in the counter-flow is higher than that in parallel flow [32].

In the condition where C_r=0, both flow configurations produce the same result. This is the special case where the maximum heat capacity is infinitely high, or otherwise stated, the "maximum fluid" does not experience any temperature change. This is called a single-stream HX, and represents the condition where one of the fluids transfers heat without temperature change, i.e. latent heat exchange such as condensation [32].

The flow configuration inside the condensing zone of the FWH therefore resembles that of a single-stream HX, while the de-superheating and sub-cooling zones are a hybrid mix of parallel and cross-flow, depending upon the internal baffle arrangement.

2.4 Transient Heat Transfer

The preceding theory only considered steady state heat transfer. However, the overall goal is to develop a transient model of the complete power plant. It is therefore necessary to consider the situations when the fluid temperatures or mass flow rates change with time inside the HX.

2.4.1 Temperature Responses

Whenever the temperatures are changing with time within any solid object, the mode of thermal energy flow is termed transient conduction or non-steady state conduction. Transients generally happen if the body is at equilibrium (energy balance) and suddenly a rapid temperature change, increase or decrease is applied. This can be done by imposing the temperature change on either the core of the object or on the surface. When this change is imposed, the body will react and try to go to its new equilibrium and during this process the body is said to be in transient heat conduction process.

There are different ways of analysing the heat transfer during a transient as reported by different authors in literature. The rate of energy accumulation and hence temperature change was investigated by Lam and Naterer [33] where a control volume of length, dx, was considered. It is shown that the transient change in wall temperature is a balance of the convective heat transfer from the hot stream and convective heat transfer to the cold stream, and can be expressed as:

$$m_w c_{pw} \frac{\partial}{\partial t} T_w = h_h(x) A (T_h - T_w) - h_c(x) A (T_w - T_c) \tag{2-29}$$

Abdelghani-Idiris et.al [34] presents a study of the response of a counter-flow double pipe HX which was carried out to predict temperature responses to step changes in mass flow rates. Their theoretical results were validated against experimental data and the two were found to coincide.

Tan and Spinner [35] investigated the effects/problems of assuming that the wall separating the two fluids does not have resistance, and the dependability of HTC on the fluids velocities. Two models were compared: one with constant HTC and the other with HTC that varies with the fluids velocities. It was concluded from the study that there is significant difference in transient responses of a HX when the velocity is changed for the two models. Also, assuming wall resistance to be negligible only predicts transient responses close to expected if the HTCs are constant. But if the HTCs vary with velocity, the model led to a significant error in transient behaviour [35].

Yin and Yensen [36] looked at the response of the HX with one stream not changing temperature (condensing) when the temperature or mass flow rate is stepped up or down. The responses of the single-phase and wall temperature distribution were investigated using the integral method from knowing the combination of initial and final temperature distributions. The results were compared against numerical simulation results over an operating range and good agreement was reported. Different combinations of HX conditions were tested and results are shown in Figure 2-21.

The dimensionless quantities N_1, N_2 and N_3 are the ratios of the heat capacities of the HX wall to the single phase stream, convective heat transfer of the condensing stream to the heat capacity of single phase and the convective heat transfer of the single phase stream to its heat capacity respectively. The NTU and temperature profiles are analytically formulated based on this quantities and working fluids temperatures only. For higher NTU value, the analytical solution overestimates the temperature at the exit of the single phase. This is a direct consequence of the increase in the ability of the single phase stream to absorb heat by convection when the other dimensionless quantities are kept constant. For the numerical solutions, DYMOLA (Dynamic Modelling Laboratory) was used to simulate the conditions.

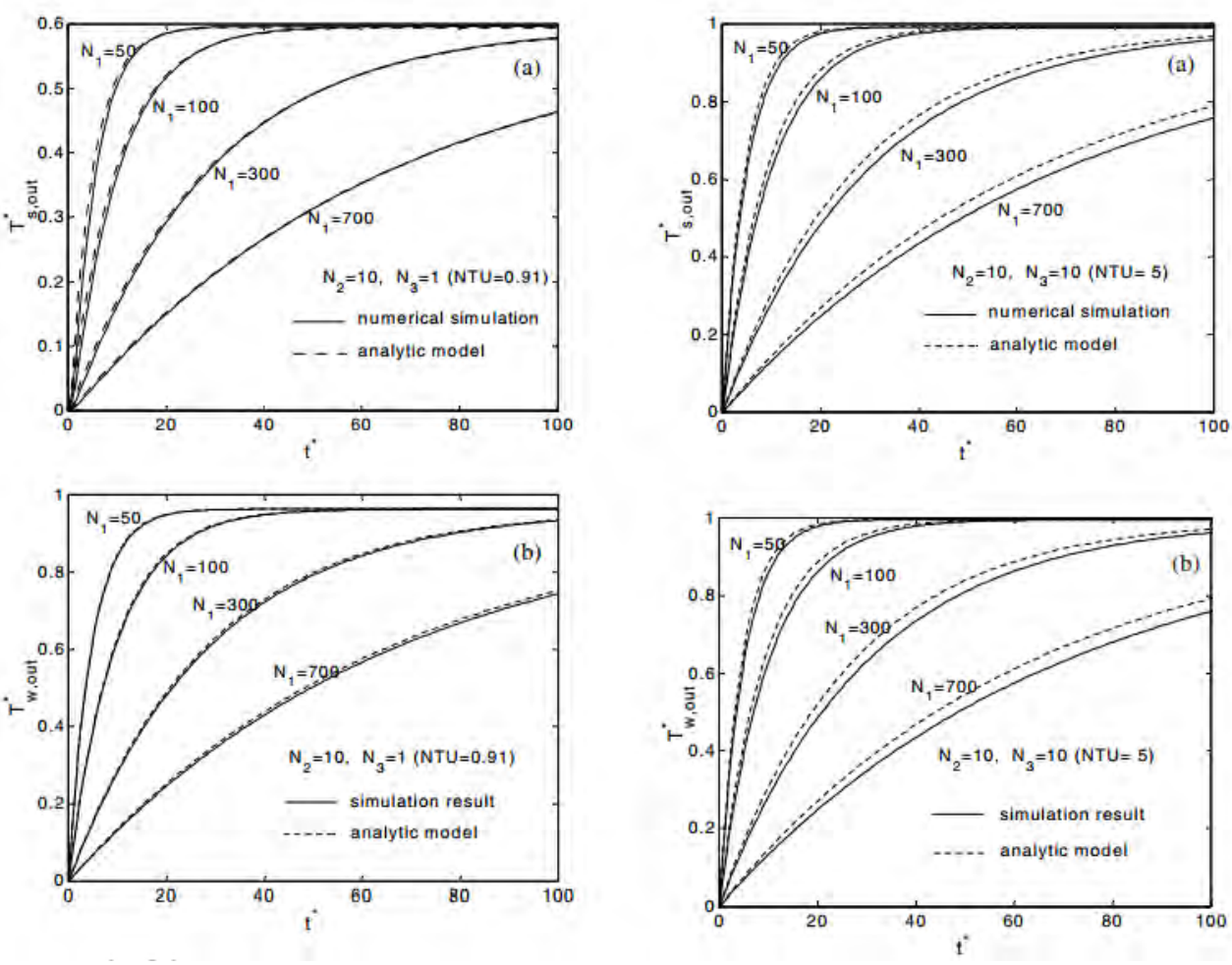

Figure 2-21: HX Exit and wall transient temperature for different NTU [36].

There are several ways of acquiring the behaviour and temperature changes within the object as the transient conduction takes place. In this study only the lumped system model and the analytical method that makes use of the Bessel function will be looked at.

Lumped System

In transient conduction of a small object/body, the heat transferred into that object during a finite time *dt* will be the increase in energy of that body for that same amount of time [26]. In essence, this is the energy conservation for that body. For the case where the body experiences constant convection all around it, the heat is given as:

$$Q_{in} = hA(T_f - T) \tag{2-30}$$

And,

$$Q_{abs} = mC_p \frac{dT}{dt} \tag{2-31}$$

But because the convective heat on the surface is the same heat that is being absorbed by the object, then the two quantities can be equated and re-arranged to give the equation below:

$$hA(T_f - T)dt = mC_p dT \tag{2-32}$$

Where, $dT = d(T - T_f)$ and, $m = \rho V$.

Substituting the above into equation (2-32) yields the following:

$$\frac{d(T - T_f)}{(T - T_f)} = -\frac{hA}{\rho V C_p} dt \tag{2-33}$$

And integrating both sides gives

$$\ln \frac{T(t) - T_f}{T_i - T_f} = -\frac{hA}{\rho V C_p} t \tag{2-34}$$

Taking the exponential on both sides of the equation gives:

$$\frac{T(t) - T_f}{T_i - T_f} = e^{-bt} \tag{2-35}$$

Where,

$$b = \frac{hA}{\rho V c_p} \tag{2-36}$$

This equation enables one to determine the temperature *T(t)* of a body at any given time during a transient scenario. Or even more strongly, it gives a feel of how long it requires for the body to come to equilibrium or to a specified temperature *T(t)* after a transient has been imposed. All parameters used in the above formulation are explained in Figure 2-22.

It must be stressed that the preceding theory is valid for a lumped system, where it is assumed that the complete body mass receives the heat uniformly through its volume. Later on this will be expanded to take the thermal conductivity of the mass into account.

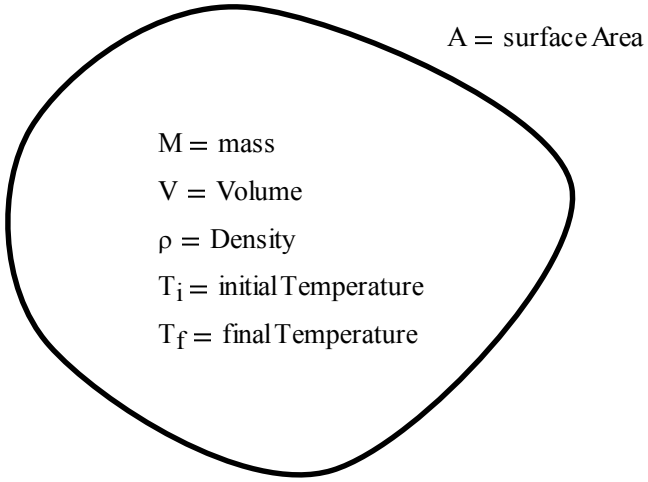

Figure 2-22: Geometry and parameters involved in the lumped system analysis.

The parameter *b* in equation (2-36) has units *1/s* and its reciprocal is the time constant, τ. It is proportional to the surface area, *A*, but inversely proportional the mass and specific heat of the body. Hence it is common for large bodies to take longer when cooling or heating. The effect of *b* on the temperature response is investigated and the graph in Figure 2-23 shows temperature profiles for different values of *b*.

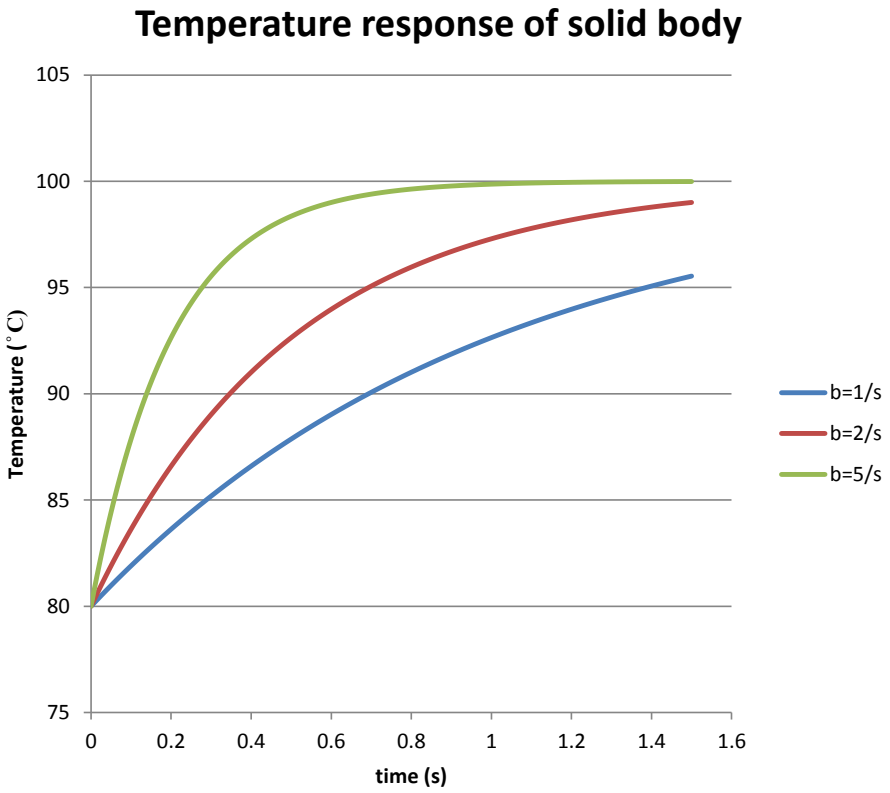

Figure 2-23: Temperature profile or response of lumped system for different b values.

From Figure 2-23 it can be seen that the body temperature approaches the final temperature exponentially as predicted by other authors [33] [36]. A larger value of *b* indicates that the body reaches the final temperature in a shorter time and the rate of decay is higher as also suggested by Talukdar [32]. The lumped analysis neglects the spatial variation of the temperature and only considers how it changes with time at a single specified point [37]. This means that the lumped analysis cannot predict the temperature profile at different locations inside the body.

The validity of the lumped analysis is measured by a constant termed the Biot (*Bi*) number. The Biot number is the ratio of the convective resistance at the surface of the body over the conductive resistance within the body. The Biot number is given as:

$$Bi = \frac{hL_c}{k} \tag{2-37}$$

Where L_c is the characteristics length of the body and is given as the ratio of the volume to the surface area:

$$L_c = \frac{V}{A} \tag{2-38}$$

The lumped analysis is accurate for *Bi* < 0.1 which is when the temperature field differs from the actual temperature by less than 5% [37]. The Biot number is seen to have the same effect in two phase as in single phase HXs where the analysis was done with the convection HTC changing along the exchanger length [33] [38]. So, for the Biot number to be less than 0.1, it means that the internal resistance is less than 10% to the external resistance and for the ambient external environment the internal thermal resistance has to be small. Small thermal resistance implies a very large thermal conductivity or small characteristic length and thus guarantees a uniform temperature within the solid [39].

Typical pipe/tube geometry is shown in Figure 2-24 below to demonstrate how the critical length is found for tubes.

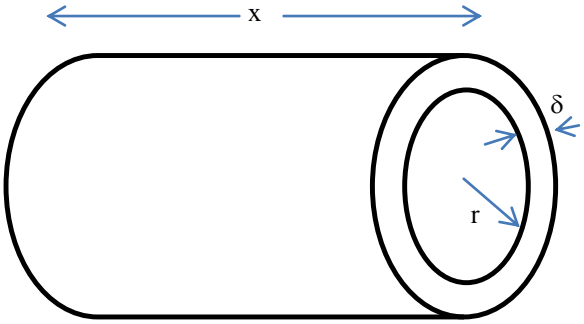

Figure 2-24: Dimensions of a tube working as a HX.

The approximate characteristic length of such a tube is given as:

$$L_c = \frac{V}{A} \simeq \frac{2\pi rx\delta}{2\pi rx} = \delta \tag{2-39}$$

Where, δ is the thickness of the tube. So, the thicker the pipe the more accuracy is lost in predicting the temperature profile when using the lumped system method [26]. In Flownex SE, which also applies the lumped analysis in its solution, this is overcome by dividing the thickness of the pipe into a number of sections and working on each thin strip as if it was an independent pipe. The characteristic length then becomes:

$$L_c = \frac{\delta}{n-1} \tag{2-40}$$

And, *n* is the number of temperature nodes, which is one more than the number of increments.

The effect of changing the critical length was investigated on Flownex SE by changing the number of increments on the thickness of the pipe. Figure 2-25 shows a schematic of the temperature distribution within conducting metal of a HX with different number of nodes/discretization.

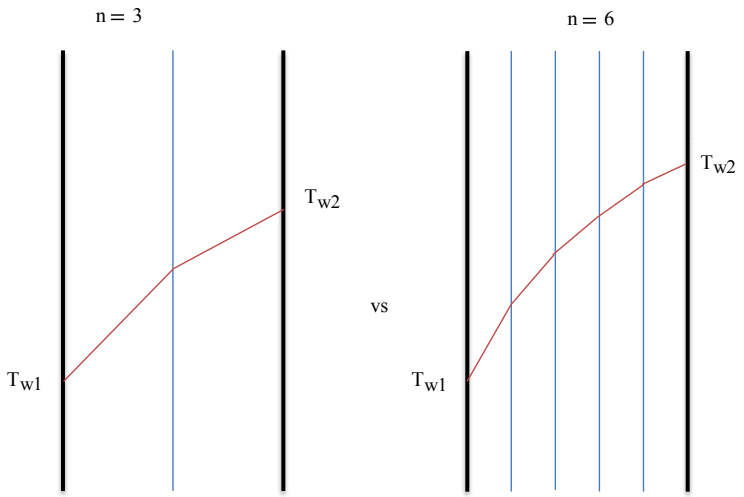

Figure 2-25: Instantaneous Temperature Field within HE with n=3 versus n=6.

Analytical Solution (using the Bessel Function)

The aim of this section is to show how the temperature variation as a function of time and/or position within an infinitely long solid cylinder can be determined analytically. The cylinder has an initial temperature T_i on the inside and T_2 on the outside. At an initial time, t_0=0s the temperature on the inside of the cylinder is immediately changed to T_1. The aim is to then solve for the temperature profiles at different times and radii of the cylinder based on the given boundary conditions. To solve this problem, the non-dimensional variables are described below:

$$T = \frac{T(t) - T_1}{T_i - T_1} \tag{2-41}$$

$$r = \frac{r_{actual}}{R}$$

$$\tau = \frac{t\alpha}{R^2}$$

The initial heat conduction for this case is outlined below with the boundary conditions:

$$\frac{d}{d\tau}T = \frac{1}{r}\frac{d}{dr}\left[r\frac{d}{dr}T \right] \tag{2-42}$$

The following boundary conditions are set for the problem:

$$\left.\frac{dT}{dx}\right|_0 = 0$$

$$T\left(x = L, \tau\right) = T_2$$

$$T(x,\tau=0)=T_1$$

The solution to this boundary value problem is obtained as described in [30] using the Bessel functions, producing the temperature profile as:

$$T(r,\tau)=2\sum_{n=1}^{\infty}\frac{J_0(\lambda_n r)e^{-(\lambda_n)^2 t}}{\lambda_n J_1(\lambda_n)} \tag{2-43}$$

Where λ_n and J_0 are the Eigenvalues and Bessel function of the first kind respectively. The solution above is for the dimensionless temperature field, and knowing the initial and imposed temperatures, the change in temperature with time can then be determined.

The following Figure 2-26 and Figure 2-27 are the solution of the temperature profiles as a function of radius and time respectively. For both diagrams, the wall is initially at a temperature of 80 ˚C on both sides and the outer wall temperature is suddenly raised to 180 ˚C to investigate temperature with time and position within material.

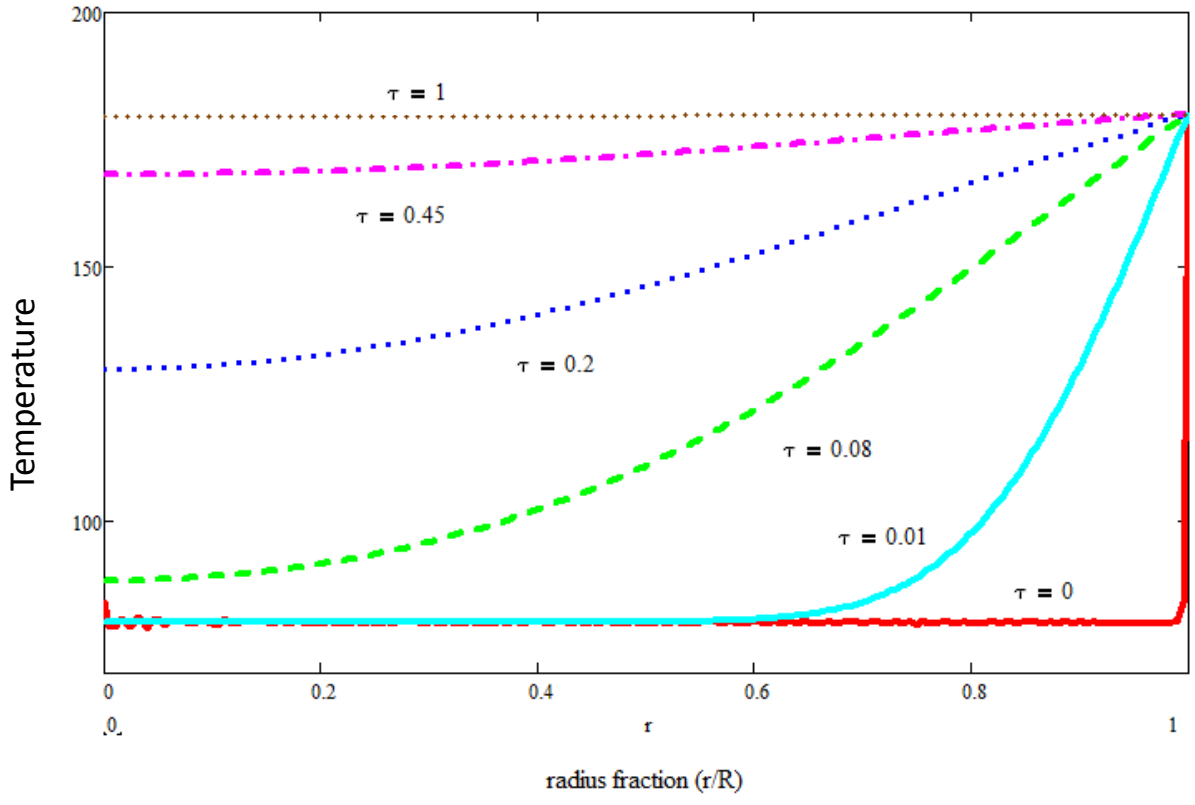

Figure 2-26: Temperature profile as a function of radius with increasing time (Analytical).

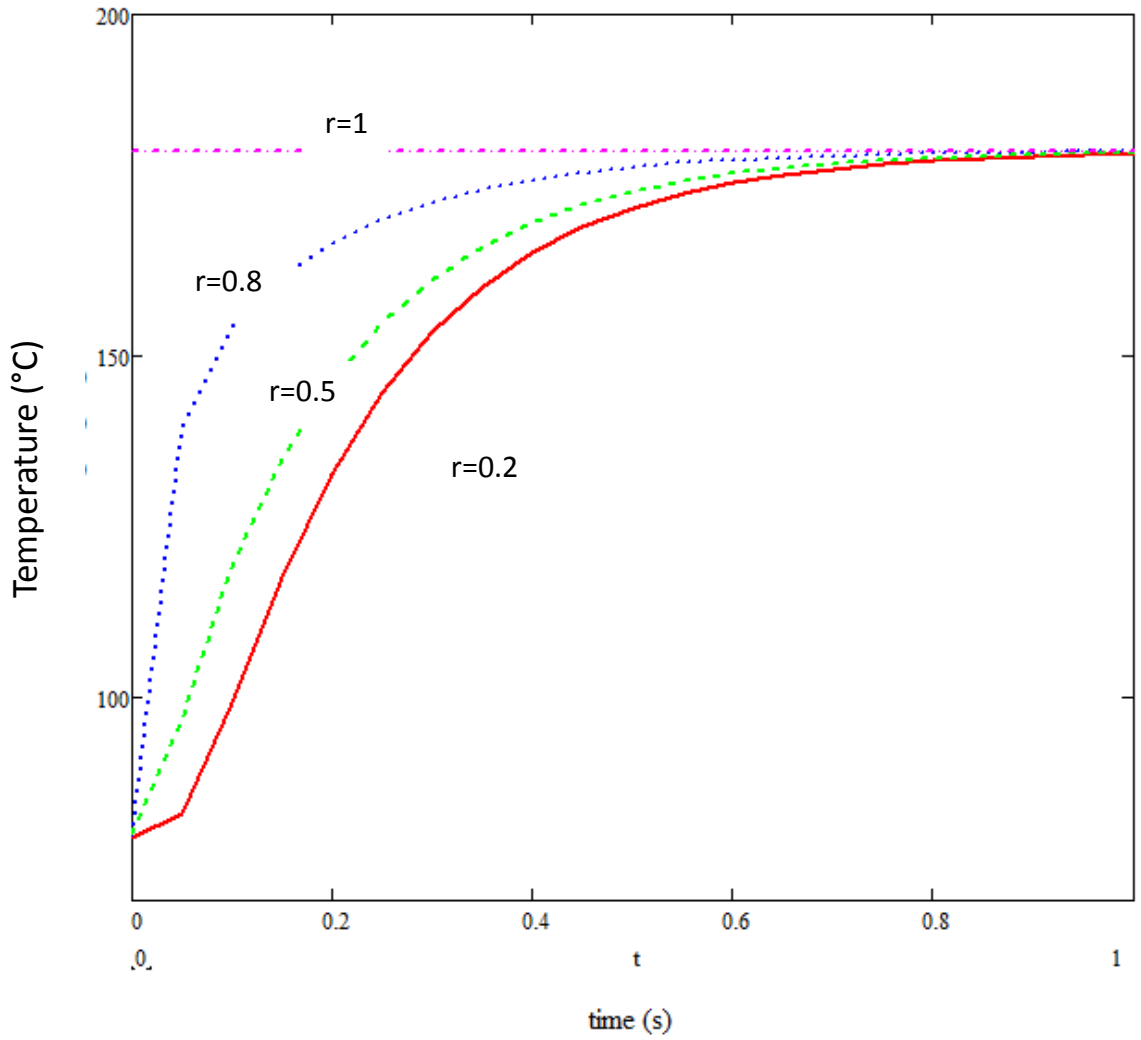

Figure 2-27: Temperature profile as a function of time with increasing radii (Analytical).

Figure 2-27 shows the temperature profiles as time changes for different radii. It is seen that the temperature gradient at a certain radius takes the same form as the one predicted by the lumped system method in Figure 2-23. The Flownex solver uses the lumped system to solve for temperature profiles across HXs. Flownex model therefore simulates a good approximate of temperature profile for criteria mentioned for lumped systems discussed under the "Lumped system" section.

Gwebu [40] investigated the effects of discretization on the temperature profile for an infinitely long pipe with convection on both the inside and outside. Figure 2-28 shows the results from the Flownex model with the tube discretized radially into 3 sections, 4 nodes. Even though the difference in Flownex and analytical results could be due to the area scheme used, there is also a contribution to the error owing to the fact that even for $Bi < 0.1$ there is still an error of less than 5% as indicated by Jiji [37]. And because the tubes of the FWH are reasonably thin, yielding a low

Biot number, the number of increments can be kept as low as possible without compromising much accuracy.

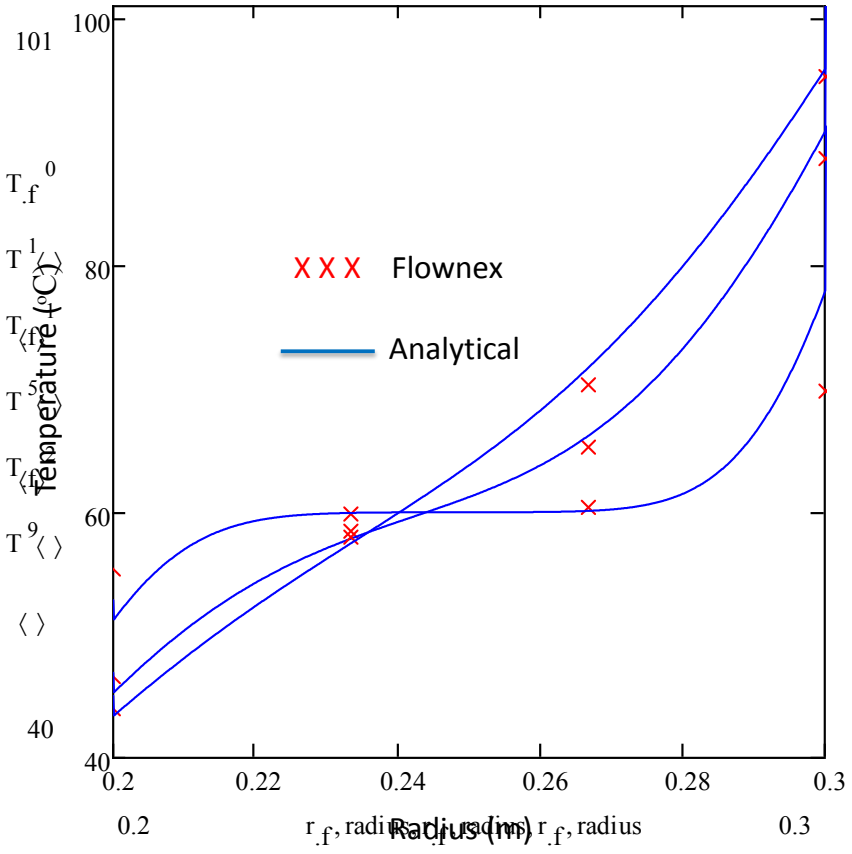

Figure 2-28: Comparison between Flownex and analytical results for an infinitely long tube subjected to convection at the boundaries to induce transients where 4 nodes and time step of 0.1s were used in Flownex [40].

2.4.2 Numerical Error

In steady state the amount of heat lost by the hot stream is the same as the heat energy conducted through the tube wall, and the amount gained by the cold stream.

$$Q_h = Q_{cond} = Q_c \tag{2-44}$$

This is valid since the temperature gradient through the pipe wall does not change. During a transient event, the temperature profiles change as was demonstrated in the previous sections. The change in temperature profile results in some energy being absorbed/released by the pipe wall in such a manner that the above steady state relationship is not valid any more.

Figure 2-29 shows a transient simulated in Flownex for a typical FWH pipe in the sub-cooler section. It is seen that the heat transfer on both streams is the same before the transient occurs at 40s. After some time in the transient the heat transfer of the two streams come back together,

but at a higher value, and it can be said that a new steady state condition was reached. During the time in-between the steady state conditions, there is a marked difference between the two stream's heat transfers. The difference between the two is the amount of heat being absorbed/released by the wall.

$$Q_{absorbed} = Q_h - Q_c \tag{2-45}$$

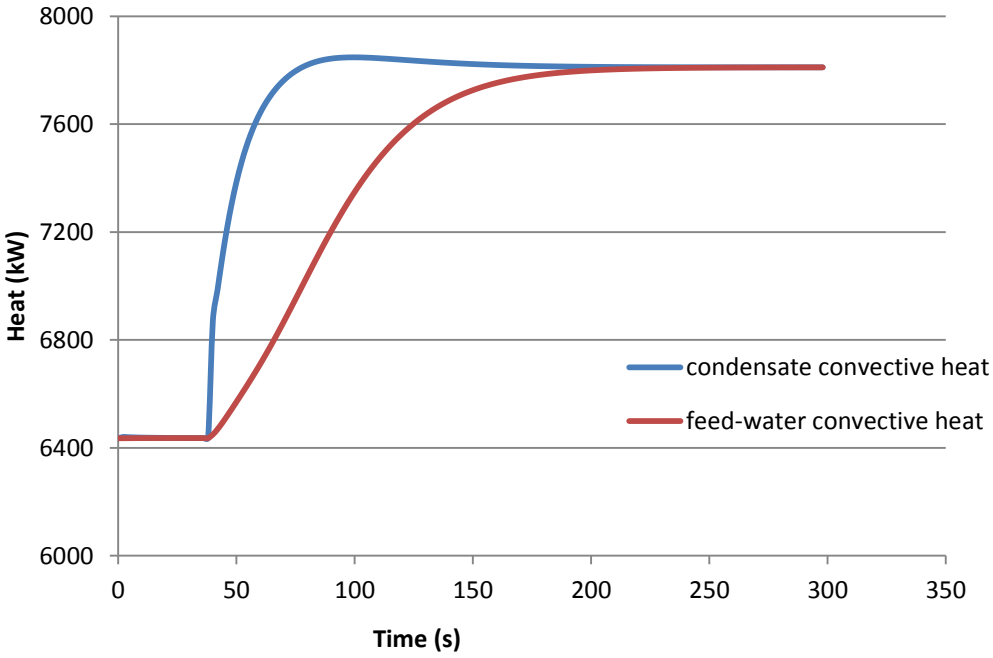

Figure 2-29: Heat transfer from the condensate to the feed-water in a typical sub-cooling zone during a simulated transient.

If the exact temperature profile is known inside the pipe material, one can integrate through the wall thickness and thus calculate the heat absorbed, and this should then match the difference observed between the two fluids. However, as was shown in the previous section, the temperature profile is not accurately calculated in Flownex with only a few nodes through the wall thickness. There is thus a heat flow error between what is actually absorbed and what the difference is between the two streams.

To gain an understanding of this numerical error, a typical FWH sub-cooling section was modelled. The feed-water stream consisted of 100 tubes in parallel of diameter 25mm and wall thickness of 2.4 mm. The mass flow of this stream was 100kg/s, and entered at 100 bar and 80 ℃. The condensate stream was a single pipe of diameter 0.3m carrying water flowing at 20kg/s, entering as a saturated liquid at 180 ℃. After 40s of steady state operation, the condensate temperature was changed to 200 ℃, saturated, and energy content of the HX observed.

The pipe wall was discretized in the direction of heat flow as shown in Figure 2-30, and analysed for different number of nodes. The heat absorbed at each time step was calculated by summing the change in energy of each element of the discretized pipe wall, as shown below, using the average element temperature.

$$Q_{absorbed} = \sum_{1}^{i} m_i C \frac{T_i^t - T_i^{t+\Delta t}}{\Delta t} \quad (2\text{-}46)$$

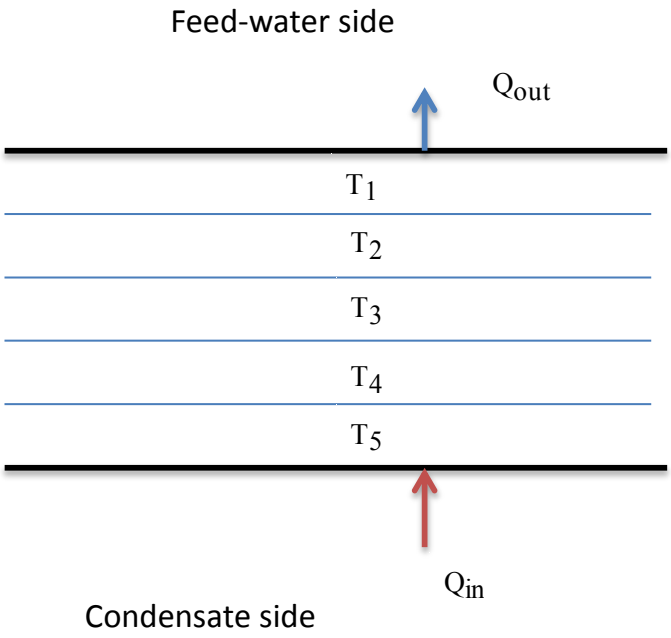

Figure 2-30: Typical discretised HX material with discrete temperatures.

The calculated heat was compared with the difference in heat flux from the two streams. A difference between these two would indicate heat flow error due to the numerical discretization. This difference is shown for the case of 20 increments in Figure 2-31.

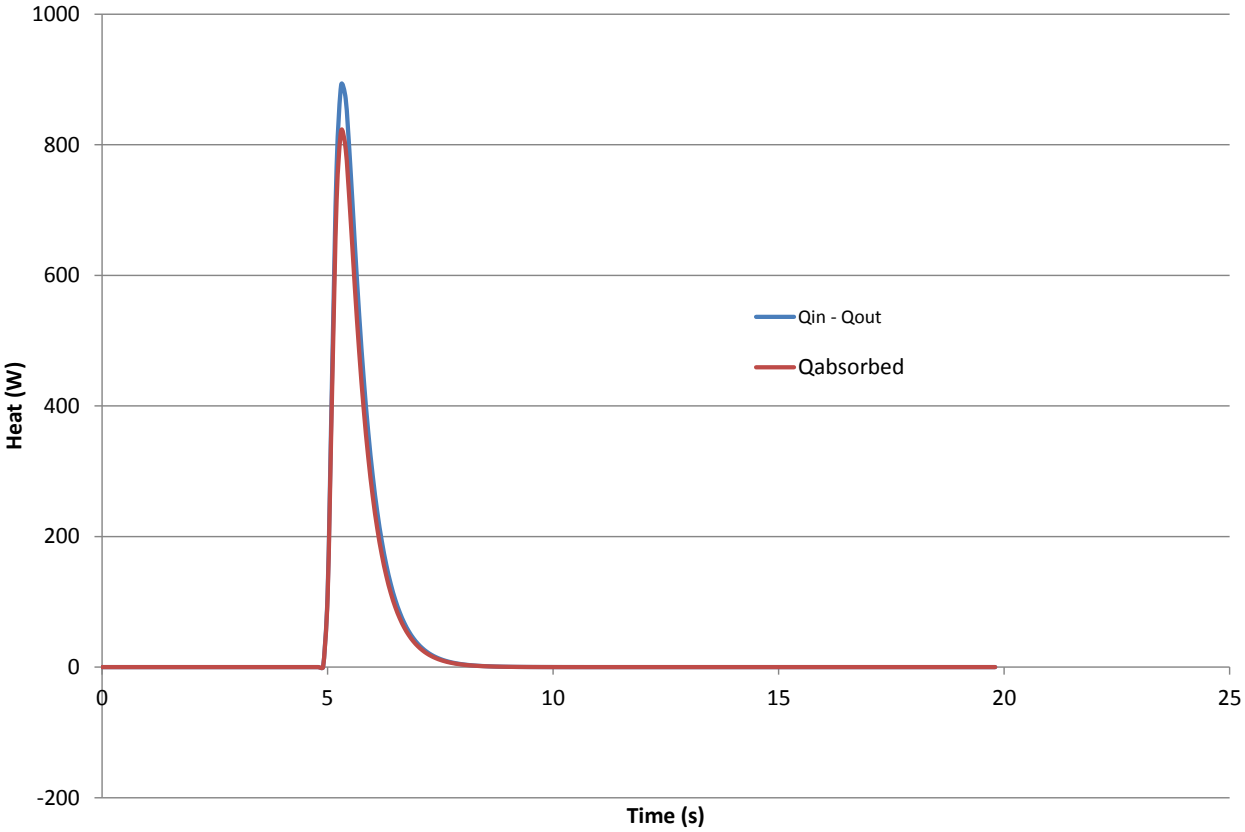

Figure 2-31: Heat energy absorbed (red) by HX and the difference of energy into and out of a HX.

The maximum error (in percentage) for increasing number of increments is shown in Figure 2-32. It is seen that the error approaches zero as the increments are increased. The optimum number of increments is a compromise between solution accuracy and computational time. This optimum has not been determined in this study. However, the maximum error only exists for a very short time after the immediate transient. For more gradual transients, as is expected in real plant conditions, this error should be negligible. For this reason, a discretization of only two elements was chosen. Also, because of the gradual transients considered in this report, a time step of 100ms was found to be sufficient. But for faster transients it might be necessary to do a time step sensitivity study.

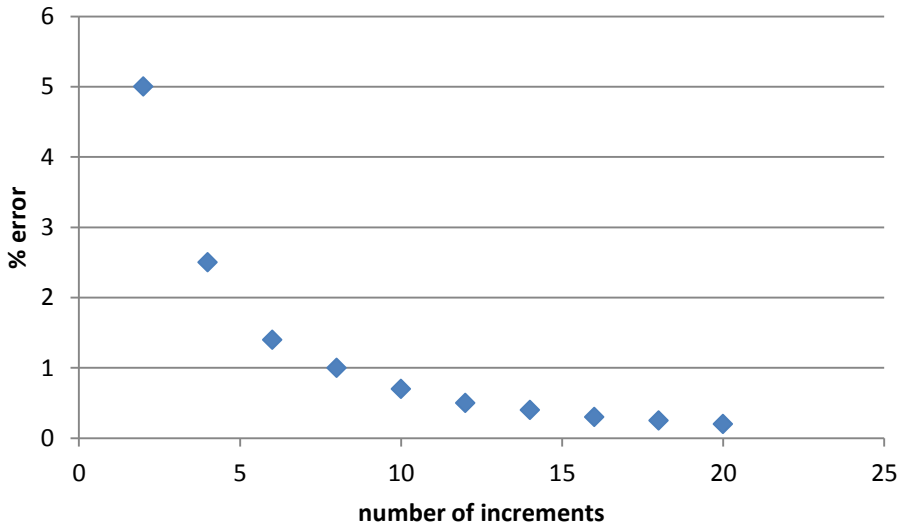

Figure 2-32: Maximum difference in energy absorbed and Q_{in}–Q_{out}, % difference for different increments.

2.5 Pressure Drop Correlation Review

The following sections look into the pressure drop correlations inside tubes for different flow regimes, and on the shell side when the fluid is two phase and single phase.

2.5.1 Pressure Drop inside Tubes

The pressure drop in pipes can be categorized into primary and secondary losses. The primary loss is associated to the viscosity of the fluid and the conditions of the tube wall, and is termed the skin friction. The friction loss also depends on the flow velocity and geometry of the pipe, and was first formulated by Darcy-Weisbach as:

$$\Delta P = \frac{fL}{D}\frac{1}{2}\rho v^2 \tag{2-47}$$

The friction factor, f, can be determined from the Reynolds number for laminar flow and turbulent flow [10]. The friction factor for laminar flow is given as:

$$f_{lam} = \frac{64}{\mathrm{Re}} \tag{2-48}$$

For turbulent flow, the friction factor can be obtained from the Moody diagram or an empirical formulation such as the one by Blasius [31]. Flownex uses the same correlation as given in equation(2-48) to calculate the friction factor in laminar flow. The Blasius correlation is also used in turbulent flow, and linear interpolation between laminar and turbulent is used to determine friction factors in the transition regime.

The secondary losses are due to disturbances to free flow of the fluid. These include the entrance and exit of tubes, bends, valves, orifices, etc. and can all be quantified in the following form:

$$\Delta P = K\frac{1}{2}\rho v^2 \tag{2-49}$$

The value of *K* is determined experimentally for different cases. So, knowing the geometry of the tube and, say, the bend radius then the value of K can be looked up.

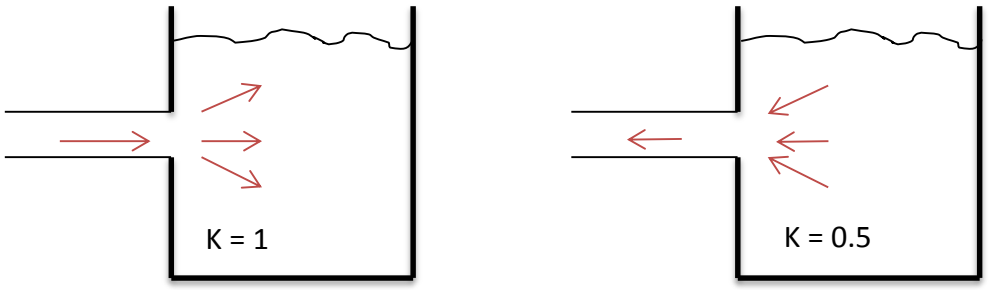

a) Exit loss factor b) Entrance loss factor

Figure 2-33: Pipe exit and entrance losses to and from a large reservoir

A typical loss factor of 0.5 is used for blunt entrances, and 1.0 for blunt exits into a larger volume as shown in Figure 2-33. These factors correlate well with the entrance and exit of the feed-water tubes in the tube-sheet.

2.5.2 Pressure Drop on the Shell Side

In a general shell and tube HX, with no baffles, the pressure drop is mainly due to three factors. Firstly, the frictional pressure loss which is a result of shear forces which are generated at the tube wall-liquid interface, at the liquid-vapour interface, and at the tube-vapour interface. The other two are the entrance and exit effects to and from the shell, and the momentum pressure drop. Correlations for two-phase frictional pressure drop in shell of a shell and tube HX are not as well understood as for flow in the tubes. The shell can be approximated as a tube and the effective diameters and lengths of steam flow path used for analysis. The basis of two phase frictional pressure drop is believed to have been set by Lockhart and Martinelli whom with their work were the first to closely estimate the pressure drop and most researchers followed their method with minor alterations [41] [42] [43] [44]. The approach is such that the two phase pressure drop is equal to that which would be experienced either by the liquid or vapour based on single-phase approaches, multiplied by a two-phase multiplier.

$$\Delta P_{fric} = \Delta P_l \phi_l^2 \tag{2-50}$$

Where,

$$\Delta P_l = \frac{2 f_l G^2 (1-x)^2}{d \rho_l} \tag{2-51}$$

$$f_l = \frac{0.079}{\mathrm{Re}_l^{\,n}} \tag{2-52}$$

The pressure loss is calculated based on the liquid properties, hence the subscript *l*, but can similarly be determined using the vapour properties. The two-phase fluid is assumed to be homogeneous, meaning the vapour and liquid have about the same velocity. Hence there is no subscript for the flow rate in equation(2-51). The superscript *n* is given as 0.25 as in the friction factor expression of Blasius.

This pressure drop for condensing zone cannot be applied in this study as most parameters are not retrievable from plant and depends on the quality which changes along the FWH. Fortunately, FWH's are often designed to have negligible pressure drop in the condensing zone, as this affects the saturation pressure and temperature inside the shell. Hence the two-phase pressure drop will be ignored and only the pressure on the single phase zones will be taken into consideration.

The pressure on the de-superheating and sub-cooling zones can be predicted from different correlations as shown by Kakac and Liu [27]. From all correlations given, a somewhat more practical method was suggested by Delaware [10]. The method assumes that the total significant pressure drop can be attributed to three factors: the entrance sections, the exit sections, and the internal sections which require knowledge of internal geometry. The internal pressure drop can further be broken down into two components: the pressure drop due to the cross-flow over the tube bundle and pressure drop in the window region as shown in Figure 2-34 and depends on the baffle geometry more than anything.

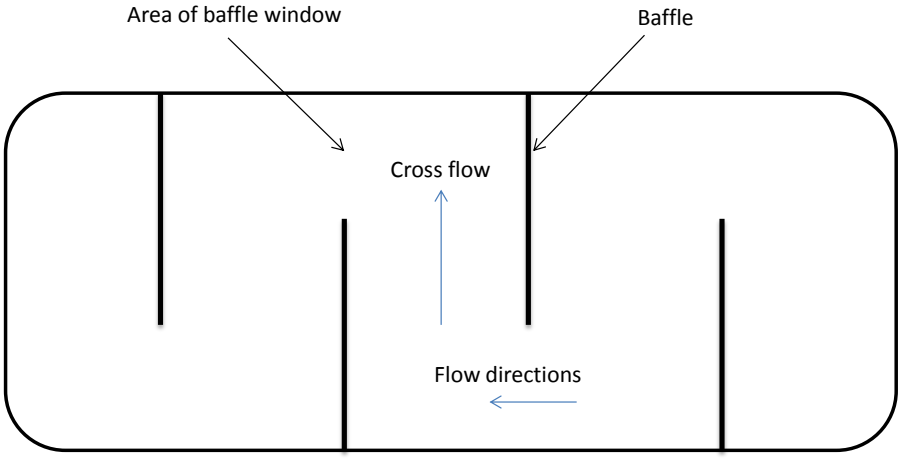

Figure 2-34: Cross-sectional view of a FWH showing baffles, baffle window and the flow directions on each segment.

The cross flow pressure drop across two baffles which is given by:

$$\Delta P_b = 2 f_s N_{rows} \frac{G^2}{g\rho}\left(\frac{\mu_w}{\mu_f}\right)^{0.4} \tag{2-53}$$

The friction factor applied in this method is determined by using the Bell-Delaware curve for the tube and pitch match under consideration and is mathematically approximated to be:

$$f_s = \frac{0.56}{\mathrm{Re}^{0.14}} \tag{2-54}$$

Once again, detail knowledge of baffle geometry and the spacing between the baffles are needed to properly calculate the pressure drop.

2.6 Level and Level Control in FWHs

Some level of condensate on the shell side is maintained to create a seal which avoids the blow-through of steam into the drain pipe line. The condensate level also forms the sub-cooling section in the FWH. The maximum heat transfer between the steam and feed-water occurs when the largest tube area is exposed to condensing steam without allowing blow-through. If the heater condensate level is higher than the design level, the condensing zone area will be less than the required area to condense, resulting in reduced HX effectiveness. A relatively small change in level in FWHs results in a greater change in heat rate, and hence the efficiency of the cycle [45].

The level in the shell has a maximum level it can reach with the heater still working. If this level is reached, the heater is bypassed to avoid the possibility of condensate induction into the steam turbine. A lower than accepted level of condensate results in high temperature steam going through into the drain cooler, as a consequence some of the condensate flashes to steam. Thus, tight optimum level is required for different load conditions for a heater to operate at maximum efficiency [46].

Originally, displacement type level systems with mechanical-pneumatic controllers were used for level control. With time, two main issues were found with them. Firstly, the nature of mechanical level controllers required high maintenance due to the failure of elements like bearings, seals and air supply components. Secondly, the varying liquid density of both the steam and feed-water streams in a FWH creates significant errors in measurement with a displacer [47].

It is suggested in [47] that to eliminate some of the maintenance problems that arise due to mechanical transmitters and controllers, new magneto-restrictive level transmitters can be used. Also, because one is looking to control the level as steadily as possible even under adverse load variation, the level can fluctuate but should stabilize as the heater acquires steady conditions for

the new load. It is of high importance in FWH operation to fully understand the function and importance of drains outlet control valve with respect to controlling the condensate level within the heater [17]. The common mistake made by operators is opening the drain valve more than it is required. The effect of this is the drop in pressure before the valve and a possibility of steam flashing. When the steam flashes, the velocity of the fluid across the valve increases and possibility of damage to the valve is high as it is designed for low flow rates and sub-cooled condensate, not steam [17]. Figure 2-35 shows the position of the drain valve relative to the whole FWH structure.

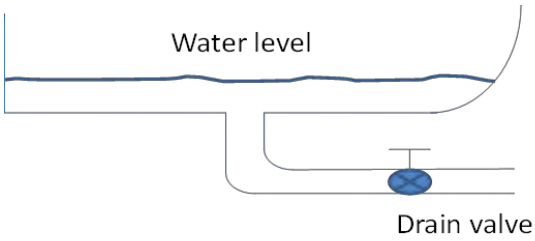

Figure 2-35: Drain valve position on a FWH.

In modelling the FWH in Flownex, the orifice of the drain pipe component can be changed to work as a valve. The orifice ensures controllability of the level within the shell. Depending on the desired level, the orifice can open wider or close to extract more or less condensate from the shell. Adding control loops was not part of this project, but the model would have ability to control the condensate level within shell.

Another check that is commonly applied to track the level change is through the effectiveness of the heater. This is done by checking the terminal temperature difference (TTD) or the drain cooler approach (DCA) temperature. Figure 2-36 shows how the DCA and TTD are determined from the temperatures of the two streams.

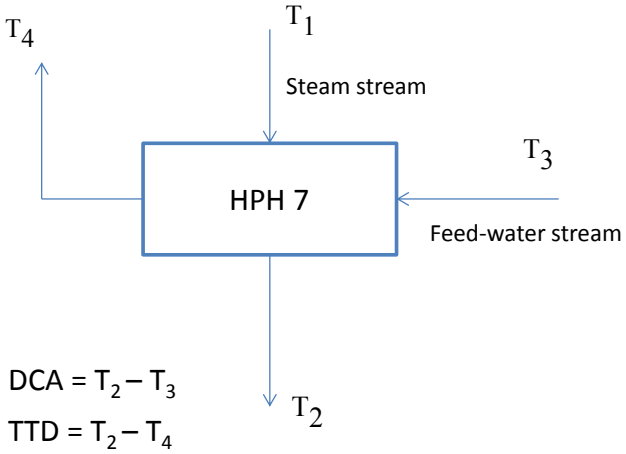

Figure 2-36: Illustration of how the TTD and the DCA are determined from a typical heater.

A decrease in the DCA is a result of the level increase for fully functioning FWH, and an increase in the TTD is also a direct consequence of level increase. This relationship is shown in Figure 2-37 with the safe operating range for typical FWHs also shown.

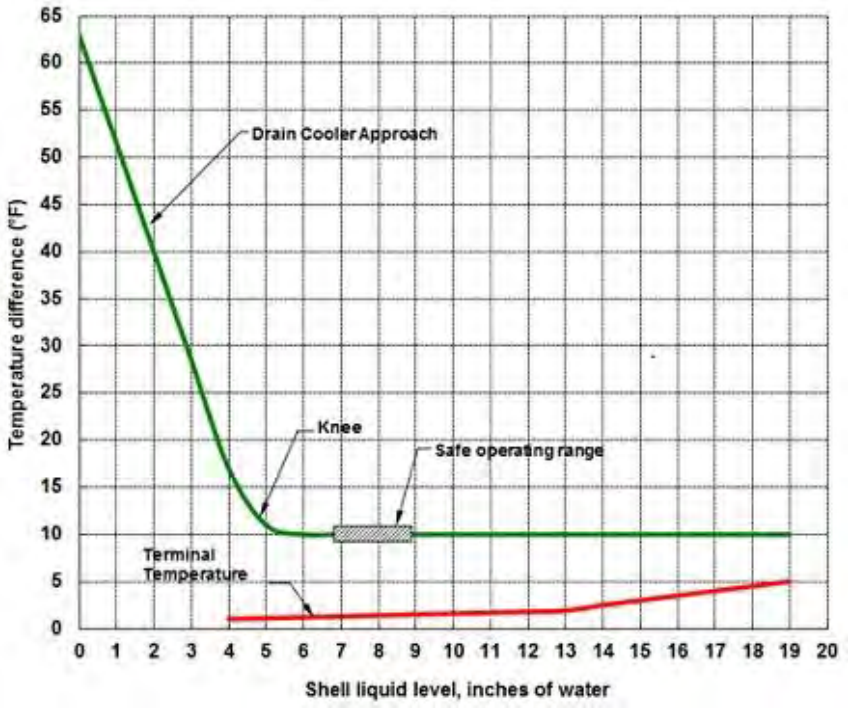

Figure 2-37: FWH level vs TTD/DCA [48].

2.7 Modelling Techniques

In modelling problems, one needs to make a good choice in the approach as there is always a trade-off between complexity, accuracy and flexibility. The following section outlines the different methodologies for building a model. There are generally three ways a model can be built: 1. White box modelling, 2. Black box modelling, 3. Grey box modelling. The three techniques are explained in detail below.

2.7.1 White-box Modelling

The model is constructed using scientific relations / first principles that fully describe the model details [49]. The detail of this kind of model is high as it has to capture all the geometrical and phenomenal aspects of the equipment. This kind of model is used when results of the model are to be exactly the same as those of the actual process. Even though this approach is complex and

requires large computing capabilities, it is very flexible and realistic. In reality, the "pure" white box model does not exist as there will always be some approximations made [50]. Figure 2-38 below shows the flow diagram of the white box modelling.

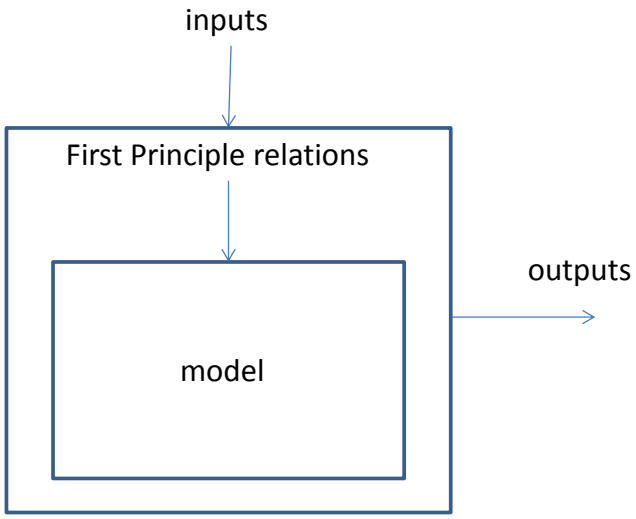

Figure 2-38: White box modelling flow diagram.

This approach is not widely used in the modelling of FWHs and in process modelling in general. Only a few cases have been reported where only first principles were used to fully define a FWH model. Laskowskia [51] made use of the mass and energy balance equations and Peclet's law to fully define a model of a simplified single zone and a three zone heater. Also, Hussaini et al. [14]only used the first principle equations in defining the model for the allocation of areas on different zones of a FWH. In the analysis of impact of fouling by Antar and Zubair [52], only the first principles were used to build and analyse the model.

2.7.2 Black-box Modelling

Black box modelling is when transfer characteristic are inferred from inputs and outputs without any knowledge of the actual process inside. Figure 2-39 shows the flow chart of how the black box can be viewed.

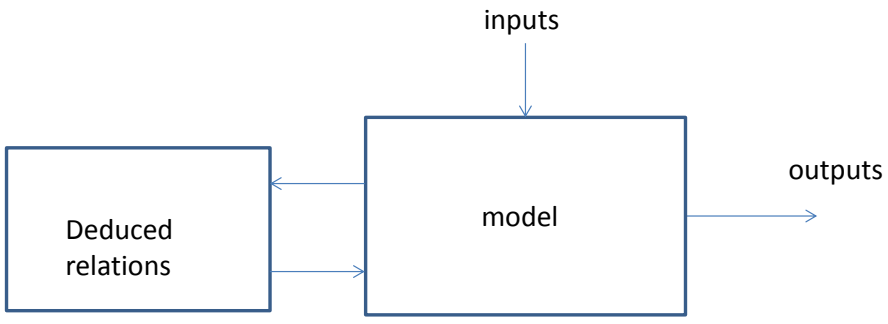

Figure 2-39: Black box modelling flow diagram.

Azman and Kocijan [53] looked at the different types of black box modelling. They mainly looked at the three types of modelling approaches: the artificial neuro networks, fuzzy models and the Gaussian process models. The artificial neuro networks and fuzzy models are the most used approaches and approximate processes from a universal point of view. Gaussian process models are, on the other hand, probabilistic and non-parametric. It searches for relationships amongst available measured data.

In places where the black box modelling is implemented in this thesis, it will be of the Gaussian process models type.

2.7.3 Grey-box Modelling

It is believed that given any set of parametric class of models, one can find a model that fits the given experimental data with minimum loss of accuracy of the process results according to any given criterion [54]. The taxonomy of the grey box modelling relies on the fact that when making a mathematical model of a physical object there are two sources of information, the response data of the process in operation and prior knowledge about the object or process characteristics [55]. Both sources of information are used in the grey box modelling. In practical modelling, prior knowledge may mean different things and it is not easy to incorporate it into the model with any member of models assumed. Each member of models requires a particular form of prior knowledge. To take prior knowledge into account, one can start with a flexible model and adapt its freedom to fit in prior knowledge. From prior knowledge of the system, one can formulate first principle relations to define physical, geometrical and phenomenological characteristics of the system [56]. With process data, one can deduce relations that best define the system. Figure 2-40 shows a flow chart of the grey box modelling.

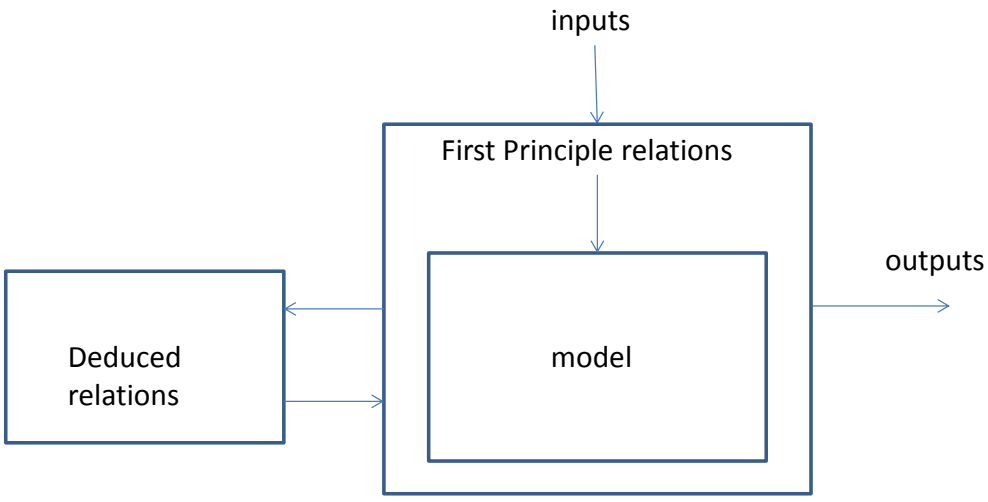

Figure 2-40: Grey box modelling flow chart.

The grey box modelling approach has power over the other types because of the balance one gets between complexity and simplification. This method was used in [1] to estimate the FWH parameters. In his work, Barszcz comments on the novelty of the work as the method of utilizing operational data to adjust phenomenological parameters of the model of a FWH derived from physical laws. The grey box modelling approach was also used in [56] in modelling a FWH intended for model-based diagnostics. In their observation Barszcz and Czop [56] report that in tuning the model, one can adjust model parameters based on operational data.

2.7.4 Utilizing Prior Knowledge

The different ways of incorporating prior knowledge are looked at in greater depth in the next sub-sections. The different branches outlined are considered to cover the main ways prior knowledge can be used to model structures of physical systems.

a) Constrained Black-box Model

The constrained black box model makes use of a model whereby specific parameters are constrained based on physical relations. This is because most of the time the linear black box model may give inconsistent parameter estimations, hence this method is employed to correct the inconsistency. The basis for this type of modelling is that a simple continuous model can be transformed into a corresponding discrete time model and known restrictions to the continuous model, such as process stability and step responses, can be used to define limits placed on a discrete time model [49].

b) Semi-Physical Modelling

Most of the processes in industry possess significant nonlinear behaviour, and giving linear relations for the black box model part would yield a poor correlation between the actual process and the model behaviour. In some cases the first principle modelling is not sufficient to model such processes, so it is possible to make use of some physical insight to transform the inputs and outputs variables into new variables which are used as regressors to develop a linear black box model [49]. The physical insight to the process is used for nonlinear transformation of measured data [1].

c) Hybrid Modelling

The hybrid model is separated into two parts, a white box part, and in some cases grey box part, which is modelled by means of first principle relations, and a completely black box part, which is identified using operating process data. The black box can be incorporated into the model either as a parallel or serial component. The serial method is used in cases where a specific physical part of a process is to be modelled. While parallel approach is used to extend an approximation of first principle model with a general black box part to

compensate for any simplifications made in the approximated model. Figure 2-41 and Figure 2-42 show the flow charts of serial and parallel approaches respectively.

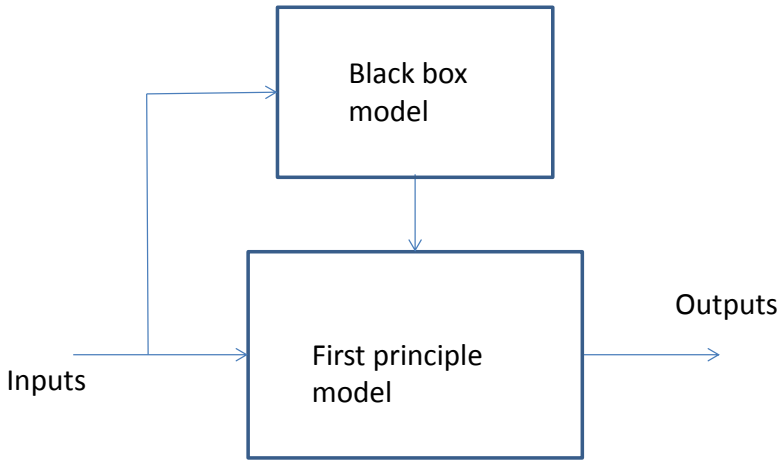

Figure 2-41: Series Hybrid grey-box Modelling.

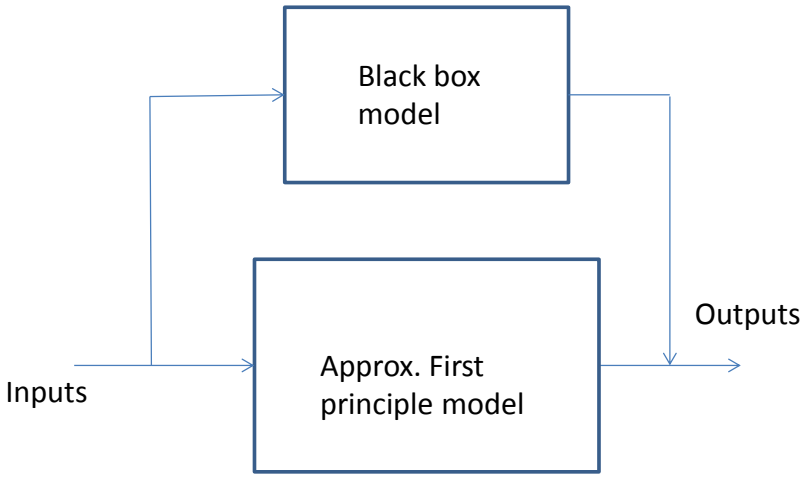

Figure 2-42: Parallel Hybrid grey-box modelling.

The parallel hybrid model is presented in [57] and it also shows that the overall model prediction is the additive combination of the output of the first principle relations and the output of deduced relations and the deduced relations compensate for the residuals between first principle relations and the actual process caused by inherent process complexities. The trick is to have the approximate first principle model working properly, otherwise the black box will misfit and the hybrid might perform poorly [49].

d) Mechanistic Modelling

In most cases, when a model is being built, some fundamental insight into the mechanisms that underlies the behaviour of the process are available and relevant balance equations can be formulated as a set of the first order equations. The main difference of this method from others is that some of the known parameters are estimated and put in parametric

form into the model and the errors are corrected by adding the black box part [58]. The activity to develop a mechanistic grey box model is said to be an object oriented procedure, which consists of basic modelling, experiments, estimations, expanded modelling and modelling appraisal [49].

With the lack of internal geometry of the FWH and insight of the process phenomenon, the white box model would not be sufficient. But with the use of some first principles and estimation of other parameters the model was built and expanded accordingly. Hence in all the analysis of the model built, the grey-box modelling approach is used and in specific the mechanistic modelling.

2.8 Previous Mathematical Models of FWHs

This section looks at some of the relevant approaches which different authors took in the mathematical modelling of FWHs and the physical implementation of the mathematics and methodologies. The models will not be discussed in detail, but an overview of the models will be looked at with the assumptions for different models also being outlined. Four models in specific are of interest and were looked into. Two of the models were formulated by the same authors [56] [1] and have similarities. They are therefore combined into one section and the differences and similarities in the approaches outlined.

2.8.1 Juan-qun Xu Model [59]

The authors looked at four high level outcomes in their work, which were to:

- Model a FWH with three working zones using the dimensional analysis.
- Characterize the model when operating at low liquid level.
- Verify the proposed model with acceptance test data.
- Attain the best efficient level and be used to reset the operating level.

In the analysis, the HPH #1 of a 330MW plant was used for all results reported. The heater model is separated into three parts: drain cooler section, condensing section and the de-superheating section. Each section was analysed separately, with different methods applied in each section. In the drain cooler section, the effectiveness-NTU method was used to calculate the heat lost by condensate to the heat gained by the feed-water. Because the feed-water mass flow is an order higher than the shell-side mass flow, it is assumed that the heat capacity ratio C_r is insignificant and is set to zero to give the simplified form of equation (2-25) of a single stream HX as:

$$\varepsilon_1 = 1 - e^{-NTU} = \frac{T_{sat} - T_{drain}}{T_{sat} - T_{fw,in}} \quad (2\text{-}55)$$

The NTU is approximated to be a function of the feed-water mass flow rate and the average temperature for the working heater pressure range. For the condensing and de-superheating zones similar analysis is done with the Dittus-Boelter correlation used for the feed-water side and the Nusselt integral method for condensation on tubes to get the HTCs. The outlet conditions of the condensing and de-superheating zones are thus determined. Analysis on the level and how it affects the overall heat transfer was then carried out. The effect of low level and level in general was shown in terms of the drain cooler approach, and how it varies. Figure 2-43 shows how the drain cooler approach changes with level.

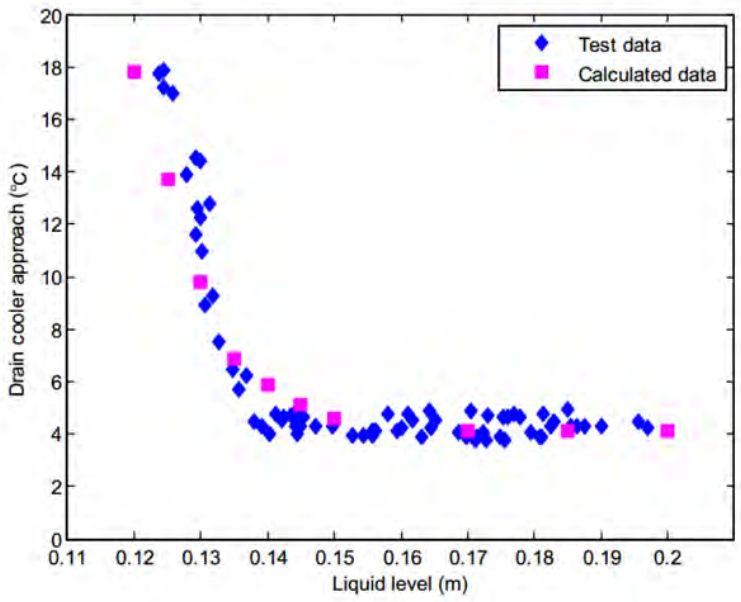

Figure 2-43: Effect of level on overall heat transfer by drain cooler approach [59].

It was concluded that, at around 0.15m of liquid level for the operating range, a decline in level significantly reduces the overall HTC, and this is evident in Figure 2-43.

2.8.2 Laskowski Models [51]

Laskowski [51] built two simple mathematical models of FWHs, one with just a single zone and the other with three different zones. The models were based on the conservation of the mass and energy, and Peclet's law. Peclet's law relates the relative importance of transportation of the convective thermal energy to its molecular thermal energy [60]. It is however worth noting that in applications like FWHs where the Reynolds numbers are very high, the Peclet's number is

relatively high and the fluid conduction along the axis of the tubes can be neglected. The accuracy of the models was tested against real plant data of a HPH supplied from a 200MW turbine. Some assumptions were made in the mathematical model, and are listed below:

- No pressures drop on both streams of the heater.
- No heat loss to the environment.
- HTCs for each zone are constant.

The model is such that all other parameters of the FWH are known, except any chosen two. And in their analysis the steam mass flow rate and the feed-water exit temperature were the unknown variables to be determined from the model. Both models were implemented with characteristics and parameters of a 200MW turbine in operation, and it was shown that the three zone model was more accurate than the single zone model with reference to the real plant data. The model showed that 75% of the heat is transferred in the condensing zone while the de-superheating and sub-cooling takes up 5% and 20% respectively. The outlet feed-water temperature of the model with three zones and the real data are shown in Figure 2-44 below:

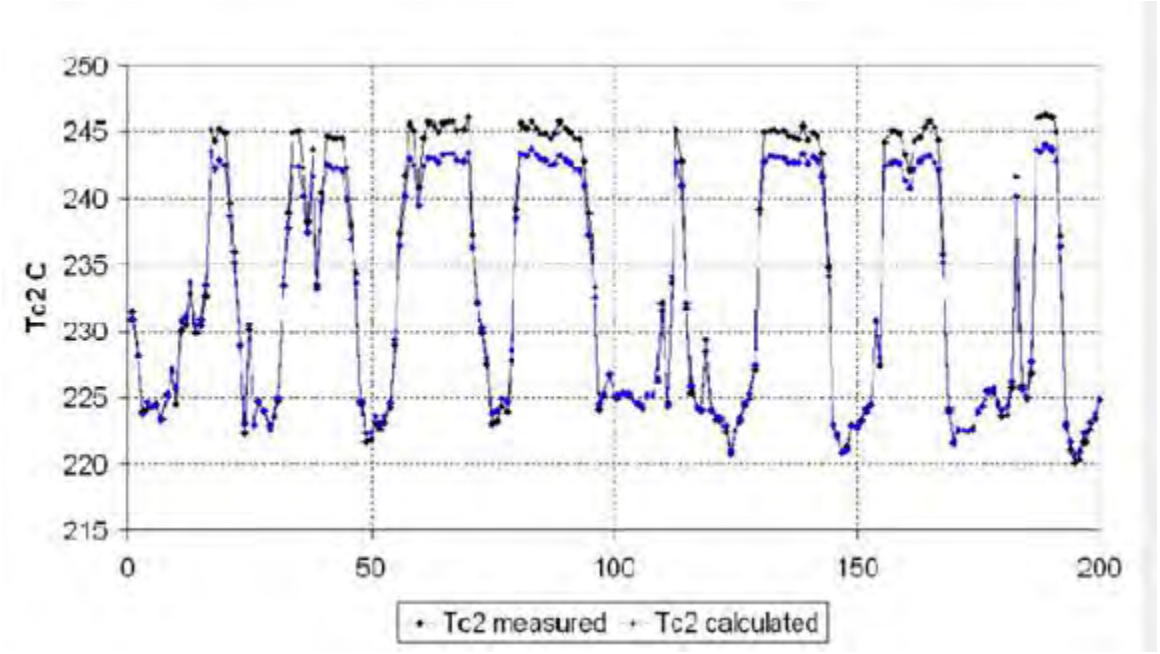

Figure 2-44: Comparison of calculated and actual feed-water outlet temperature [51].

The results showed good agreement with real plant data, except for when the FWH is operating in high temperatures as seen in Figure 2-44. The authors then suggest that the HTCs used should be varied with varying Nusselt, Prandtl, and Reynolds numbers for more accuracy. The same conclusion was given by Tan and Spinner [35] in their analysis of shell and tube HXs.

2.8.3 Barszcz Models [56] [1]

Barszcz and Czop [1] looked into the mathematical modelling of a high pressure FWH for a coal fired plant. The authors discuss some of the structural simplifications in building a model, how some of the parameters can be estimated, and the dynamic validation of the model on Virtual Power Plant (VPP) simulating environment. The author goes on to describing some of the modelling techniques which arise from problems associated with dynamic modelling of systems. Firstly, if fully analytical mathematical models are used, it gets very costly determining all model parameters. Secondly, if fully data-driven models are used, then there is not a clear interpretation of some of the internal process phenomenon. The approach in [1] is such that both approaches are used in parallel to compensate one other. The model is tested against a heater supplied by a 225MW turbine. Some assumptions are made prior to system identification, and are given below:

- The pressure in the heater cavity is constant and is equal to the pressure of the bled steam at the inlet of the FWH.
- The pressure of the condensate is constant and is the same as bled steam pressure at inlet.
- No heat conduction in the longitudinal direction of the pipe or the working fluids.
- There is no de-superheating section although superheat is accepted into the condenser control volume.
- Geometry and high level properties are constant for a given scenario.

The transient model was a generalization of available steady states, and the HTCs found for different loads were used to predict the trend of the system and as initial conditions. The model assumes no de-superheating and the steam de-superheats in the condensing zone control volume. There are then two control volumes and the mass and energy balance are performed on them. The heat absorbed by the tube is also formulated assuming that there is no energy loss to the atmosphere as follows:

$$\frac{dQ_w}{dt} = \dot{Q}_{steam} - \dot{Q}_{fw} \tag{2-56}$$

Where,

$$Q_w = m_w c_{pw} T_w$$

In the extension of their work [56], Barszcz and Czop looked at all the three zones of the heater but this brought about a loss in accuracy in predicting some of the model parameters. The simulation times were also rated against real time to see which approach was more economical. The basis of all mathematical analysis in both approaches is fully outlined in [61].

3. Model Development

3.1 Overview of Model Development

This chapter looks at how the heat balances data is taken and converted into relations that can then be used on Flownex model as inputs by just specifying one input. The parameters to be converted that will depend on one variable are the high level inputs of the FWH and the heat transfer characteristics of the different zones. The modelling approach taken in determining the heat transfer characteristics on the condensing zone of the FWH is what was explained in section 2.7.3 as the grey-box modelling. The inputs and outputs of the process are known and some first principle relations are used to predict the characteristics of the process. This is done without knowing the little details of the process itself in a similar way as shown by Bohlin [55]. Also, from technical data, the amount of tube mass is estimated from the knowledge of shell length and diameter, and the typical diameter of tubes in a FWH. The FWH is separated into three different zones and the heat transfer on each zone is determined from knowing the inlet and outlet conditions, and estimating the saturation conditions. The heat transfer on the de-superheating and sub-cooling zones is added straight to the feed-water as heat input. But for the condensing zone, the overall HTC is inferred from the heat transfer obtained from plant performance data. The overall HTC is split into the two convective parts and a conductive part. The conductive part is not accurately determined as the linear formulation is used instead of the radial one due to lack of detail. The convective HTC cannot be accurately determined on both streams as the real geometry is not known, so a typical ratio of the outer to the inner HTC based on correlations introduced in section 2.3.2 is determined using typical geometry and working conditions of HPHs. The obtained average ratio is then used for all load conditions to get the two HTCs. The method of application of heat transfer in the de-superheating zone on the model is the black box modelling outlined in section 2.7.2. The FWH model is described by showing all components, their inputs and the significance of such components towards the model as a whole. The model is then explained as a whole working in steady state and in transient. The initial state settings of each state are also outlined.

3.2 Operating conditions

To illustrate the methodology followed in modelling the FWH, the Kriel HPH 7 is used as a case study. Kriel power station was commissioned in 1979 and was largest coal fired station in the ESKOM fleet at that time. It consists of six 500 MW units shown in Figure 3-1 and only unit five has the right instrumentation to give sufficient information on the feed-water heating system.

Figure 3-1: Kriel power station [3]

The HPH 7 is also shown in Figure 3-2 on the heat balance with its location relative to the complete power generation cycle also indicated. And the high level inputs used in the FWH model are taken from the heat balance. The enthalpy reported on the heat balance could not be used to predict other parameters like pressure because pressure is very sensitive to enthalpy change. It was therefore concluded that using mass flows, pressures and temperatures only would be sufficient to fully define the FWH model.

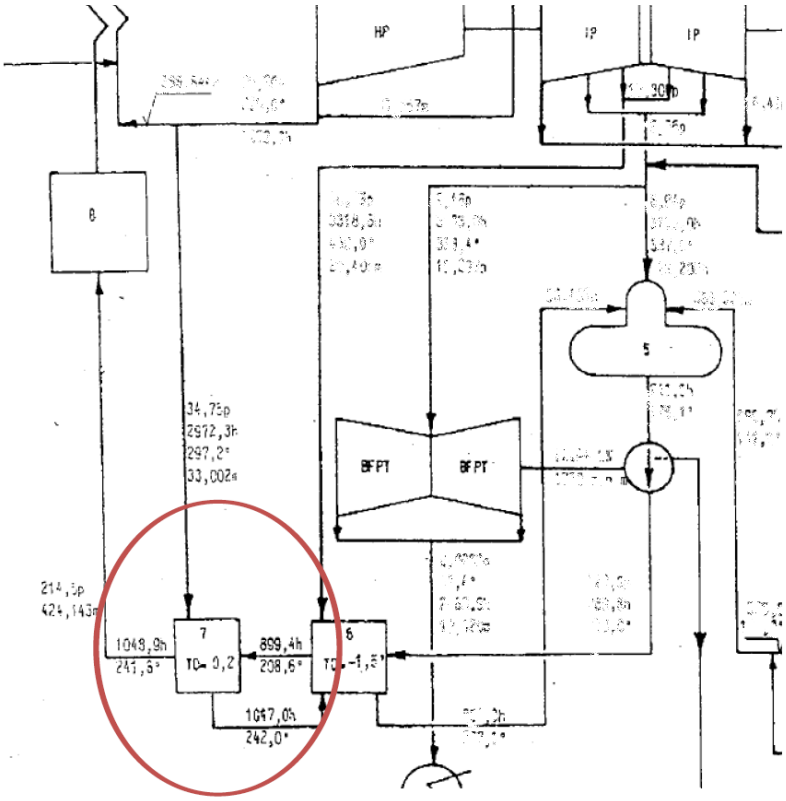

Figure 3-2: Data from heat balance of Kriel power station

The operating conditions of the model are given in Table 3-1. The operating conditions were converted to trends to predict for conditions in between given load conditions. This will be shown in section 3.7.

Table 3-1: Inlet conditions of the HPH 7.

Load condition	Steam temperature (°C)	Steam flow (kg/s)	Feed-water flow (kg/s)	Feed-water pressure (Bar)	Feed-water temperature (°C)	Bled steam Pressure (Bar)	Condensate temperature (°C)	Feed-water temperature (°C)
40%	268.8	8.632	168.283	172	171.1	13.61	194.3	196.4
60%	277.4	15.194	251.322	184	186.9	20.38	213.3	215
80%	286.5	23.145	334.565	199	198.5	27.09	228.1	229.2
100%	296.6	32.037	415.662	213	207.8	34.07	240.9	240.8
Full Load (105%)	297.2	33.032	424.143	214	208.6	34.75	242	241.6

3.3 Determining the Heat Transfer Characteristics

To understand the heat transfer and energy flow across the HX material of a FWH, first the steady state analytical calculations were carried out using data from the acceptance tests. The main aim

is to extract the data to quantify the overall HTCs and pressure losses using analytical methods. These are then applied to a FWH model on Flownex with the same input properties as those used in the analytical solution method. The aim is for the Flownex model, which is numerical software, to produce outlet properties of both streams to be the same as given in the data thus validating the methodology and application of the HTC on the Flownex FWH model. The preceding analysis is a general methodology and can be applied for any horizontal FWH but for illustration purpose a specific heater was analysed in this report, the Kriel HPH 7.

Heat Transfer Characteristics Determination

The steam on the shell side has to de-superheat, condense and then be sub-cooled before being cascaded out to the next lower heater or pumped into the feed-water line. The feed-water on the tube side absorbs the energy from the steam and increases the temperature as a result. Figure 3-3 shows a typical temperature profile of the steam and feed-water for the three zones of a FWH as indicated.

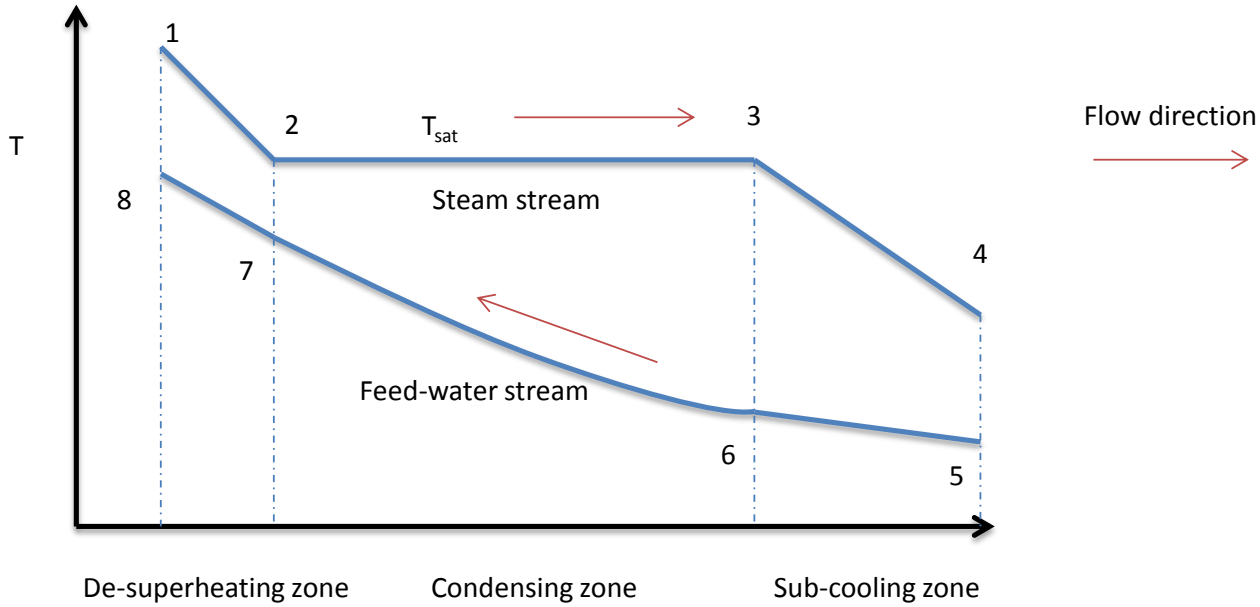

Figure 3-3: Temperature profile of a typical three zones FWH.

The shell side HTC changes drastically from zone to zone. This is because the fluid on the shell side changes states and the properties change. Also, the effective path diameter and velocities change on the different zones on the shell side [7]. So determining the total HTC for all zones on the steam would not give a good representative of the three zones FWH as the HTC would be dominated by the highest of the three. To get accurate heat transfer characteristics, the heater is split into

parts/zones. In the analytical solution, only the overall HTC for the condensing zone is determined because it generally carries more of the heat duty, 85% or more [52]. The de-superheating and condensing zones are incorporated into the model as heat lost on the steam side and heat gained on the feed-water side. The sub-cooling heat, as will be shown in the calculation in Appendix A, is insignificant to the overall energy for the Kriel HPH 7 but for modelling purposes its significance will be included and explained in section 3.6.

The steam enters the FWH from the turbine with superheat for all HPHs in coal fired plants and the first stage is the de-superheating zone. It is assumed that there is negligible pressure drop on the shell side for the preceding analysis. This was seen not to affect the performance of the model by Barszcz [56] and the inlet pressure is assumed to be the same pressure as in the cavity. To get the amount of energy that is lost in the de-superheating zone, the enthalpy of the steam when it reaches saturation (quality is 1), is determined from the inlet pressure at point 1 in Figure 3-3.

$$h_{s2} = f\left(P_{sat}, x = 1\right)$$

The enthalpy of the steam as it enters the FWH is almost always readily available or can be obtained from other measurable parameter (pressure and temperature). So knowing the enthalpy of the steam as it enters the FWH, the enthalpy as it exits the de-superheating stage, h_{s2}, and the mass flow rate makes it possible to determine the amount of energy the steam loses at any load across the de-superheating zone. The amount of heat energy is therefore given as:

$$Q_{des} = \dot{m}(h_{s1} - h_{s2})$$

Where h_{s1} is the steam enthalpy as it enters the FWH. The energy for each load characteristic is determined using above relation and a plot of the de-superheating zone energy vs the feed-water mass flow is created as shown in Figure 3-4. This is to estimate the other loads, not reported, based on the reported load characteristics. The maximum capability load is also included and the de-superheating energy is assumed 0 MW for 0 kg/s mass flow in creating the trend of the de-superheating energy.

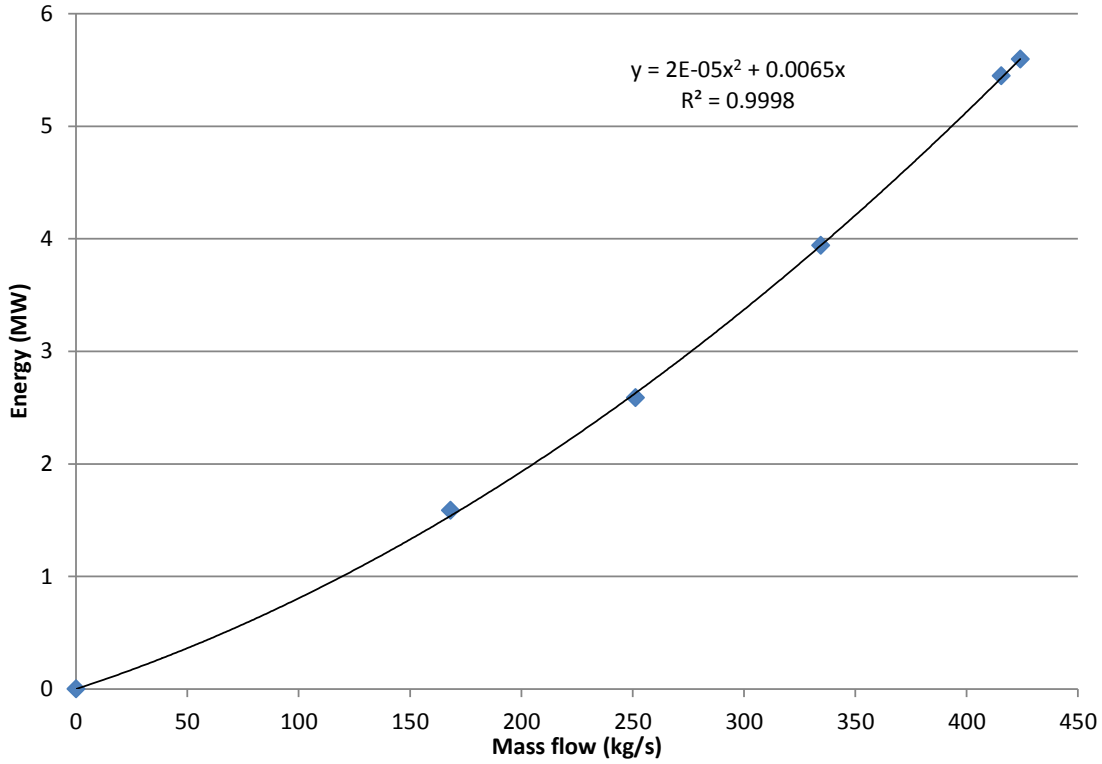

Figure 3-4: De-superheating energy vs feed-water mass flow rate of HPH 7.

The total heat lost by the steam in the shell across all three zones can also be determined by knowing the steam outlet and enthalpies for different load conditions, and is given as:

$$Q_{total} = \dot{m}(h_{s1} - h_{s4})$$

The energy extracted from the steam during condensation is the energy extracted at constant pressure to get the steam from quality of 1, as it exits the de-superheating zone, to quality of zero, i.e. from saturated vapour to saturated liquid. The enthalpy can be determined by knowing pressure and quality as already shown above in obtaining h_{s2}; therefore the energy lost in the condensing zone is given by:

$$Q_{cond} = \dot{m}(h_{s2} - h_{s3})$$

The difference between the total heat lost by the steam and heat lost in de-superheating and condensing zones is the heat lost in sub-cooling zone.

$$Q_{sub} = Q_{tot} - (Q_{cond} + Q_{des}) \quad (2\text{-}57)$$

The temperature of the feed-water at the outlet without de-superheating stage (i.e. at point 7 in Figure 3-3) is calculated by first determining the enthalpy at that stage. This is done by assuming that all the energy lost by the steam is transferred into the feed-water at the de-superheating

stage and the enthalpy of feed-water at outlet of FWH, point 8 in Figure 3-3, is given or obtainable from other outlet conditions. It is also assumed that the pressure drop on the feed-water side is also negligible. The enthalpy and temperature of the feed-water at point 7 in Figure 3-3 are determined as follows:

$$h_7 = h_8 - \frac{Q_{des}}{\dot{m}_{fw}}$$

$$T_7 = f(h_7, P_{fw})$$

In a similar manner, the temperature of the feed-water as it enters the condensing zone is determined. But in this case it is from knowing the enthalpy of the feed-water as in enters the FWH at point 5 and the sub-cooling heat transfer from equation(2-57).

Knowing the exit and inlet temperatures on the condensing zone shown in Figure 3-5, and the heat lost enables for usage of the LMTD method to get the overall HTC for the condensing zone. Because the details of the tubes are not fully known, and hence the condensing area is not known, the HTC is combined with the area and *UA* is determined instead of just *U*.

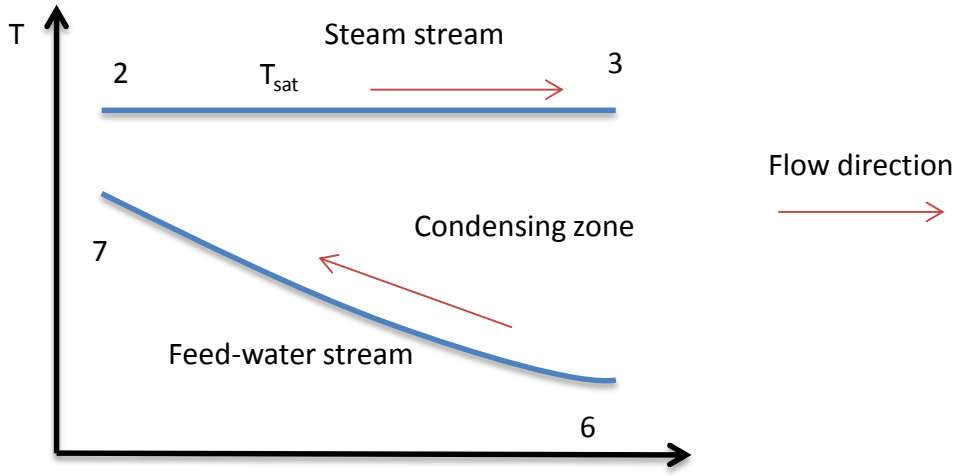

Figure 3-5: Condensing zone temperature profile.

$$UA = \frac{Q_{cond}}{\left(\frac{(T_2 - T_7) - (T_3 - T_6)}{\ln\left(\frac{T_2 - T_7}{T_3 - T_6} \right)} \right)} \tag{2-58}$$

The initial model is built without consideration of the effect of conduction resistance in the overall HTC, and the overall UA value is split into the steam side and feed-water HTC. A sample calculation for the typical HTCs on both streams using correlations outlined in section 2.3.2 was carried out to estimate the ratio between the two sides. The calculations are shown in Appendix B. Also, typical film HTC value of condensing water vapour over tube bundle is given to be in the range 5500 – 17000 W/m^{2}K. And, for water in tubes it ranges 1700 – 11000 W/m^{2}K [62]. This gives a ratio of the shell to the tube side HTC of up to 10. Further research is needed to get the range of film HTC for the FWHs and not just the typical HXs. The HTC on the tube side was then determined with the knowledge of the overall HTC and the assumption made on the feed-water HTC that it is a factor, FX, times more than the shell side HTC as follows:

$$hA_{shell} = FX \cdot hA_{fw}$$

$$UA = \left(\frac{1}{hA_{shell}} + \frac{1}{hA_{fw}} \right)^{-1} \tag{2-59}$$

$$hA_{fw} = \frac{UA \cdot \left(FX + 1 \right)}{FX}$$

Advancement to the HX analysis was made to include the heat conduction in the analytical solution for the convective HTC. The overall HTC now comprises of three components, which are:

$$\frac{1}{UA} = \frac{1}{h_{in}A} + \frac{1}{h_{out}A} + \frac{L}{kA}$$

The conductive resistance is determined by taking the average area, *A*, of the typical HPHs from specifications [63] and reports from the Kriel power station. The thermal conductivity of stainless steel was extracted from the Flownex material library at temperatures of operation. This was similar to what is reported in the design books [64] [65].

The conductive resistance is defined in section 2.3.1 as follows for linear conducting elements:

$$R_{cond} = \frac{kA}{L}$$

In a similar way as demonstrated for a case without conduction, the convective HTC is split into internal and external parts after removing the effect of conductivity on the overall HTC. And different internal and external HTC are obtained. The conduction part removed is estimated using the flat plate formulation whereas the tubes are circular. This brings about a small error in the conductive resistance determination.

3.4 Thermal Mass Determination

The thermal mass of tubes and headers is the most important factor when the working conditions of the FWH are changed regularly. The amount of mass within the shell determines the amount of time it takes and energy required from one steady state to the next in operation. Therefore quantifying this mass and correctly applying it in the model is a necessity. The amount of mass within the shell can be obtained from the drawings and dimensions of the heaters. The mass of tubes can be estimated provided the tube thickness is known. In [63] the total mass, including the outer casing mass, of the heater is given but in this analysis only the mass of the tubes are considered as the shell mass does not contribute much in transients. Table 3-2 shows some of the geometrical data of a HPH 7 with the total heating surface area also given. In all the analysis, the density of the tubes is taken to be 7850 kg/m^3.

Table 3-2: HPH 7 shell geometric data [63].

Total vessel length	10830 mm
Vessel diameter	1750 mm
Surface Area of tubes	789 m^2
Dry weight	40500 kg

The number of tubes in a HX is mainly dependant on the fluid flow rates inside tubes and available pressure drop. The limits on velocity are 0.9 m/s, below that there is a high risk of fouling, and 2.4 m/s is the higher limit, where above it is a risk of tube erosion [12]. Also, area requirements for the required heat transfer may determine the number of tubes employed in HX. However, for a given shell with dimensions, Kakac and Lui [27] suggest that a maximum number of tubes that can be fitted in a shell can be approximated as a function of the shell and tubes diameters. This is done by dividing the projected area of tube layout by single tube.

$$N_t = \left(\frac{CTP}{CL} \right) \frac{\pi D_s^{\,2}}{4(PR)^2 d_i^{\,2}} \tag{2-60}$$

CTP is the tube count calculation constant accounting for the fact that the tubes do not fully cover the entire shell circumference due to necessary clearances between outer tube and shell. The CTP value for a two tube pass HX is given to be 0.9 [27], i.e. 10% clearance. CL is the tube layout constant and depends on the angle of tube layout. Most of Eskom FWHs in place have tubes in 30° layout and for this layout a CL value of 0.87 is used. PR is the tube pitch ratio to the diameter and ranges from 1.25 to 1.5 for all HXs and is defined as shown in equation (2-61) [12] [27]. D_s and d_i are the shell inner diameter, and tube diameter respectively and P_T is the centre distance of adjacent tubes.

$$PR = \frac{P_T}{d_i} \tag{2-61}$$

Figure 3-6 shows other tube layouts with the flow direction indicated for all cases. The pitch length is shown on the 60° triangular pitch and is found in a similar way for other layouts.

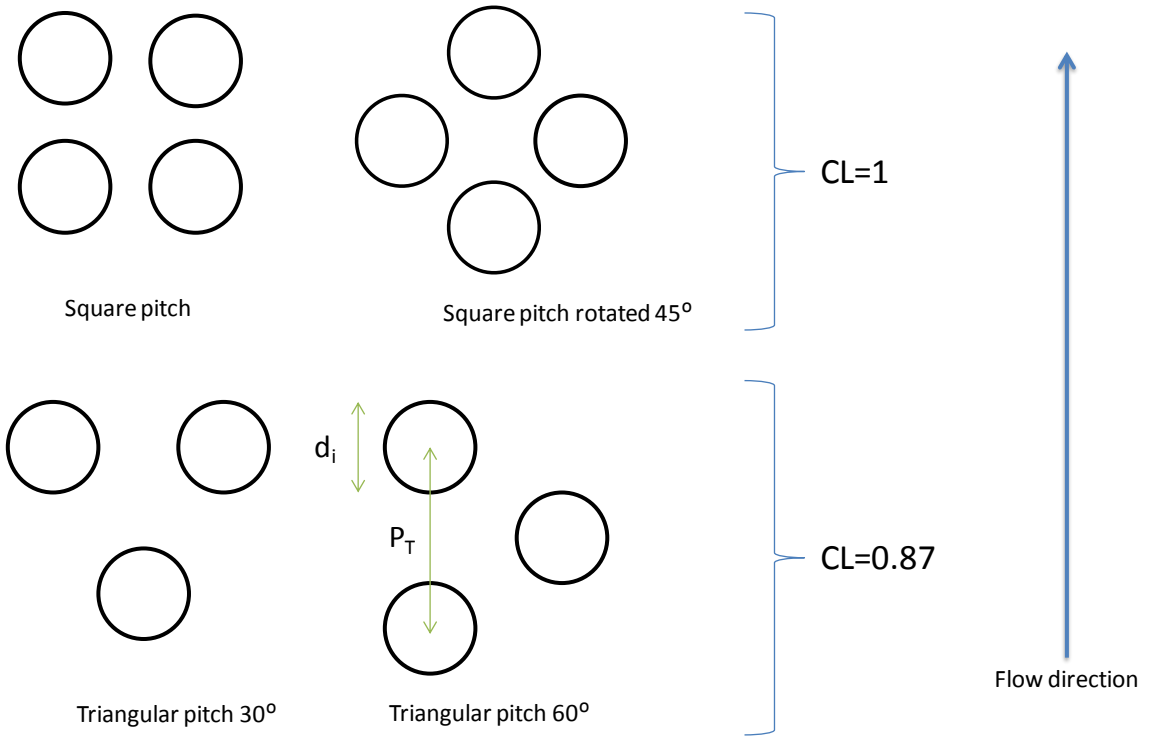

Number of passes	CTP
1	0.93
2	0.9
3	0.85

Figure 3-6: Summary of the tube layout in HXs and the accompanying characters in tube count analysis.

The standard internal tube diameters for HXs are 19.6 mm and 25 mm, and most of Eskom HPHs have the 25 mm tubes [63].

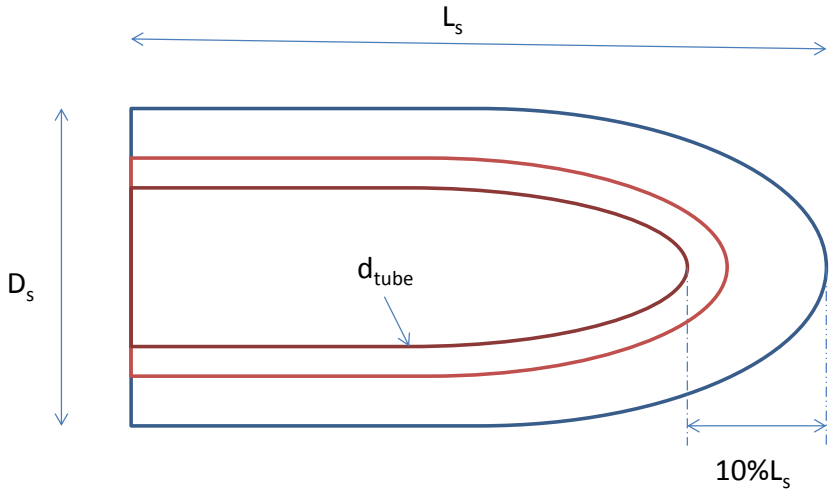

Figure 3-7: Schematic drawing of a FWH indicating dimensions and the clearance of tubes to the end cap.

Figure 3-7 shows the dimensions of a shell and tubes in a FWH, and the clearance between tube bend and the end cap of the shell. About 10% of the shell length is left between the tube bundle and the shell end-cap to allow for thermal expansion [10].

Table 3-3: Illustration of tube mass determination showing required parameters.

D_s (m)	L_s (m)	CTP	CL	d_i (mm)	t_{tube} (mm)	N_t	L_{tube} (m)	Mass (kg)
✓	✓	✓	✓	✓	✓	eqn(2-60)	$90\%L_s$	
1.5	10.83	0.9	0.87	25	2.4	**1290**	**9.747**	**18605**

Table 3-3 shows the inputs and the resulting estimate tube count, tube length and eventually the mass of tubes for the HPH 7. From Table 3-2 it was reported that the heating surface area for the FWH is 789 m^2. This is used with the tube thickness to get the real mass of the FWH tubes to see how good the approximation method is before applying it to the model development. The actual mass was calculated to be **14864 kg**. It was therefore seen that the mass reported in Table 3-3 is an overestimate. The 10% clearance on the tubes and end cap is for the outer longest tube. This means that there are other tubes which the 90% L_s shown in Table 3-3 does not hold and needs to be accounted for. The shortest inside tube can be estimated to bend at the centre of the bundle, about a shell radius away from the outer tube. Another factor not taken into consideration is the fact that the tubes do not extend to the end of shell at inlet and exit of tubes. Taking both this two factors into consideration yields the average tube length of about 75% L_s. The mass of the tubes was calculated with this new assumption and was found to be **15504 kg**. The error after taking this into consideration is 4.3% compared to the initial one of 25.1%. The same estimation was done for a HPH 6 using dimensions given in [63]. The mass found using the number of tubes estimated was

found to be **14172 kg** while the real mass using area was found to be **13018 kg** and an error of 8.8%. The mass obtained from the method of Kakac is higher because the number of tubes estimated is the maximum that can be fitted and not exactly what is fitted into a shell.

The mass is incorporated into the model as the area and the thickness as seen in Figure 3-20.

3.5 Pressure Drop Determination

The pressure drops in the tubes and on the shell side are not reported for the data that was made available. So there is no methodology for determining this pressure drop from data. Therefore, the model is built with negligible pressure drop on the shell side. The pressure drop in the tubes is only attributed to the frictional pressure drop for smooth tubes, and the inlet and exits of tubes. The implementation of the pressure drop will be shown in section 3.6.

3.6 Detail Model Description

This section looks at the model components and their significance in building up the entire FWH model. The inputs will be described in each case with the simplifying assumptions in some cases. The model description will be separated into three sections; the de-superheating, condensing and sub-cooling sections of the heater. The model will be presented for the HPH7 at a 100% load case.

Model Assumptions and Limitations

- No pressure drop in the analytical determination of the HTC, but model built with pressure drop (negligible compared to absolute pressures) on both streams to allow for flow.
- The heat energy (transfer) on the shell side can either be removed from a flow resistance element or node before it. It would not make any difference as there is no length associated with the shell side. On the other hand, the heat energy has to be transferred and distributed along the tube length. And all heat transfer elements have to be connected to the pipe elements on the tube side.
- The shell material is assumed to not take part in the heat transfer, either for steady state or transient scenarios.
- No heat is lost to the atmosphere in developing the analytical model.
- The model has level control capabilities, but there are no control loops in place.
- The analytical model is realised for 40% to 100% load, and the Flownex model is expected to give credible results for the same range. Below 40% the model can still produce results as all trends were made to range from 0% but may not be as accurate. This is because there are no working conditions reported for conditions lower than 40%.

- No significant heat energy determined from analytical model on the sub-cooling zone, but some heat energy is removed on the Flownex model to avoid flashing of the condensate back to steam.

Figure 3-8 shows the three different parts that will be described in this section circled with three different colours on the complete FWH model.

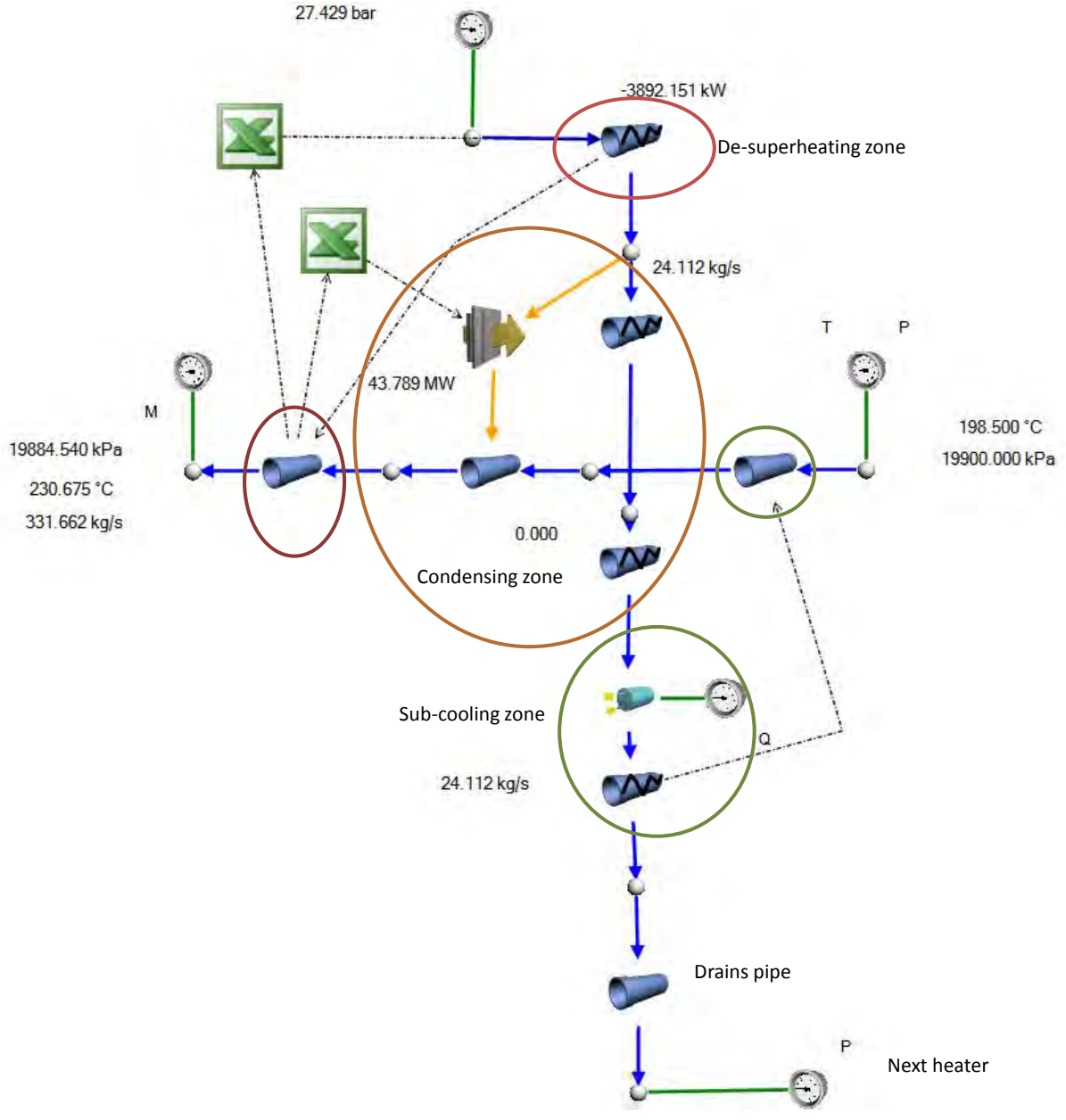

Figure 3-8: Complete transient model of a FWH showing with three different zones.

De-superheating component

In section 3.3, the de-superheat energy for various loads was determined analytically. The heat energy is removed from the bled steam and added to the feed-water on the de-superheating zone. The shell side of the de-superheating zone is modelled as a flow resistance element with a relatively large flow admittance so as not to create any significant pressure drop. Figure 3-9 shows the de-superheating zone shell side component with the inputs options. The heat input to the shell is specified as negative under inputs, and at 100% load in steady state was found to be 5445 kW and is shown in Figure 3-9. The Excel component changes this value according to the curve-fitted data as a function of feed-water mass flow shown in Figure 3-4.

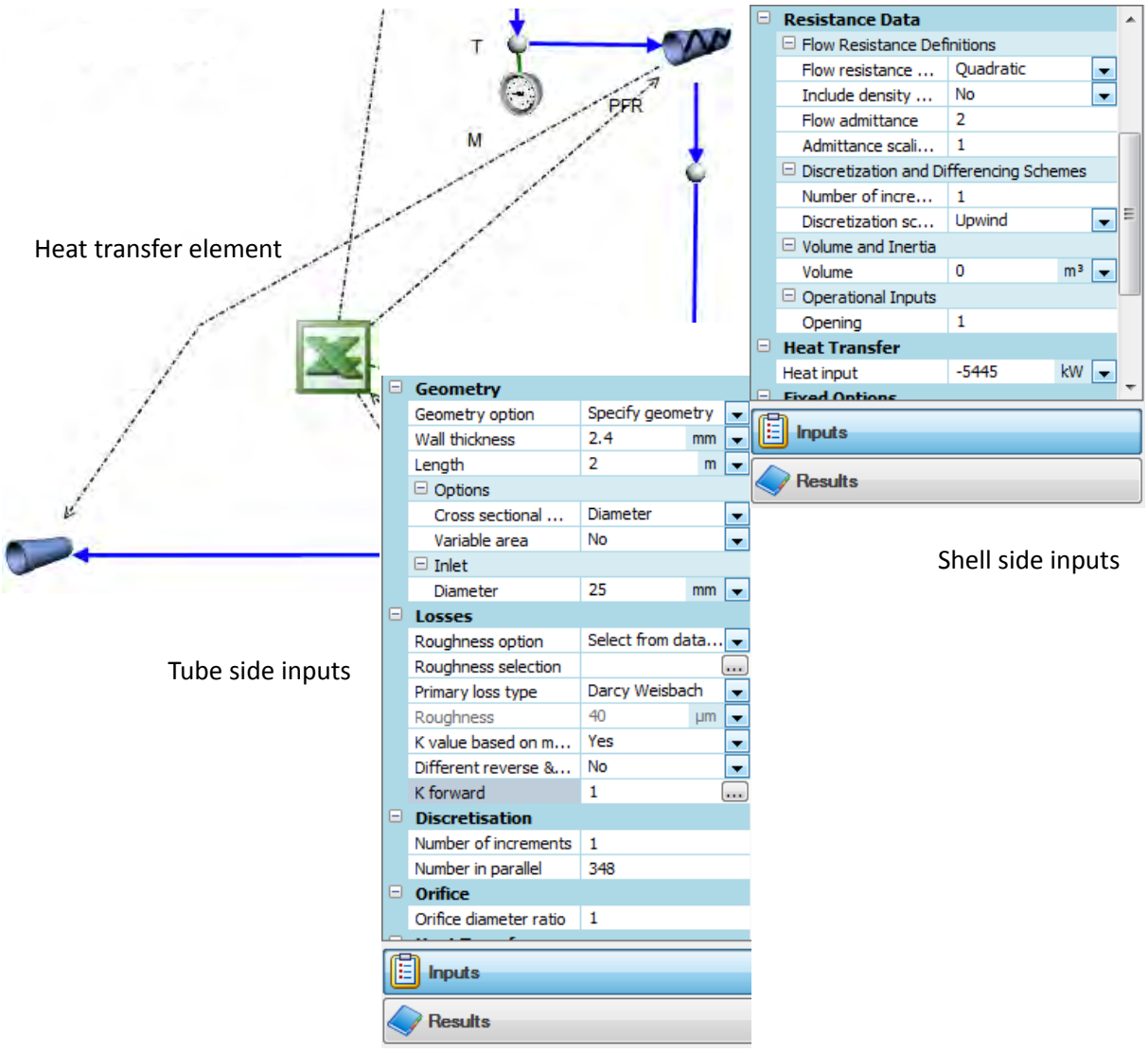

Figure 3-9: De-superheating zone showing both inputs of shell and tube sides.

The volumes of all flow resistance elements are set to zero to ensure that the full volume of the shell side can be accurately accounted for in the two-phase tank where the condensate collects. The tube side is modelled using some of the geometry from Table 3-2 and the pressure drop is

estimated from the working mass flow. This is done by specifying the tubes roughness and loss coefficient, *k*, value which is specified as 1 as seen in Figure 3-9. The coefficient is for the flow exiting to a larger diameter as the feed-water leaves the FWH.

The number of pipes used in the model is estimated from using typical FWH tube diameters given in section 3.4 such that the design point flow is possible in the number of pipes chosen. So the number of tubes can always be adjusted to accommodate flow of the FWH being modelled. The heat input is specified as positive for the tube side because energy is being added. The data transfer link is used as a heat transfer element in the de-superheating zone as also shown in Figure 3-9. The link takes the value of heat specified to be lost in the steam side and adds it on the tube side. The downfall to using the data transfer link in transient situations is that the effects of thermal mass are not captured. However, in the steady state mode operation, the properties at inlet and outlet of the de-superheating zone can still be accurately predicted as the thermal mass plays no significant role in steady state operation.

Sub-cooling zone

In the analytical determination of the heat energy transfer in the Sub-cooling zone, for the Kriel HPH 7, it was found that there is insignificant heat energy transfer from the heat balances used. However for modelling purposes, it was included in the model to avoid “flashing” of the saturated liquid as it flows in the drain pipes. The sub-cooling zone is modelled as flow resistance the same way as it is in the de-superheating zone. The only difference in this case is that the amount of heat that is removed from the saturated liquid on the shell side. The heat to be removed was estimated from the maximum load working conditions such that the saturated liquid in the pipes does not flash back into steam for the given flow rate. The same amount of heat energy is removed from the steam side for other plant load conditions because it was found that adding that amount of energy to the feed-water does not change its temperature significantly. The data transfer link is also used as a heat transfer element as shown in Figure 3-10, taking the energy lost on the shell side and adding it to the tube side.

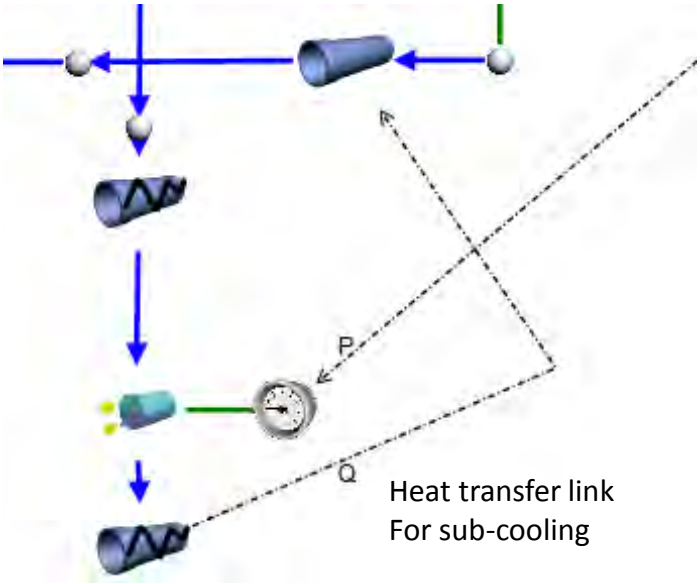

Figure 3-10: Sub-cooling zone with the data link as heat transfer element.

The tube side pressure drop is attributed to the roughness of the tubes and the entrance loss coefficient to the tubes. The loss coefficient is specified under the 'k forward' option in the similar manner as in Figure 3-9, but for entrance the loss coefficient is 0.5. Coupled to the sub-cooling zone is the level of liquid in the shell side and this is modelled as a two phase tank between the sub-cooling and condensing zones as shown in Figure 3-11.

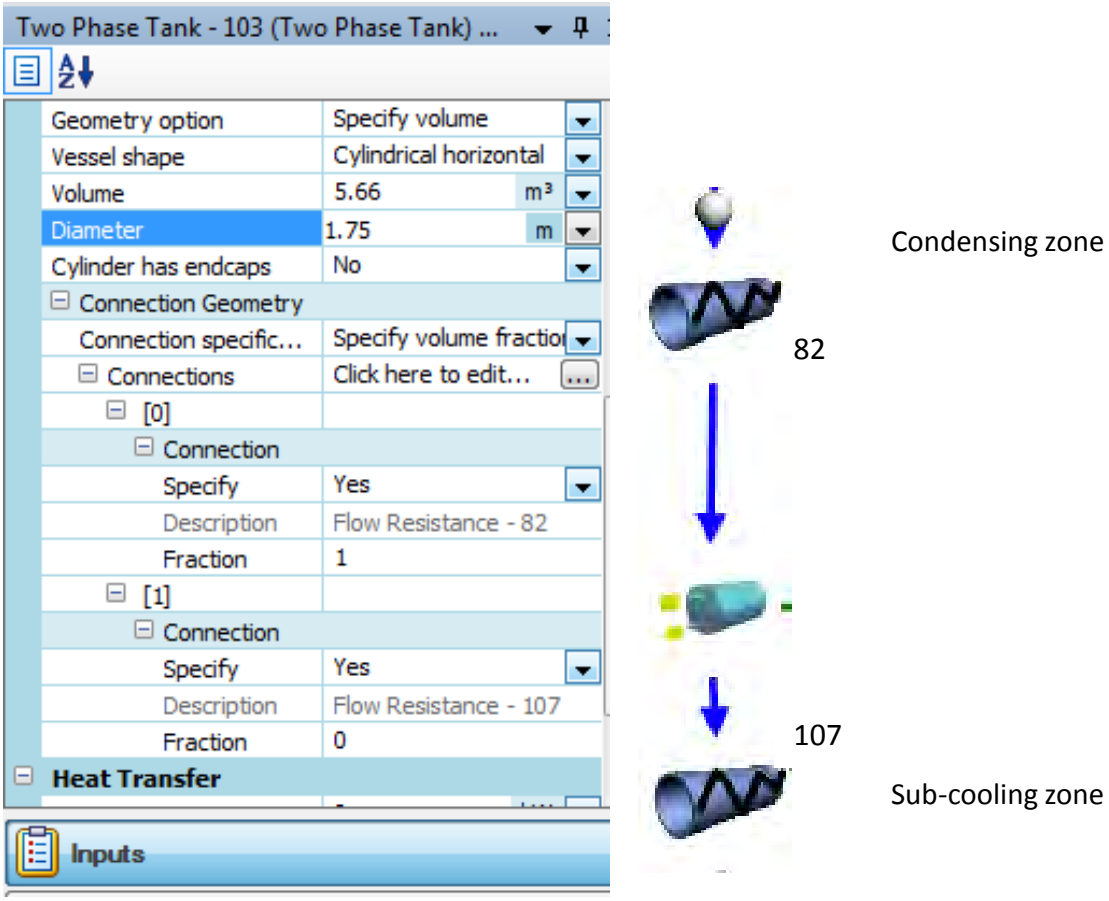

Figure 3-11: FWH shell and inputs required in the model.

Both the volume and the diameter are entered as inputs of the shell. The volume of the tank cannot be specified as total shell volume as some of the shell volume is occupied by the tubes. To get an approximate volume to be occupied by steam and level of condensate, the correlations used in section 3.4 are applied to determine the free volume. This is done by taking 10% of the outer clearance volume and the 13% of the remaining 90% due to tube arrangement added together. The total shell volume was found to be 26.049 m^3 yielding free volume of 5.66 m^3. Even though this approach does not give a good enough level change approximation, it sets a starting point in understanding the effect of submerged tubes and level variations in a FWH. The dynamic heights are taken into consideration by specifying the inlet of the steam to be at the top of the shell and exit at the bottom. In steady state solving the level is maintained by specifying the quality of steam within the shell, and this gives the ratio of the steam to liquid. In transient situations the pressure and quality are specified for the shell cavity to initialise the model and are then turned off as the simulation is started to let the dynamics be controlled by the fluids and heat transfer properties.

Condensing zone

The condensing zone is the most critical in the model as it has most inputs that depend on the analytical solutions determined in section 3.3 earlier. On the shell side, like all the other zones, the flow resistance element is used to exclude the volume effects. The only difference is that there are increments specified as shown in Figure 3-12 below.

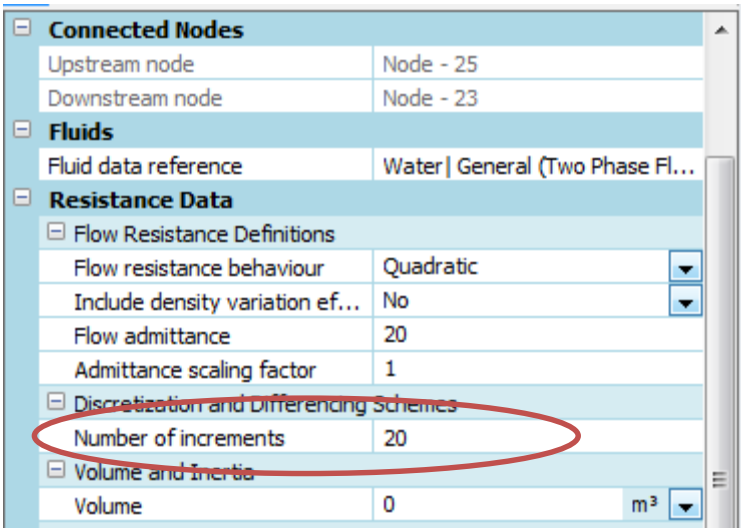

Figure 3-12: Condensing zone shell side inputs.

The increments are so that the temperature profile of the feed-water, on the tube side, across the condenser is close to realistic one and is not just a straight line from inlet to outlet temperature. All components that form the condenser are then to have the same number of increments. So the shell side of the condensing zone also has 20 increments as a result and all other inputs are the same as the tube side. The length of the tubes is estimated based on the length of the shell length. Even though the length might not be important with respect to the condensing area, it is still necessary to accurately capture the frictional pressure drop. In the condensing zone, only friction contributes to the pressure loss since it connects the other zones and there are no inlets or exits. The shell and tube sides on the condensing zone are connected by a heat transfer element as shown in Figure 3-13 and the heat transfer characteristics are set as inputs.

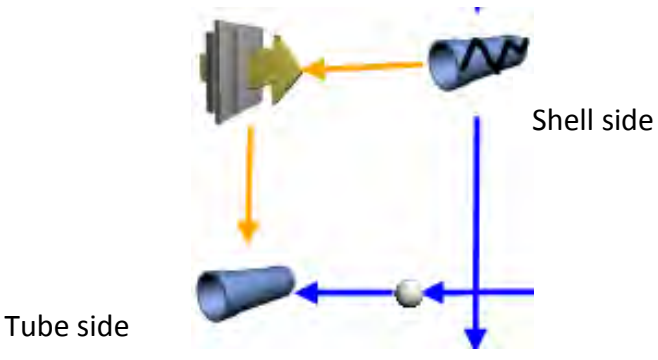

Figure 3-13: Heat transfer element connecting shell and tube sides.

The overall HTC of the element has three components to it; the internal tube convective HTC, tubes conduction, and the shell side convective HTC. The tubes conduction inputs are shown in Figure 3-20 and are the same for all load conditions. The conductivity was seen to vary with temperature but does not to change significantly, ± 3 W/mK, in the operating range. The 100% load conductivity was used for all load characteristics, when the tubes are at 240 ℃. The external HTC was chosen to be ten times (FX=10) more than the internal HTC for all load characteristics and varies as determined in section 3.3. The HTCs were determined combined with the area and in the inputs of the heat transfer element the convective areas are specified to be 1 m^2 as shown in Figure 3-14.

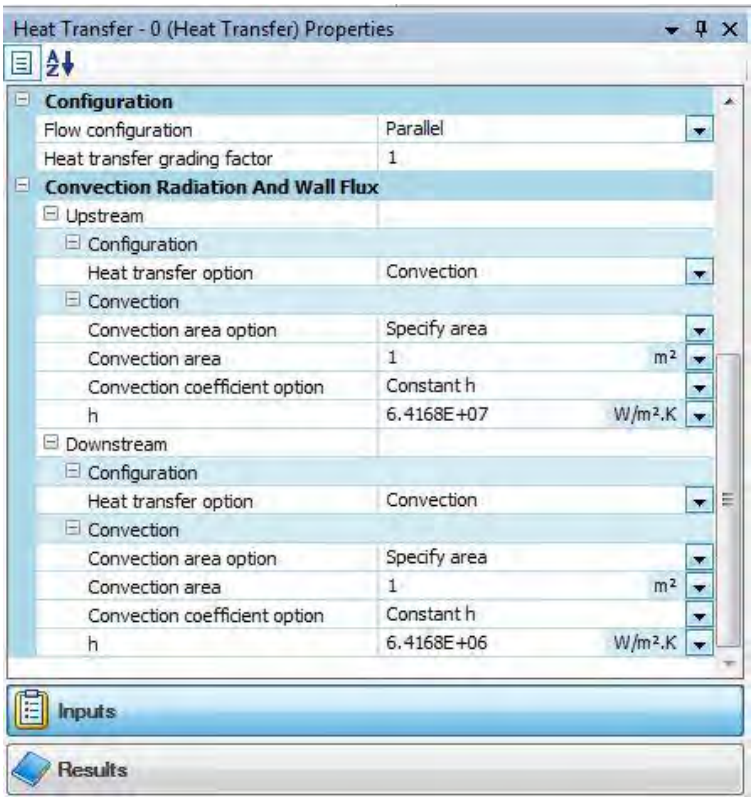

Figure 3-14: Convection HTC inputs on a condensing zone.

This implies that the HTC is input combined with the area under the convection coefficient option by specifying it to be constant in the dropdown options. The analytical solutions are presented in the Appendix A.

Once again the Excel component drives the HTC for different feed-water mass flows.

High Level Inputs

The high level inputs for the heater are the inlet properties of the two streams of the FWH and were obtained from the heat balance of the Kriel HPH 7. They are not necessarily part of the model, but are properties from other systems if the FWH was connected to a whole power plant

model. These inputs are driven by an Excel component which uses as input the plant load condition.

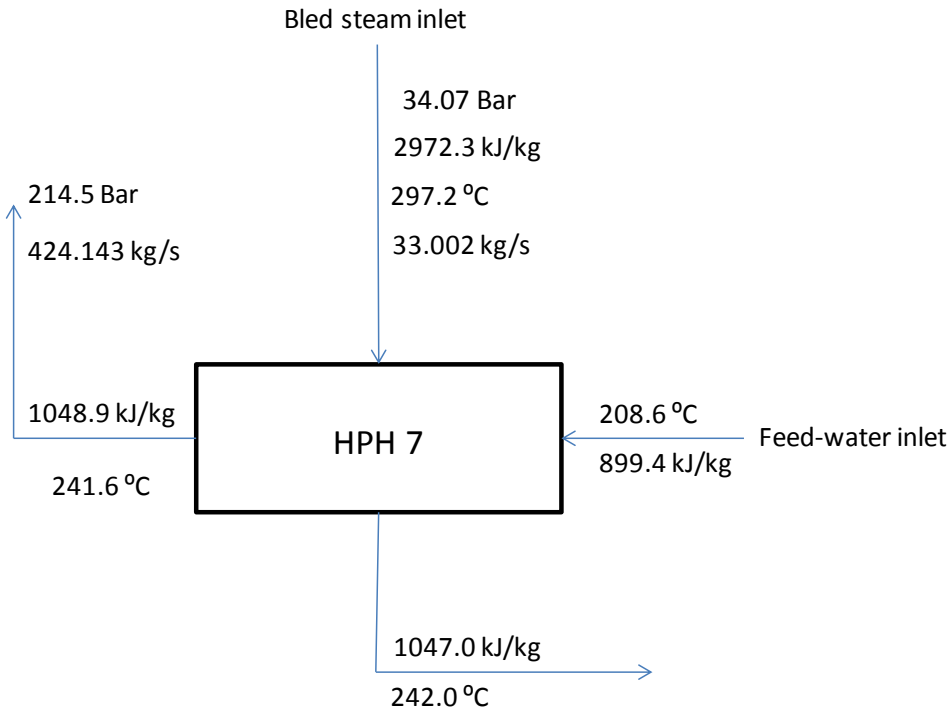

Figure 3-15: Typical HPH 7 high level inputs and results.

Figure 3-15 shows the inlet properties of the shell and tube side presented as vertical and horizontal lines with arrows respectively for maximum load capacity.

In steady state, the inputs are set under the boundary conditions element at both the shell and tube inlet. The shell side inlet conditions are shown in Figure 3-16 to demonstrate.

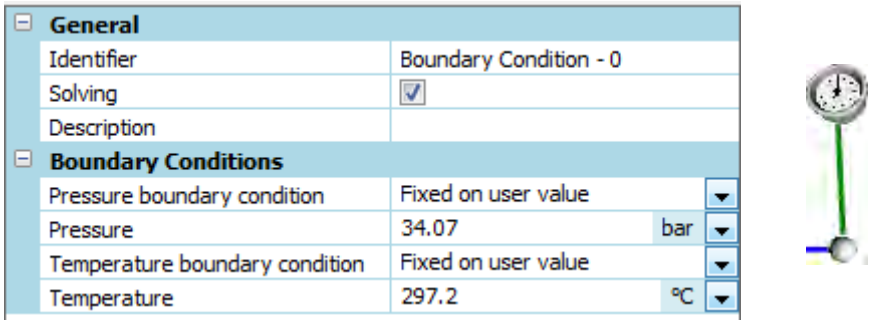

Figure 3-16: Inputs to the shell side inlet properties.

For every load condition, the high level inputs are set and not altered in solving for the steady state scenario for a given plant condition. This is not the case in transient situation where characteristics are changing depending on the demand of electricity. On a whole plant point of

view, the feed-water mass flow can be seen as the driving factor in determining at what load the plant is operating.

Steady state model

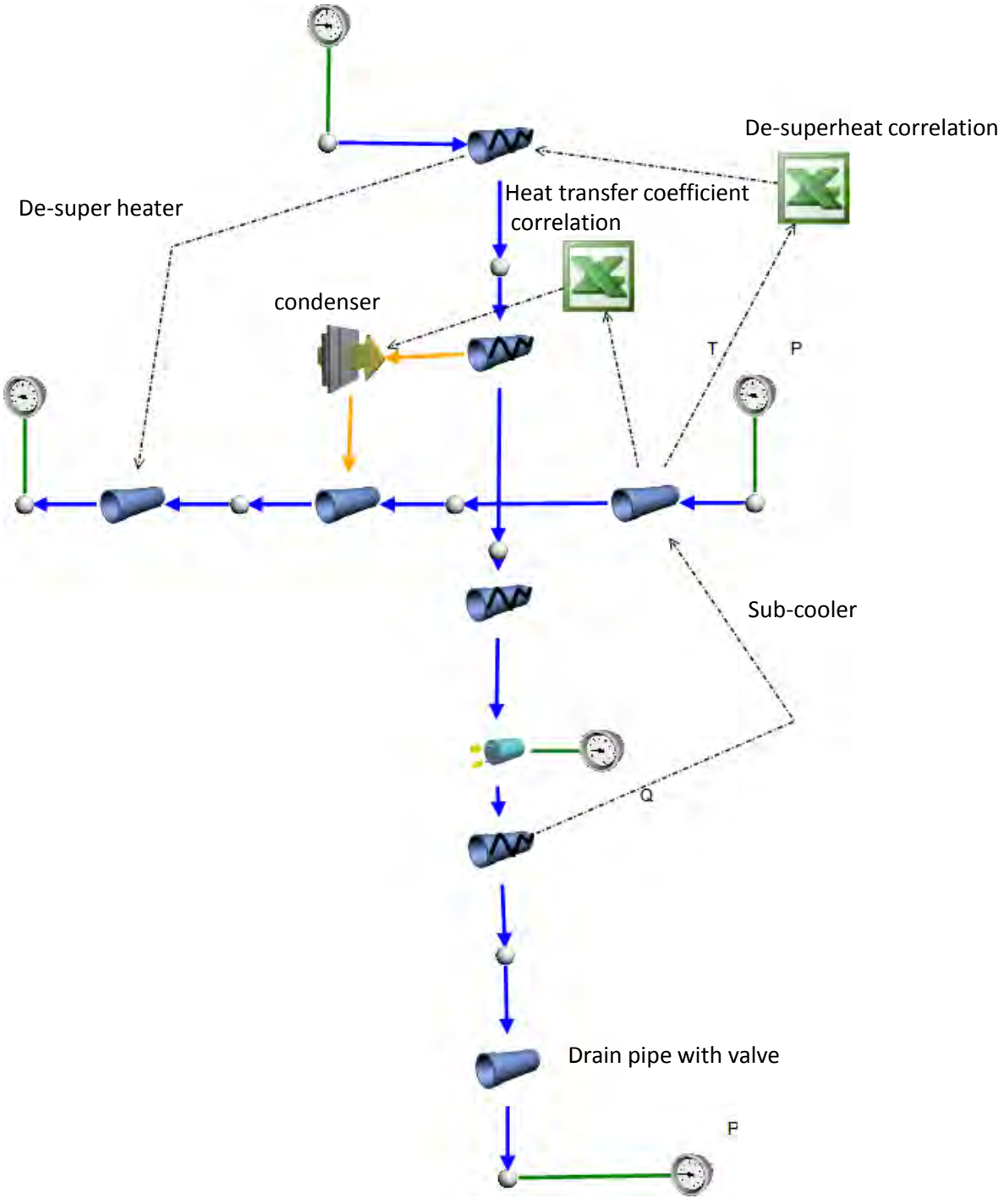

Figure 3-17: Steady state Flownex model of a FWH

Figure 3-17 shows the steady state model of a FWH on Flownex. For any steady state working condition to be investigated, the high level inputs have to always be specified for that condition. The amount of de-superheat to be extracted from the steam is determined from the relation given

in Figure 3-4 by reading up the feed-water mass flow rate using the "links" as shown in Figure 3-17. The internal and external convective HTCs on the condensing zone are also scripted in the excel component and change with different load conditions. For every load condition specified by the "USER", the designer function on Flownex is set up. This is to determine the amount of steam mass flow required to fully condense in the condensing zone for the given heat transfer characteristics. The Flownex designer function is used to adjust an orifice in the drains-pipe to allow the correct amount of bled steam associated with the heat load inside the heater. This is similar to the controller changing the value in practice such that the level in the tank stays constant. For all cases in the steady state Flownex model, the pressure in the next FWH is assumed to be 100 kPa below the inlet pressure to drive flow. In a complete process model, this pressure will be determined by the receiving heater.

Transient Model

The transient model high level inputs can change depending on the feed-water mass flow. This then changes the heat transfer characteristics in the heat transfer element in condensing zone according to Figure 3-22. The heat transfer on the de-superheating zone is also driven by the amount of feed-water mass in a similar way as for the steady state. The bled steam mass flow into the FWH is determined by the heat transfer characteristics and the pressure drop at the heater inlet. Depending on the heat duty on the condensing zone, the FWH extracts enough steam such that it leaves the zone fully condensed.

The model has to be solved in steady state to initialize the transient. In this steady state, the quality inside the shell is specified and the pressure at the exit of the drains line is set as the pressure of the next heater, HPH 6. The drain pipes to the next heater have a non-return valve to prevent the flow of condensate back into the shell in case of malfunction. The same valve is put in place in the pipeline that carries bled steam into the FWH to prevent blow back of steam back into the turbine. The transient model of a FWH is shown in Figure 3-8.

When running transients, the quality of the tank is released and the level changes depending on the characteristics of the FWH and plant as a whole. To maintain the level within the tank, a valve (orifice) in the drains line can be manually opened slightly to lower the level or closed to increase the level of condensate in the FWH. The changing of the orifice allows for more or less mass to flow out of the shell per given time. In this model the exit properties of both streams and the condensate level variations are monitored and compared to data.

3.7 Pre-processing Results and Model Implementation

The high-level inputs for the transient model have to be converted into some form of polynomial correlations that are a function of the feed-water mass flow as mentioned in section 3.6. From the working conditions of the heater at different loads, trends are predicted for each property using regression analysis. The estimate of coefficients of the functions for the different properties is only up to the second order. In some cases the coefficient of the second order is so small that it can be neglected, and leaving out the whole term does not change the accuracy of prediction.

The parameters are defined in the model inputs and for different heaters different coefficients will result and the user can manually adjust the coefficients of correlations accordingly.

The feed-water mass flow is the main parameter that changes with the load and all the other parameters are driven by the changing mass flow.

The sub-cooling heat was found to contribute less than 0.5% of the total heat in the analytical solution for the Kriel HPH 7 and not including it in the model/analysis would not change the output results on the Flownex model. Also, from a temperature point of view, the difference between the condensing temperature and drain temperature was found to be about 0.1˚C for all loads, hence not significant heat is transferred at the sub-cooling section for the HPH 7. However, as already explained, there is a certain amount of sub-cooling required to avoid flashing and resulting in numerical instabilities. A fixed sub-cooling load of 800 kW was therefore added. This does not affect the outlet properties of both streams significantly.

The HTC calculated in section 3.3 on the condensing zone was tested on Flownex for a 100% load condition with the overall HTC split into two convective parts as shown in Appendix B. The superheat is extracted from the steam stream before it goes to the condensing zone in this test. The model on Flownex is initially implemented without the layers across the HX as a conductive medium. Figure 3-18 shows the inputs of heat transfer element and the highlighted layers option is left empty to exclude effects of conduction.

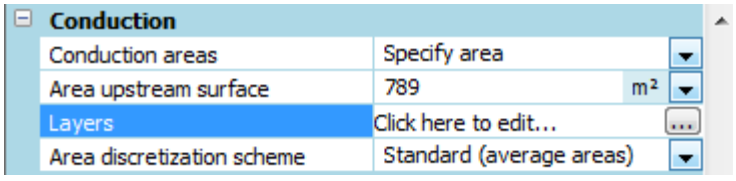

Figure 3-18: Inputs of the heat transfer without conducting layers.

The model produced quality at inlet and outlet of 1.001 and 0 respectively as seen from Figure 3-19. The energy content across the HX element shown in Figure 3-19 compares well with the one determined analytically in Appendix A for the 100% load case.

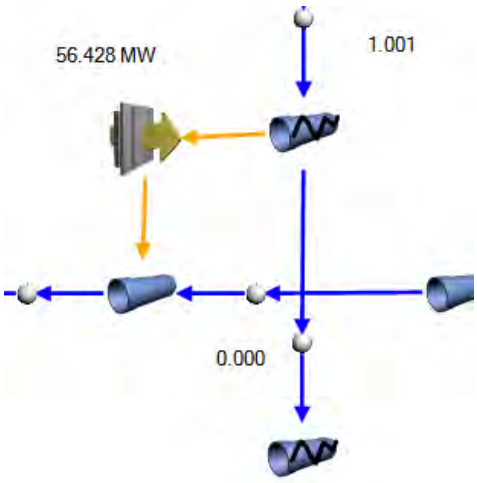

Figure 3-19: Condensing zone section showing inlet and outlet quality, and heat energy without conduction

For illustration purpose the thickness of the HPH 7 given in [63] is used to demonstrate the effect of adding a conductive medium/layer. However, this does not necessarily mean all heaters are of the thickness specified and can readily be changed in both the analytical solution and Flownex model. The conductivity resistance of the whole tube bundle was found to be 1.742 x 10^6 W/K. The new convective HTC is determined with the effect of conduction and the same assumption of the feed-water to shell side HTC ratio in Appendix B is used. The overall convective HTC is then obtained to be **6.4281 x 10^6 W/K** compared to the **4.52985 x 10^6 W/K** where there was no conduction. The conductive resistance is incorporated into the model by adding "layers" in the heat transfer element as shown in Figure 3-20.

Layers	Click here to edit...	...
[0]		
Description		
Geometry		
Thickness in element ...	2.4	mm
Thickness in cross dir...	1	m
Number of nodes	20	
Area downstream sur...	789	m²
Material Data		
Material option	Select from data reference	
Material major conduc...	Parallel	
Material	Carbon Steel - AISI 1010| Met...	
Area discretization scheme	Standard (average areas)	
Configuration		

Figure 3-20: Inputs to the conductive layers option.

Adding the "layers" for conductivity and adjusting the HTC in the condensing heat transfer element to the newly obtained one yield the same results as those without conduction in terms of the quality and energy content transferred across as can be seen in Figure 3-21.

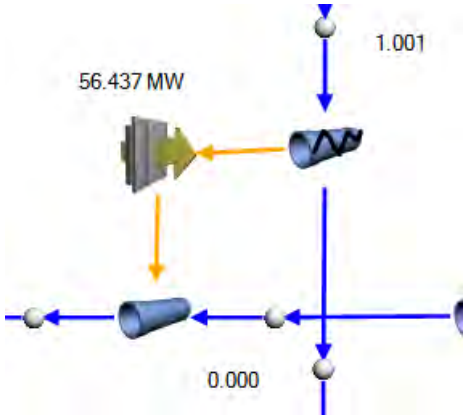

Figure 3-21: Condenser section showing inlet and outlet quality, and heat energy with conduction.

The analytical solution, for all load characteristics available from plant data and acceptance tests, of HTCs is given in Appendix A with all assumptions as described above. The above analysis shows that Flownex takes the effect of conduction into consideration through addition of layers, and accurately predicts its effects.

From the results obtained on the HTCs for different load characteristics of the power plant, a graph is plotted as shown in Figure 3-22 to relate the heat transfer to the feed-water mass flow rates. For graphical purposes, the HTC at maximum operating point is included and is at 424.143 kg/s.

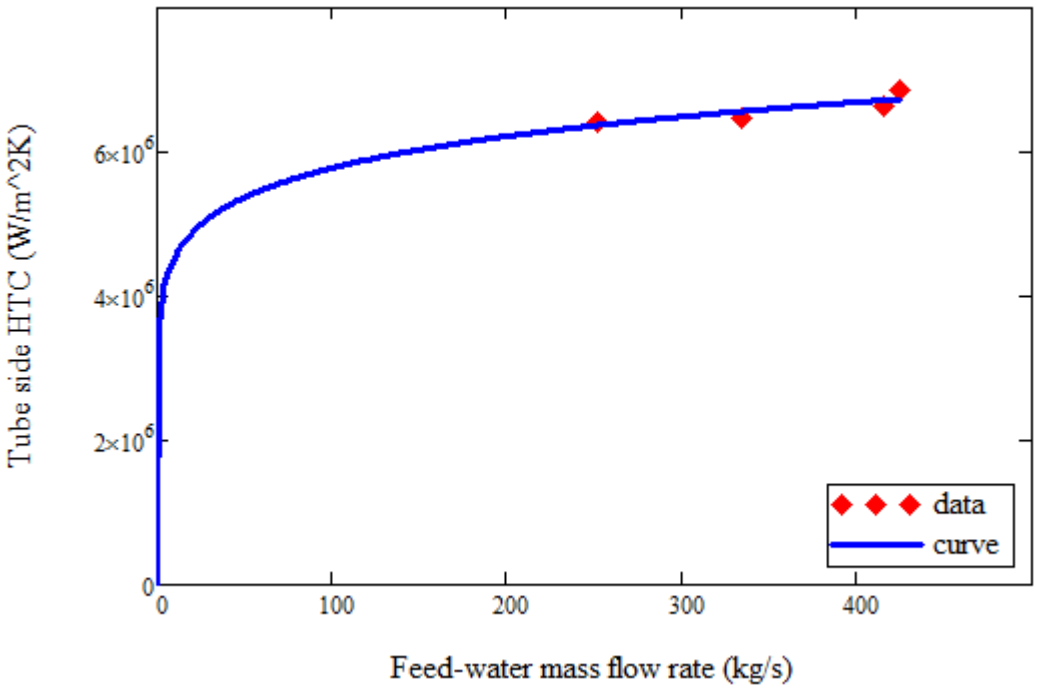

Figure 3-22: Feed-water side HTC varying with load.

Four operating points were used to predict the behaviour of the tube side HTC. From literature in section 2.3.2 it was shown that the HTC on the tube side takes the power law form in terms of the flow rates and a power law fit was done on the four points as shown in Figure 3-22. The resulting correlation for the HTC was found to be:

$$h_{Tube} = 3.549 \times 10^{6} m_{fw}^{\ 0.106}$$

The most important aspect in the analysis of the HTCs is that the tube side convective HTC does not exactly follow the expected trend. This is because it is made to depend on the outside shell HTC which is assumed to be just a multiple of it in this analysis. However, it is expected to take form of the overall HTC which would still be of a power law form but distorted due to the bit of effect by the shell side HTC.

4. Model Validation, Observations and Discussions

This section looks at validating the model by looking at some of the key parameters under different load variations and working conditions of the FWH. In steady state operation, the main parameters which were results are the amount of bled steam required to fully condense across condensing zone for the given heat characteristics, exit temperatures of the two streams and the amount of heat transferred. The model working condition is outlined and the initial set-up is given for the different model runs and some observations are made for different scenarios.

4.1 Steady State Tests

4.1.1 Conditions and system set-up

The steady state model is setup as explained in section 3.6. The high level inputs for each load characteristic are set in the model with the corresponding heat characteristics of the condensing surface and de-superheating zone. The quality of the steam in the shell is specified for a given inlet pressure and mass flow rate to indicate the level in the shell. The model solves for the bled steam mass flow rate for each load case. This is done by setting up a designer on Flownex as shown in Figure 4-1. All the bled steam must be fully condensed (quality = 0) when exiting the condensing zone.

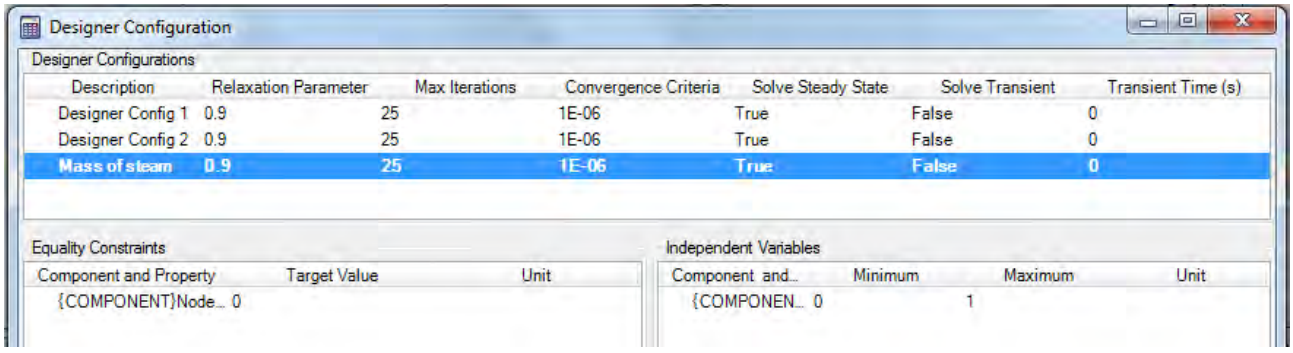

Figure 4-1: Designer set-up to determine the required Bled steam mass flow for thorough condensation.

4.1.2 Model Results

The steady state model was solved for the four known load cases, and the results are reported in Table 4-1. The condensate temperature from the model is taken to be the temperature of the two phase fluid in the shell or saturated liquid as it leaves the condenser. The heat transfer reported is the heat in the condensing zone only.

Table 4-1: Flownex steady state model results.

Plant condition	Bled steam mass flow (kg/s)	Feed-water exit temperature (˚C)	Condensate temperature (˚C)	Heat transferred (MW)
40%	8.387	195.723	193.721	16.481
60%	15.229	215.14	213.325	28.836
80%	23.121	229.26	228.249	42.267
100%	32.016	241.0	240.802	56.439

It was found that the model has a strong dependency on the pressure drop in the shell side components. And the pressure drop was kept to a minimum while still maintaining the flows required. The effect of higher pressure drop on the shell side is shown in Table 4-2 with pressure drops of 0.2 kPa and 56 kPa used to demonstrate. From the results it is seen that a lower pressure drop results in a higher outlet feed-water temperature and hence better performance. This effect was also looked into by Cumo [12] in the discussion of the thermal and hydraulic rating of HXs. The same conclusions on performance were made by Cumo.

Table 4-2: Effect of pressure drop on FWH performance.

Feed-water exit temperature (˚C)	Condensate temperature (˚C)	ΔP (kPa)
228.924	228.84	0.2
227.72	227.726	56

The pressure drop is dependent on the geometry and size of the FWH and its components. And Patel [66] comments that in all HXs, there is a close physical and economical affinity between heat transfer and pressure drop. The model results in Table 4-1 were generated with pressure drop of 0.51 kPa on the condensing zone and an average pressure drop of 28 kPa from inlet to outlet on the shell side of FWH at 100% load.

4.1.3 Actual Plant Results

The heat balance for the Kriel power station FWHs was used as the actual plant data results and the results are shown in Table 4-3. The acceptance data results for the tests carried out at Kriel were used to verify some of the heat balance values used.

Table 4-3: Actual FWH 7 working data.

Plant condition	Bled steam mass flow (kg/s)	Feed-water exit temperature (˚C)	Condensate temperature (˚C)	Heat transferred (MW)
40%	8.632	196.4	194.3	16.929
60%	15.194	215	213.3	28.653
80%	23.145	229.2	228.1	42.141
100%	32.037	240.8	240.9	56.403

4.1.4 Discussions

The model results in Table 4-1 are seen to be in the range of what the real plant produces. Figure 4-2 shows the percentage errors of the model results compared to the real plant data, and the errors for all measured load cases are below 3%.

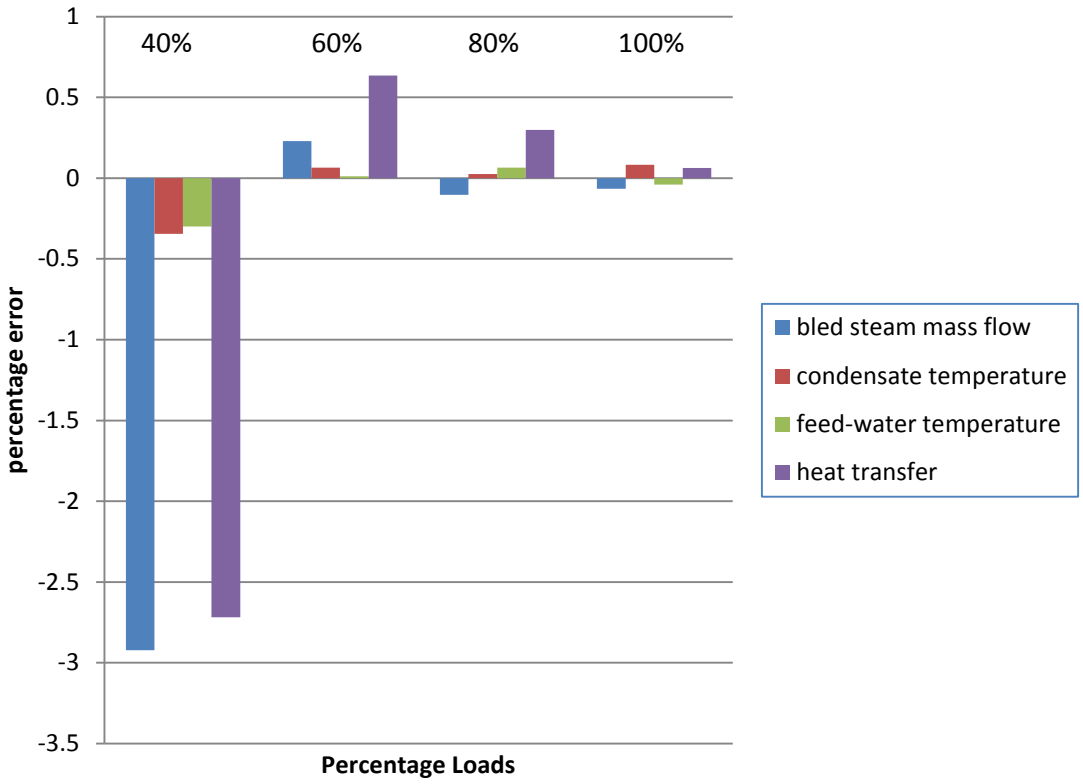

Figure 4-2: Percentage error in the model results for different load conditions.

At 100% and 80% loads the bled steam mass flow rate from the model results compared very well with the plant data results. For both the load characteristics the errors for all measured parameters are less than 0.5%. At 40% the bled steam mass flow rate required to fully condense was found to be less than that given in the plant data and the error was found to be 2.83%. This is

as a result of the heat transfer which is less by 2.64%. This error is most probably due to the curve fits used to approximate the heat loads for the various zones of the FWH.

The rest of the errors may be attributed to properties which changes slightly due to the pressure drop as calculated in Flownex. These pressure drops were not incorporated in the analytical process. It was shown in [1] that the effect of assuming no pressure drop results in an error of less than 5%. The same model assumptions were made in [61], before Barszcz model [1], and the same conclusions were made. So the assumption of no pressure drop was validated, and the combined pressure drop in the de-superheating and condensing zones of the Flownex model was found to be about 1.01 kPa. For bled steam at about 20 bars, a pressure drop of 1 kPa does not change the latent heat significantly.

It can therefore be concluded that the model is a close representative of the analytical solution and a good enough estimation of what the FWH does in steady state operation.

4.2 Transient Tests

4.2.1 Condition and system set-up

Simple simulation with model running at steady state 80% load

The model is setup with high level inputs set for 80% load conditions. The quality on the shell was set to initialize the model in steady state. When initiating transient simulation the shell properties are released and let to solve based on high level inputs and extraction rate of the condensate without any change in high level inputs.

Ramp up 80% to 100% load

The model is initiated at 80% load with the high level inputs set for a FWH working at this load. The shell quality is set in the initialization of the model in steady state. As the model is started, the quality on the shell is released and the pressure starts to change depending on the model dynamics, high level inputs and heat transfer characteristics. After 2 seconds the feed-water mass flow rate is ramped up linearly from 80% load to mass flow that corresponds 100% load in a space of 200 seconds. The outlet temperatures and shell side flow rates are recorded as the load goes from 80 % to 100% load.

4.2.2 Model Results

Simple simulation with model running at steady state 80% load

The model was let to run for 300 seconds without changing any of the high level inputs or the drain extraction rate. Figure 4-3 shows the exit temperatures FWH.

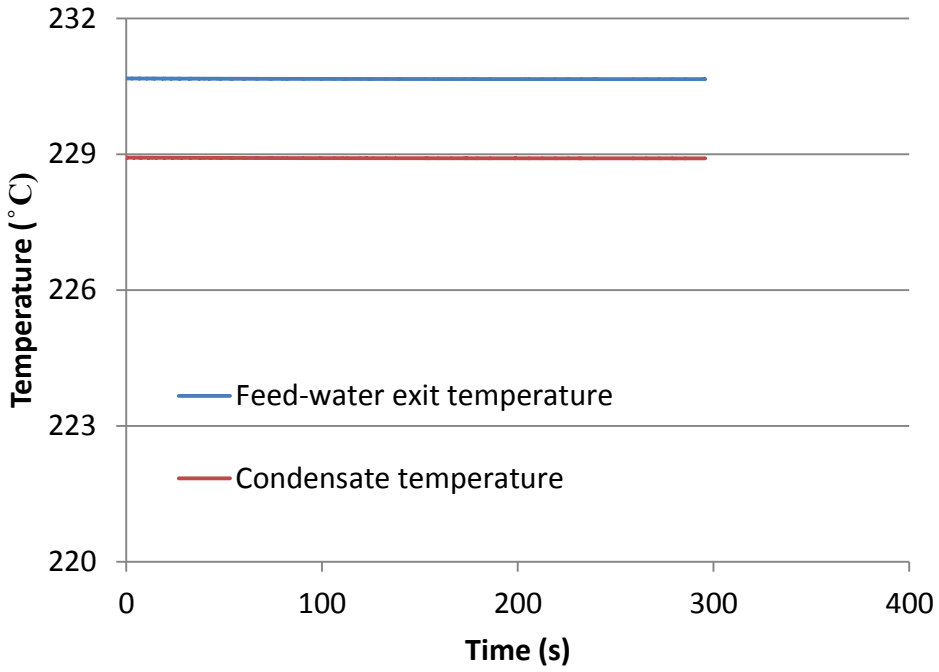

Figure 4-3: Exit temperatures of the two FWH streams at 80% load.

From Table 4-3 it was reported that the feed-water exit and condensate temperatures at 80% were 229.2 ° C and 228.1 ° C respectively. From Figure 4-3 the feed-water exit temperature is higher, 230.4 C, than plant acceptance data and this could be due to inaccuracy in predicting the heat transferred in the condensing zone.

Ramp up 80% to 100% load

The model was run with conditions as described in the previous section. Figure 4-4 shows the mass flow of the bled steam, the condensate drain mass flow rate and the level within the shell. In the ramping stage, the bled steam mass flow starts off more than that of the condensate being drained. As a consequence, the level inside the shell starts off increasing as shown in Figure 4-4. As the load is increasing, the pressure at the inlet of the steam side increases and thus increasing the pressure within the shell. The higher shell pressure results in in a higher pressure drop on the drains line and thus more condensate being drained. This is evident on Figure 4-4 after 50 seconds where the level within the shell settles and eventually decreases. The bled steam mass flow is seen not to increase linearly from 80% to 100% load. This is because bled steam sucked into the FWH is

dependent on the inlet pressure and the heat transfer characteristics of the condensing zone. After 200seconds, as the FWH reaches 100% load, the inlet pressure on the steam line stops increasing and the bled steams dips due to a sudden stop in pressure drop increase before settling at a steady flow rate of 33.47 kg/s.

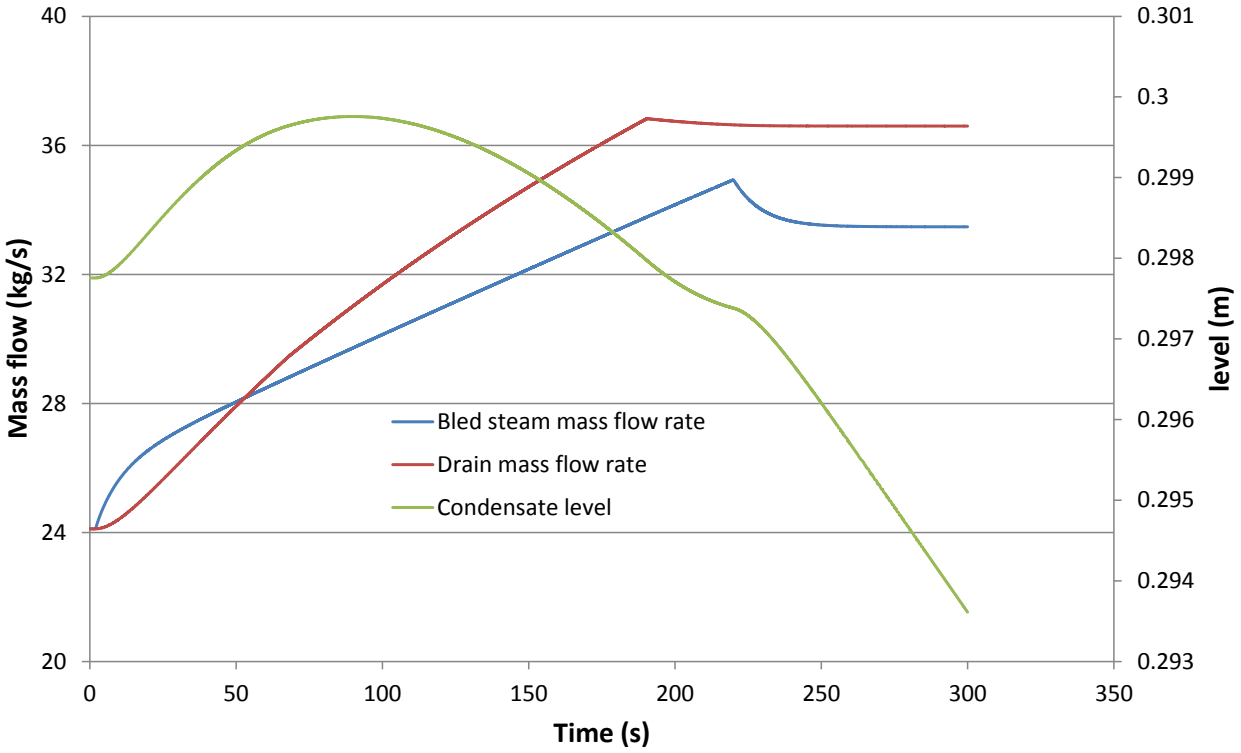

Figure 4-4: Bled steam and condensate drain flow rate, and level for changing load characteristics (80% to 100%).

In this exercise the level was not being controlled and at 100% load more condensate is being drained than the bled steam entering the FWH. To maintain a settled level one would adjust the orifice ratio to balance the mass flows in and out.

The exit temperatures of the two streams were also monitored as the plant load changed from 80% to 100%. The feed-water exit temperature starts at 230.8˚C and settles at 242˚C as shown in Figure 4-5. On the other hand, the condensate temperature starts off at 229˚C and settles at 240.8˚C at 100% load.

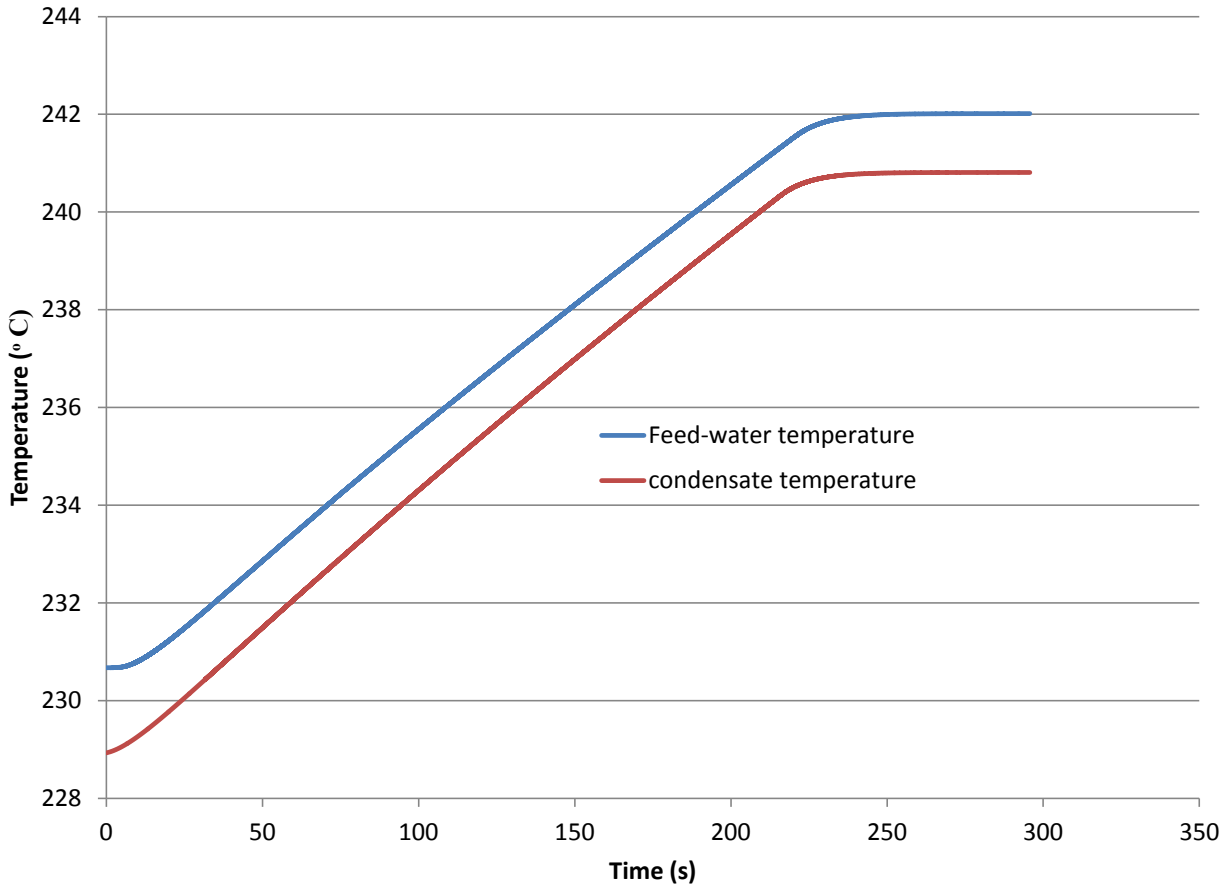

Figure 4-5: condensate and feed-water temperatures for changing load conditions (80% to 100%).

Figure 4-6 shows the heat transfer on the condensing zone during the load change. At 80% the heat being transferred was reported to be 43.78 MW and changes to 58.6 MW at 100% load. The 100% load heat transfer is higher because the model is not fully in steady state and the bled steam is a bit higher than expected.

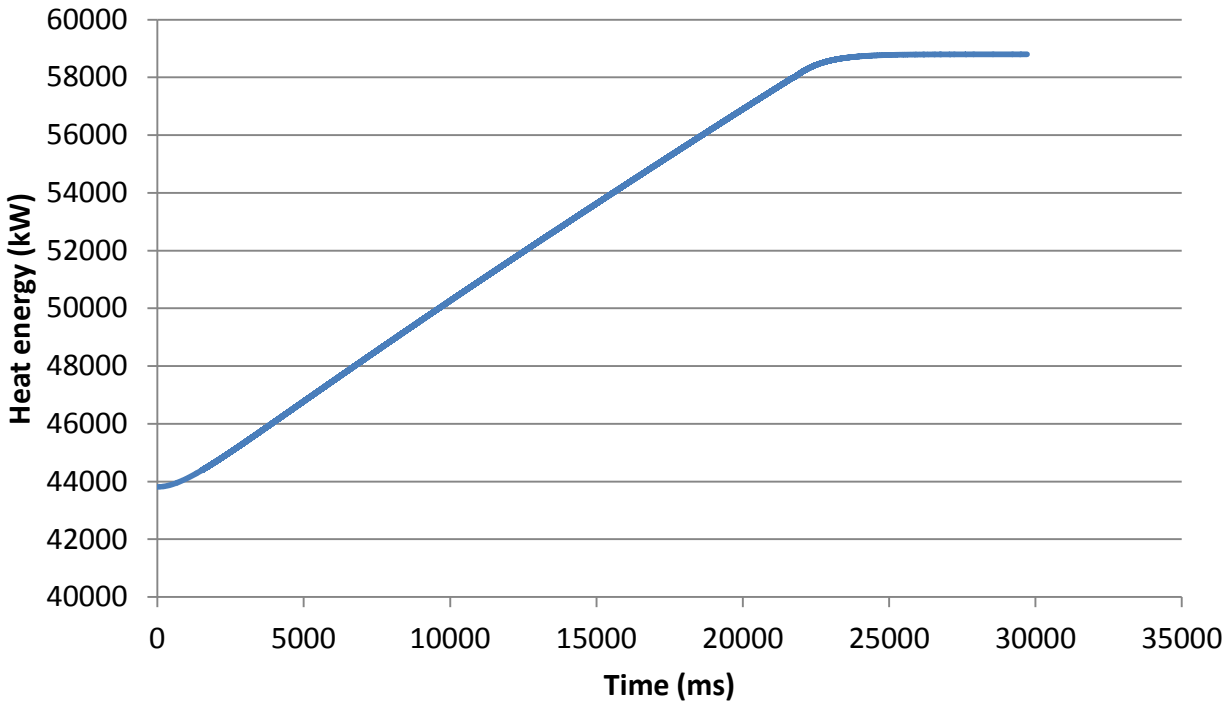

Figure 4-6: Heat transfer across FWH and the level for changing load conditions (80% to 100%).

4.2.3 Actual Plant Results

Figure 4-8 shows the feed-water temperatures of the two HPHs in operation at Kriel power station while a performance test was conducted. In the analysis only HPH 7 was considered, and even here only the HPH 7 results are of interest. It is worth noting that the feed-water temperature at HPH 6 exit is the temperature of HPH 7 at inlet. The temperature was recorded to be 211˚C as compared to 207.8˚C in the specification [3]. The inlet temperature for the transient test on the feed-water was therefore taken as 211℃ to get a good comparison with the acceptance data. The reason for the difference was attributed to the erosion of the tubes in the HPH 6, shown in Figure 4-7. The erosion decreases the tube thicknesses and decreasing the resistance of heat transfer.

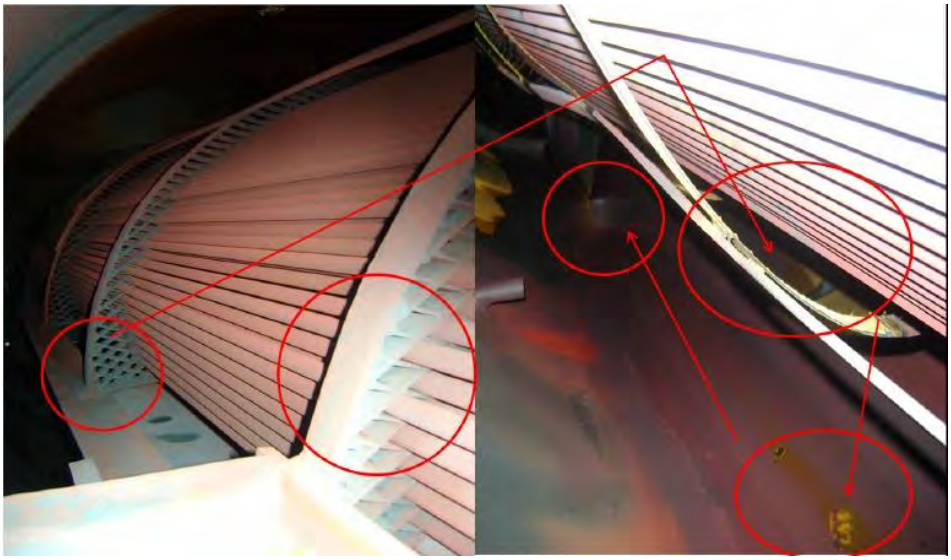

Figure 4-7: HPH 6 corrosion at Kriel power station [3].

The effect of erosion was tested on the analytical model by changing the thickness, and this was used to validate the conclusion made in [3]. The temperatures and load are also shown to fluctuate at a specified load. The feed-water temperature after HPH 7 at 80% load was recorded to be 229°C and 239°C at 98% load as indicated by the purple line in Figure 4-8 below.

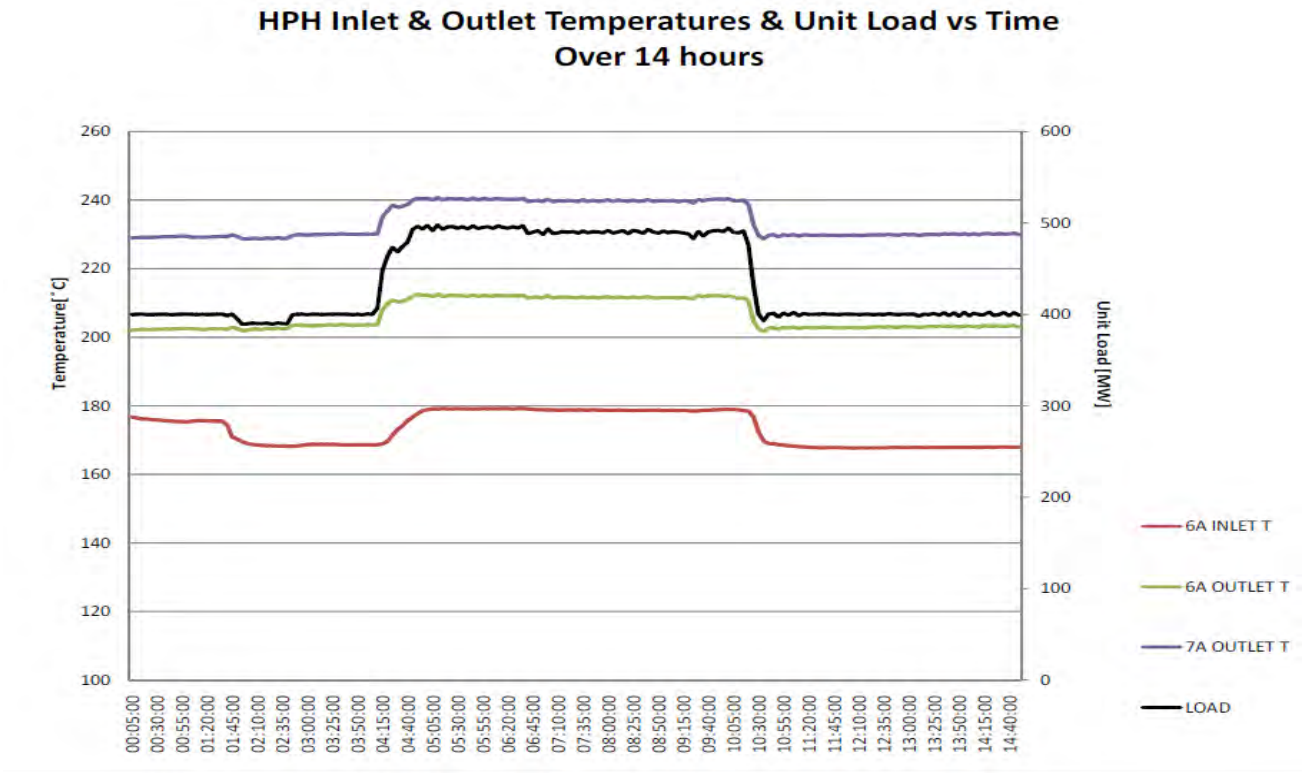

Figure 4-8: Plant data for HPH7 over 14 hours [3].

The Flownex model results for a ramp from 80% to 100% load are compared to the acceptance data given in Figure 4-8 and are shown in Figure 4-9. At 100% load, the average feed-water

temperature at HPH 7 was recorded to be 242 °C from the Flownex model. Figure 4-9 shows that there is good agreement between the model results and the acceptance data values.

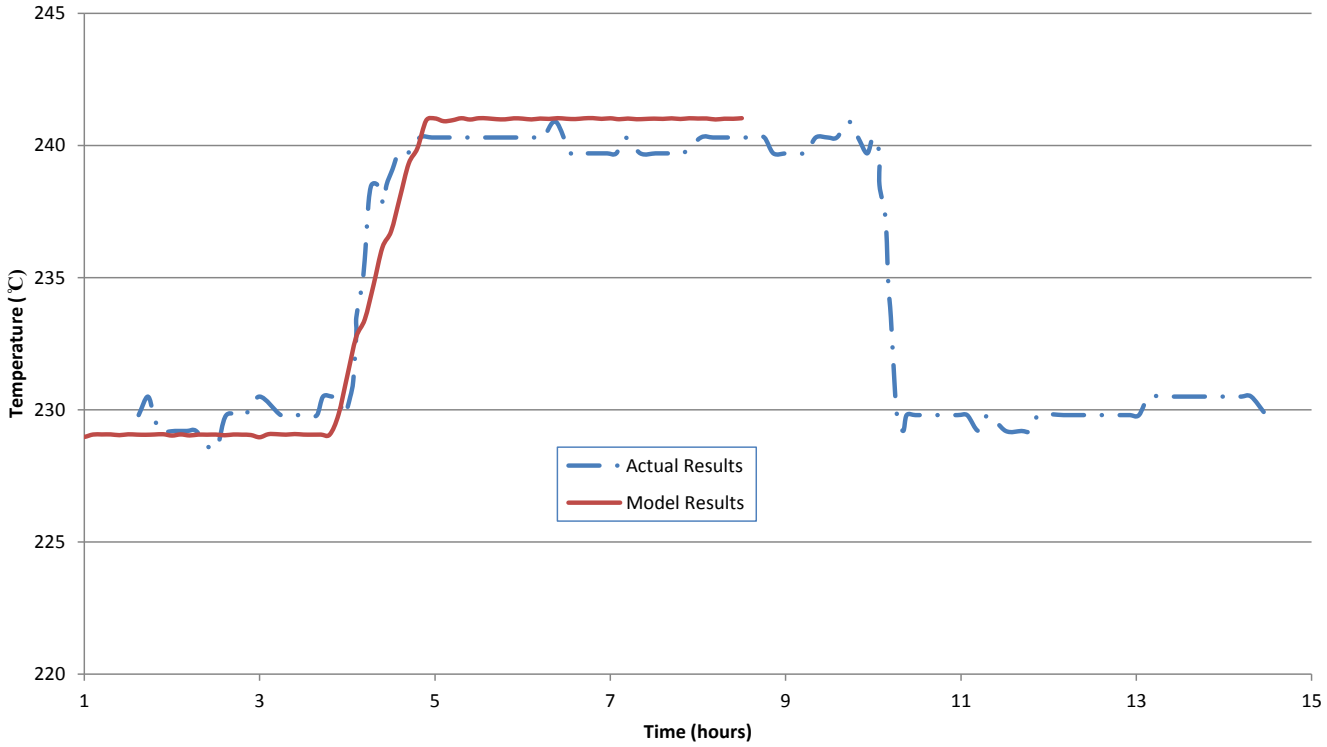

Figure 4-9: Comparison between acceptance test results and Flownex model results.

It is worth noting that the model results do not ramp at the same time scale given on the graph but is put on same scale only for comparison.

5. Conclusions and Recommendations

The main aim of this report was to formulate a mathematical methodology for modelling FWHs and implementing the model suggested on Flownex. The model built will be used to help in fault finding on the heaters in the Eskom fleet. Also, the model is part of the components of a complete power plant simulator. The model will eventually be brought together for a complete transient power plant simulation. Most models used for analysis at Eskom are only steady state models and this study brought about a better understanding of transients and processes in transient. The thesis also looks at the amount of detail required to fully define a FWH model. The conclusions start off by looking at answering some of the main objectives of the report. It then looks at conclusions based on empirical findings and theoretical implications of the findings, and ends off by looking at the conclusions from results of the steady and transient state models and the observations from both scenarios.

The mathematical method was successfully formulated from first principles and heat balance data (grey-box model) with the assumptions outlined in section 3.3, and the HTC of the condensing zone for different loads were predicted to acceptable accuracy. To verify the predicted HTC they were tested on Flownex model with just a condensing zone in place. For all load cases, the HTCs with and without the effect of conduction were formulated and were tested on Flownex. The results in section 3.7 Figure 3-19 and Figure 3-21 show that the HTC produce the required conditions for the condensing zone for both cases.

The mathematical model was implemented on the Flownex model as a whole for both the transient and steady state. The steady state tests showed good agreement with acceptance data and will be discussed in more detail in the next section. The transient model is built with look-up tables for high level inputs and heat transfer characteristics as explained in section 3.6.

The first theoretical conclusion drawn from literature was that there is need for the thermal mass of the HX to be included if the dynamics of the process are to be precisely captured during transient scenarios. The effects of the thermal mass were shown in the form of temperature responses of the HX and fluids in streams. Also heat energy accumulation in HXs during changes in operation was used to show the same effects. The mass was added as a lump, and it was shown in literature that temperature gradients in transients could be estimated for a lumped system for cases where the Biot number is less than 0.1. Secondly, using typical parameters of a FWH and working conditions the typical HTCs values for condensation over tubes and flow inside tubes were determined using correlations discussed in section 2.3.2. The ratio was used for all analysis in this report.

The model needs to be revisited in order to fully represent the performance of the FWH in terms of the pressure drop across both streams. The understanding of how pressure drop in both streams is outlined in section 2.5. But due to lack of FWHs' internal data the pressure drop in both streams is not accurately modelled. A check however was made on the model to see how pressure drop affects the performance of the FWH. And results obtained are consistent with theory in that as more pressure is lost the saturation temperature is lowered and hence the performance is also lowered [12]. However, the Laskowski and Barszcz models and in this thesis, it is evident that assuming no or minimum pressure drop on both of the FWH streams does not change the performance significantly. Laskowski model suggests that constant HTC lead to a loss in accuracy of the feed-water temperature at high load. In the analysis of this report, the HTCs vary with load and better agreement with the results was obtained even for higher load conditions.

5.1 Steady State Model

5.1.1 Conclusions

The steady state model was successfully modelled with satisfactory accuracy in terms of the key indicators of FWH performance mentioned in section 4.1. The feed-water temperature is the most accurately predicted parameter for the four load cases considered with errors less than 0.5%. The model result parameter which was most out of the plant data result is the heat load predicted from the analytical solution at 40% and thus yields a bled steam mass flow that is off by 2.83%. The amount of heat transfer in steady state model for all loads was found to correspond with the one on the mathematical model for other loads. It can therefore be concluded that the steady state model showed good agreement with acceptance data in terms of performance of the FWH.

5.1.2 Recommendations

The steady state model required that the mass flow rate for the operating load be determined first, using the "designer" function on Flownex. This was done for every run/test for different loads. There could however be better ways, that are not known by the author, that could produce the required mass flow rate from input load conditions without the aid of the "designer".

5.2 Transient State Model

5.2.1 Conclusions

The transient model built is a good representative of what the FWH would do in operation. The change of load from one steady state to another was achieved and the results for the Kriel HPH 7 were in agreement with the model results. The level in the heaters was seen to respond as expected with the given conditions and changes imposed. The model was therefore successfully built with level control capabilities but realising the control loops was not part of this project.

5.2.2 Recommendations

The following are recommendations for future work and changes that can be made on the bits and pieces that make up the transient model:

- The HTCs ratio applied in the analysis needs to be investigated further as this ratio could change with load in transients.
- There is more work to be done towards understanding the transient behaviour of thick HXs on Flownex for different Biot numbers as headers in FWHs form part of the heat exchanging material and also accumulate or release energy in transients.
- Inclusion of pressure drop in the model analysis as it was realised in the later stages of the project that some of the FWHs at Eskom report pressure drops in the bled steam inlet pipe lines.

5.3 Closing Remarks

As a starting point to developing a FWH model on Flownex SE, this project has been a success not only in modelling the FWH but also in finding the limitations to the modelling tool and how to overcome some of them. A fairly robust methodology has been created and can be used to tackle similar problems where geometry of the FWHs is not known, and can be altered to accommodate other phenomenon not included in the current model.

6. List of References

[1] T. Barszcz and P. Czop, “Estimation of feed-water heater parameters based on a grey box approach,” vol. 21, no. 4, 2011.

[2] G. Minner, D. Flemming and W. Kettenacker, “Feedwater heater calculations,” *PEPSE,* vol. II, pp. (9-1)-(9-22), 2004.

[3] S. Xulu, A. Hoosen and R. P, “LP and HP heater assessment for Kriel power station”.

[4] M-Tech, “Flownex library manual,” Johannesburg, 2014.

[5] M-Tech, “Flownex library theory manual,” Johannesburg, 2013.

[6] T. Ghosh and M. Prelas, Energy Resources and systems:Volume I: Fundamentals and Non-Renewable Resources, Springer Science + Business Media B.V, 2009, pp. 19-28.

[7] R. Grosseer and G. Bouwer, “Lethabo turbine and turbine plant training course,” Alstom, Johannesburg, 2007.

[8] P. K. Nag, Power plant Engineering, New Delhi: Tata McGraw-Hill Publishing Company, 2007.

[9] M. W. Hubbell, The fundamentals of nuclear power generation: Q & A, New York: authorhouse, 2011.

[10] K. Thulukkanam, “Shell and Tube Heat exchanger Design,” in *Heat exchanger Design Handbook*, CRC Press, 2013, pp. 237-336.

[11] R. K. Shah, E. C. Subbarao and R. A. Mashelkar, Heat Transfer Equipment Design, Hemisphere publishing Co, 1988.

[12] M. Cumo and A. Naviglio, Thermal Hydraulic Design of Components for Steam Generation Plants, New York: CRC Press, 1991.

[13] Rathakrishnan, fundamentals of engineering thermodynamics second edition, new delhi: Asoke k. Gosh, Prentice-Hall of India private limited, M-97, Connaught circus, 2006.

[14] I. Hussaini, S. Zubair and A. M, "Area allocation in multi-zone feedwater heaters," *Energy conversion and management,* vol. 48, no. 3, pp. 568-575, 2005.

[15] M. Youssef, "tpowertec," [Online]. Available: http://tpowertec.com/heatexchangers.htm. [Accessed 20 November 2014].

[16] W. K. Laskowskia R, "Comparison of two simple mathematical models for feed water heaters," vol. 91, no. 1, 2011.

[17] L. F. Wadsworth and T. J. Kielar, "Recommended Guidelines for the Operation and Maintenance of Feedwater Heaters," in *INTERNATIONAL ENERGY ASSOCIATES LIMITED*, Washington, 1983.

[18] W. D. Mackowski, Conduction Heat Transfer: Notes for Mech 7210.

[19] M. Thurumaleshwar, Fundamentals of Heat and mass transfer, New Delhi: Dorling Kindersley, 2006.

[20] Y. Cenel and M. Boles, Thermodynamics: an Engineering approach, New York: McGrawHill, 2006.

[21] A. Bejan and A. D. Kraus, Heat transfer Handbook, volume 1 ed., New Jersey: John Whiley, 2002.

[22] E. N. Sieder and G. E. Tate, "Heat transfer and pressure drop of liquids in tubes," *Industrial Engineering Chemistry,* no. 28, p. 1429, 1936.

[23] J. W. Palen, "Heat exchangers, vapourizers and condensers," *Mechanical Engineer's Handbook Energy and Power,* vol. 4, pp. 295-332, 20096.

[24] J. McNaught, "Two phase forced convection during condensation on horizontal tube bundles," *Heat transfer,* vol. 5, pp. 125-131, 1982.

[25] Q. Kern, Process Heat Transfer, New York: McGraw-Hill, 1965.

[26] M. Rathore, Comprehensible Engineering Heat Transfer, New Delhi: LAXMI PUBLICATIONS (P) LTD, 1998.

[27] S. Kakac and H. Liu, Heat exchanger selection, rating and thermal design, London: CRC press, 2002.

[28] Wolverine, "Wolverine Tube Inc.," [Online]. Available: http://www.wlv.com/wp-content/uploads/2014/06/databook3/data/db3ch13.pdf. [Accessed 18 07 2014].

[29] P. Rousseau, Practical thermal-fluid system simulation, 2013.

[30] A. V. Luikov, Analytical Heat Diffusion Theory, Chicago: Academic press inc, 1968.

[31] Y. V. Rao, Heat Transfer, New Delhi: Universities Press (India) Limited, 2001.

[32] P. Talukdar, "Transient Heat Conduction," Department of Mechanical Engineering, New Delhi, -.

[33] C. Lam and G. Naterer, "Transient Response of two-phase heat exchanger with varying convection coefficients," *Heat Transfer,* vol. 128, pp. 953-962, 2006.

[34] M. A. Abdelghani-Idiris, F. Bagui and L. Estel, "Analytical and Experimental response time to flow rates along a counter flow double pipe heat exchanger," *International Journal ofHeat and Mass Transfer,* vol. 44, pp. 3721-3730, 2001.

[35] K. S. Tan and I. H. Spinner, "Dynamics of a shell and tube Heat Exchanger with a finite tube wall capacity and finite shell-side resistance," *Ind. Eng. Chem. Fundam.,* vol. 17, no. 4, pp. 353-357, 1978.

[36] J. Yin and M. K. Jensen, "Analytical model for transient Heat exchanger response," *International Journal of Heat and Mass Transfer,* vol. 46, no. 17, pp. 3255-3264, 2003.

[37] L. M. Jiji, Heat Conduction, New York: Springer, 2009.

[38] N. Siavellas and D. Georgiou, "1D heat transfer through a flat plate submitted to step changes in changing heat transfer coefficients," *Thermal Science,* vol. 5, no. 44, pp. 452-464, 2005.

[39] P. K. Nag, Heat and Mass Transfer, New Delhi: McGraw-Hill, 2008.

[40] E. Gwebu, "TRANSIENT BOILER HEAT EXCHANGER THERMAL BEHAVIOUR ANALYSIS," Cape Town, 2014.

[41] C. I. Kleinstreuer, Two-Phase Flow: Theory and Applications, London: Taylor and Francis, 2003.

[42] M. Dobson, J. Chato and W. J.P, "Optimal sizing of Two-phase Heat Echanger," Mechanical & Industrial Engineering Dept. University of Illoris, Illoris, 1993.

[43] D. Chisholm, "Pressure gradients due to friction during the flow of evaporating two-phase mixture in smooth tubes and channels," *Heat Mass Transfer,* vol. 16, pp. 147-158, 1973.

[44] L. Friedel, "Improved friction drop correlation for horizontal and vertical two-phase pipe flow," in *European two-phase flow group meeting*, Ispra, 1979.

[45] Hambrice K., "Topics: Pump Zone," K-TEK coorporation, 2013. [Online]. Available: http://www.pump-zone.com. [Accessed 18 January 2014].

[46] C. Herrera, "Blog: Magnetotrol," 11 December 2012. [Online]. Available: http://levelandflowsolutions.magnetrol.com. [Accessed 28 July 2013].

[47] K. Hambrice, "Topics: Pump Zone," K-TEK coorporation, 2013. [Online]. Available: http://www.pump-zone.com. [Accessed 18 January 2014].

[48] F. Todd and I. Jacobson, "FSRUG," 2012. [Online]. Available: http://www.fsrug.com. [Accessed 24 July 2014].

[49] B. Sohlberg and E. Jacobsen, "Grey Box Modelling- Branches and Experiences," Seoul, 2008.

[50] M. Tarr, "Courses/Topics: ami," 2013. [Online]. Available: http://www.ami.ac.uk/courses/topics/0199_mod/index.html. [Accessed 22 01 2014].

[51] R. Laskowskia and K. Wawrzykb, "Comparison of two simple mathematical models for feed water heaters," vol. 91, no. 1, 2011.

[52] M. A. Antar and S. M. Zubair, "The impact of fouling on performance evaluation," *Apllied Thermal Engineering,* no. 27, 2007.

[53] K. Azman and J. Kocijan, "Apllication of Gaussian processes for black box modelling of biosystems," *ISA Transactions,* vol. 46, no. 4, pp. 443-457, 2007.

[54] L. Ljung, System Identification: Theory for the User, Linkoping: PTR Prentice Hall, 1987.

[55] T. P. Bohlin, Practical Grey-box Process Identification: Theory and Applications, Stockholm: Springer, 2006.

[56] T. Barszcz and P. Czop, “A feedwater heater model intended for model-based diagnostics,” Ossy, 2010.

[57] M. Mujtaba and M. Hussain, Application of Neural Networks and other Learning Technologies in Process Engineering, London: Imperial College Press, 2001.

[58] J. A. Roubos and R. Babuska, “Semi-Mechanistic Modelling and it Application to Biochemical Processes,” Netherlands.

[59] J. Xu, T. Yang, Y. Sun, K. Zhou and Y. Shi, “Research on varying characteristics of feed-water heater considering level,” *Applied Rhermal Engineering,* vol. 67, pp. 179-189, 2014.

[60] M. Rathore and R. J. Kapuno, Engineering Heat Transfer second edition, 2011.

[61] D. Flynn, “Model-based fault detection in a high-pressure heater line,” in *Thermal power plant simulation and control*, London, The Institute of Electical Engineers, 2000, pp. 269-308.

[62] H & C Heat Transfer Solutions, “H & C Heat Transfer Solutions,” Design tips, 2008. [Online]. Available: http://www.hcheattransfer.com/coefficients.html. [Accessed 8 02 2015].

[63] Steinmuller, “ high pressure heater replacement: operation and maintenance manual,” Steinmuller (Pty) Ltd, Johannesburg, 1996.

[64] J. R. Davis, copper and copper alloys, ASM international, 2001.

[65] P. Makelainen and P. Hassinen, Light weight steel and aluminium structures, London, 1999.

[66] V. Patel and R. Rao, “Design otimization of tube and shell heat exchanger using particle swarm optimization technique,” *Applied Thermal Engineering,* vol. 30, pp. 1417-1425, 2010.

[67] W. Parry, j. Bellows and A. Harvey, ASME International Steam Tables for Industrial Use (Based on IAPWS -IF97), New York: ASME Press, 2000.

[68] F. du Preez, “Feedwater heaters Part A,” 2008.

[69] A. N. Karayannis and N. C. Markatos, “A method to predict and analyse the performance of high pressure feedwater heaters using computational fluid dynamics techniques,” in *IMECH E Conference Transactions: Heat Transfer*, London, Mechanical Engineering Publications, 1995, pp. 399-404.

[70] D. Kothari and P. Subbarao, “Power Generation,” *Springler Handbook of mechanical Engineering,* pp. 1361-1419, 2009.

Appendix A. Methodology Summary

Inputs to the model from working conditions

$$\begin{pmatrix} MM \\ PP \\ TT \\ HH \\ HHO \\ TTO \\ Mm \\ hh \\ tt \\ hho \\ tto \\ ppo \end{pmatrix} :=$$

Temp [?C	M_flow [k	Ent [kJ/kg	Temp [?C	Ent [kJ/kg	Temp [?C	Press [bar]
515.15	424.143	899.4	481.75	1049.9	514.75	214
514.05	415.662	895.8	480.95	1044.4	513.95	213
501.25	334.565	853.8	471.65	991.1	502.35	199
486.45	251.322	802.6	460.05	926.8	488.15	184
276	0.5	0.5	274	0.5	277	50

The last row on the inputs section is made up conditions and the inputs are kept close to zero as possible. These conditions are for 0% load condition. All calculations of the steam and feed-water properties use the steam-water tables [67].

De-superheating Zone

Calculation of the temperature and enthalpy of steam after de-superheating zone

$$Tdes_i := T_{steam}(P_i, "", "", "")$$

$$Hdes_i := h_{steam}(P_i, "", "", 1, "")$$

$$Tdes = \begin{pmatrix} 242.15 \\ 241.019 \\ 228.266 \\ 213.338 \\ 120.212 \end{pmatrix} \cdot °C$$

$$Hdes = \begin{pmatrix} 2.803 \times 10^3 \\ 2.803 \times 10^3 \\ 2.803 \times 10^3 \\ 2.799 \times 10^3 \\ 2.706 \times 10^3 \end{pmatrix} \cdot \frac{kJ}{kg}$$

Energy lost by the steam during de-superheating

$$Qdes_i := M_i \cdot (H_i - Hdes_i)$$

Where H is the enthalpy of the steam as it enters the FWH

$$Qdes = \begin{pmatrix} 5.594 \\ 5.445 \\ 3.939 \\ 2.586 \\ -0.271 \end{pmatrix} \cdot MW$$

Sub-cooling zone

Qrem is the energy left from the total energy after removing de-superheating energy, Qdes.

Energy extracted in the subcooling region

$$Qsub_i := Qrem_i - Qcond_i$$

$$\Delta T_i := Tdes_i - TO_i$$

$$Qsub = \begin{pmatrix} 0.026 \\ 0.025 \\ 0.014 \\ 7.413 \times 10^{-3} \\ 0.05 \end{pmatrix} \cdot MW$$

$$\Delta T = \begin{pmatrix} 0.15 \\ 0.119 \\ 0.166 \\ 0.038 \\ 117.362 \end{pmatrix} K$$

INSIGNIFICANT

Condensing zone

Heat transfer across FWH without desuperheating

$$Qrem_i := QS_i - Qdes_i \qquad Qcond_i := \left(h_{steam}\left(P_i, "", "", 1, ""\right) - h_{steam}\left(P_i, "", "", 0, ""\right)\right) \cdot M_i$$

$$Qrem = \begin{pmatrix} 57.945 \\ 56.428 \\ 42.154 \\ 28.66 \\ 0.271 \end{pmatrix} \cdot MW \qquad Qcond = \begin{pmatrix} 57.9185546 \\ 56.4031439 \\ 42.1405089 \\ 28.6525894 \\ 0.2201557 \end{pmatrix} \cdot MW$$

The overall heat transfer Coefficient using the LMTD on the condensing surface

$$UA_i := \frac{Qcond_i}{\left[\frac{\left(Tdes_i - Tfw_i\right) - \left(Tdes_i - t_i\right)}{\ln\left(\frac{Tdes_i - Tfw_i}{Tdes_i - t_i}\right)}\right]}$$

$$UA = \begin{pmatrix} 4.595 \times 10^6 \\ 4.48514 \times 10^6 \\ 4.393 \times 10^6 \\ 4.37323 \times 10^6 \\ 4.69017 \times 10^3 - 5.43359i \times 10^3 \end{pmatrix} \cdot \frac{W}{K}$$

Not part of the solution, made up to fill the matrix

$$\frac{1}{UA} = \frac{1}{hin} + \frac{1}{hout} + \frac{L}{kA}$$

$$ua_i := \left(\frac{1}{UA_i} - R_{cond}\right)^{-1}$$

$$ua = \begin{pmatrix} 6.239 \times 10^6 \\ 6.04 \times 10^6 \\ 5.874 \times 10^6 \\ 5.839 \times 10^6 \\ 7.704 \times 10^6 \end{pmatrix} \cdot \frac{W}{K}$$

The convective resistance is then determined from the overall HTC by removing the conductive part of the HTC as shown above.

$$FX := 10$$

$$hin_i := \left(\frac{FX + 1}{FX}\right) \cdot ua_i$$

$$hout_i := FX \cdot hin_i$$

$$hout = \begin{pmatrix} 6.86246 \times 10^7 \\ 6.64389 \times 10^7 \\ 6.46139 \times 10^7 \\ 6.42258 \times 10^7 \\ 8.47401 \times 10^7 \end{pmatrix} \cdot \frac{W}{K} \qquad hin = \begin{pmatrix} 6.862 \times 10^6 \\ 6.644 \times 10^6 \\ 6.461 \times 10^6 \\ 6.423 \times 10^6 \\ 8.474 \times 10^6 \end{pmatrix} \frac{W}{K}$$

Appendix B. Typical HTCs Calculation

The test carried out in this analysis assumes fluid conditions of the fluids close to 100% load conditions of the Kriel HPH7. It is also assumed that the inner diameter of the tubes is 25 mm and the same for the outer diameter, thickness is not taken into consideration.

condensation Kriel HPH 7

Reference:C:\Users\User\Desktop\Water-Steam IAPWS-IF97 rev A.xmcd

Shell side typical parameters and steam conditions

$a := 0.725$

$T_b := 293\,°C$

$T_w := 292.5\,°C$

$P := 33bar$

$D_o := 0.025m$

Steam properties

$k := \lambda_{steam}(P,"","",0,"","") = 0.63\,\frac{W}{K \cdot m}$

$v_f := v_{steam}(P,"",0,"","") = 1.228 \times 10^{-3}\,\frac{m^3}{kg}$ $v_g := v_{steam}(P,"",$

$\Delta H_{fg} := h_{steam}(P,"","",1,"") - h_{steam}(P,"","",0,"") = 1.769 \times 10^{6}\,\frac{m^2}{s^2}$

$\mu_f := \mu_{steam}(P,"","",0,"","") = 1.115 \times 10^{-4}\,\frac{kg}{m \cdot s}$

$T_f := 0.375 \cdot (T_b - T_w) + T_w = 292.688\,°C$

Nusselt Integral correlation

$$hout := a \cdot \left[\frac{k^3 \cdot (v_g - v_f) \cdot \Delta H_{fg} \cdot g}{\mu_f \cdot D_o \cdot (T_f - T_w) \cdot v_f^{\,2} \cdot v_g} \right]^{\frac{1}{4}}$$

$hout = 3.494 \times 10^{4} \cdot \frac{W}{m^2 \cdot K}$

Tube side typical parameters and conditions

$$m_{fw} := 415.662\,\frac{kg}{s}$$

$$d_i := 25mm$$

$$T_{fw} := 207\,°C$$

$$P_{fw} := 213bar$$

Feedwater properties

$$Pr := Pr_{steam}(P_{fw}, T_{fw}) = 0.881$$

$$k_{fw} := \lambda_{steam}(P_{fw}, T_{fw}, "", "", "", "") = 0.676\,\frac{m \cdot kg}{K \cdot s^3}$$

$$\mu_{fw} := \mu_{steam}(P_{fw}, T_{fw}, "", "", "", "") = 1.346 \times 10^{-4}\,\frac{kg}{m \cdot s}$$

$$Re := 4 \cdot \frac{m_{fw}}{730 \mu_{fw} \cdot \pi \cdot d_i} = 2.154 \times 10^5$$

Dittus Boelter correlation

$$hin := 0.023 \cdot \frac{k_{fw} \cdot Re^{0.8} \cdot Pr^{0.4}}{d_i} = 1.092 \times 10^4 \cdot \frac{W}{m^2 K}$$

Ratio of the two HTCs

$$ua = \frac{1}{hin} + \frac{1}{hout}$$

$$hout = FX \cdot hin$$

$$FX := \frac{hout}{hin} = 3.201$$

The ratio of the shell to the tube side HTC was found to be 3.201 for the estimated geometry and working conditions of the FWH. For all analysis in this report the ratio was used as 10 as the 3.201 was just for estimation of order of the ratio.